

Fire Protection of Industrial Process Equipment

Joachim Søreng Bjørge

Thesis for the degree of Philosophiae Doctor (PhD)
University of Bergen, Norway
2019

UNIVERSITY OF BERGEN



Fire Protection of Industrial Process Equipment

Joachim Søreng Bjørge



Thesis for the degree of Philosophiae Doctor (PhD)
at the University of Bergen

Date of defense: 09.12.2019

© Copyright Joachim Søreng Bjørge

The material in this publication is covered by the provisions of the Copyright Act.

Year: 2019

Title: Fire Protection of Industrial Process Equipment

Name: Joachim Søreng Bjørge

Print: Skipnes Kommunikasjon / University of Bergen

Acknowledgements

First of all, I would like to thank my main and technical supervisors, Dr. Maria-Monika Metallinou and Professor Torgrim Log, for support and valuable guidance throughout this marathon of a research project. I am extremely grateful for all the help, motivation, discussions and feedback in both realizing and conducting the project.

I would also like to thank Professor Øyvind Frette for valuable guidance and administrative support, Gunnar Birkeland for his initiative in realizing the project and PDS Protek for their support throughout the project.

Finally, I would like to thank my fiancée, Linn Lønning, for enduring four years of long nights and weekends while my focus was on the research project. I'm looking forward to spending more time with you and our two wonderful daughters.

Abstract

Active and passive measures are two main branches in Fire Protection Engineering (FPE). The present thesis, entitled “Fire Protection of Industrial Process Equipment”, studies parts of these topics:

1. A study of the cooling efficiency of water upon impingement onto hot metal surfaces.
2. A study of industrial grade thermal insulation as a means of Passive Fire Protection (PFP).

The first part of the thesis studies the cooling efficiency of water droplets impinging onto heated metal substrates. A method for studying this was developed, and measurements were performed in the temperature range from 85 °C to 400 °C, i.e. covering the boiling regimes experienced when applying water to heated objects in fires.

Stainless steel and aluminum test discs (with 50 mm diameter, 10 mm thickness, and a surface roughness of Ra 0.4 or Ra 3.0) were suspended horizontally by four thermocouples, simultaneously used to record the disc temperatures. The discs were heated by a laboratory burner prior to the experiments and left to cool with and without applying 2.5, 3.2 and 3.7 mm diameter water droplets to the discs, while the disc temperatures were recorded. The droplets were generated by the acceleration of gravity from hypodermic injection needles and hit the disc center at an impingement speed of 1.5, 2.2, 3.1 and 4.4 m/s, depending on the fall heights. The water application rate was 0.022 g/s, and the discs were aligned at 0° (horizontal), 30° and 60° inclination.

Based on the recorded rate of the temperature change, as well as disc mass and disc specific heat, the absolute droplet cooling effect and the relative cooling efficiency relative to complete droplet evaporation at 100 °C were obtained. Distilled water droplets were tested on both aluminum and stainless steel. Droplets of acetone solution (300 ppm and 700 ppm) and NaCl (35 g/kg) solution, emulating seawater, were tested on aluminum discs, to evaluate the influence of an active surfactant on cooling efficiency. Typically, the water-cooling efficiency was above 60% at the temperatures of boiling crisis and below 10% at temperatures above the Leidenfrost temperature.

There were significant differences in the cooling efficiency as a function of temperature for the two metals investigated. There was, however, no statistically significant difference with respect to whether the surface roughness was Ra 0.4 or Ra 3.0. The droplets of higher impact speed resulted in lower cooling efficiency, especially at disc temperatures above the Leidenfrost temperature, likely due to more vigorous droplets bouncing at higher impact speeds. Larger inclination did, as expected, result in lower cooling efficiency. At temperatures associated with nucleate boiling, the water droplets with NaCl conspicuously displayed higher cooling

efficiency at about 110 °C. This may be explained by the formation of small salt deposits at the disc surface, thus improving the cooling efficiency. At temperatures between 120 °C and the Leidenfrost temperature, acetone and NaCl additives did not significantly alter the cooling efficiency. Above the Leidenfrost temperature, a minor increase in cooling efficiency was observed for the acetone solutions. Overall, the additives only marginally changed the water droplet cooling efficiency.

Heat fluxes in the range 250–350 kW/m² may be expected in industrial hydrocarbon fires. According to the NORSOK S-001 standard, a firewater flux of 10 L/m²min is mandatory for protecting pressurized equipment containing hydrocarbons. At 100% efficiency, heating and boiling this water flux requires about 430 kW/m². At temperatures associated with boiling crisis, the suggested fire water flux would be just sufficient to mitigate the expected heat fluxes. If the metal has already been heated close to, or above, the Leidenfrost temperature, this application flux is much too low. At 10% cooling efficiency, it would only be able to withdraw 43 kW/m² from the fire-exposed surface.

The simple and straightforward technique, based on the differences in cooling rate of metal discs, with and without droplet application, proved to be well suited for assessing the cooling efficiency of water droplets from 80 °C to 400 °C. The test rig also worked well for demonstrating droplet boiling regimes and water droplet cooling efficiency to fire safety engineering students and gave them valuable insight into the limited performance of water droplets cooling when applied to hot metal surfaces.

The very low water droplet cooling efficiency for temperatures close to or above the Leidenfrost point underlines the importance of early detection of fire and early activation of fire water in industrial fires to prevent escalation. The fact that fire water provides increased safety for some temperature areas, but not for all, may lead to a more nuanced appreciation of this safety measure in the total risk analysis. The results also invite a discussion of other means to prevent escalation, for example lay-out based on inherent safety principles and use of passive fire protection (PFP).

The second part of the thesis focuses on current industrial challenges involving insulation of pressurized equipment containing hydrocarbons. Historically, a 50 mm layer of thermal insulation, covered by an additional layer of 50 mm PFP has been applied. Experience shows that humidity from the air has wetted the thermal insulation, at areas where the temperature is below dew point, resulting in corrosion attacks. Corrosion-related incidents are among the costliest problems facing the oil and gas industry today, especially in aging facilities. According to the new standards for thermal insulation of process equipment, 25 mm spacing should be allowed between the metal object and thermal insulation, to prevent/reduce Corrosion Under Insulation (CUI). However, the new requirements will increase the total diameter of the equipment by more than 50 mm, which may not be available without major modifications. Improved knowledge about the contribution of thermal insulation as a means of PFP can be part of a solution. In order to test thermal insulation in a configuration compliant with the new standards for insulating process equipment, a prototype/mockup was built. Thereafter, a concept for small-scale testing of mockups, resembling a part of a typical hydrocarbon distillation column, with thermal insulation in accordance with the modern requirements has been developed.

The second part of the thesis demonstrates a conceptual methodology for small-scale fire testing of mockups, resembling a section of a distillation column. The concept was first tested on 16 mm thick steel walls, and the mockups were exposed to a small-scale propane flame. In order to give heat flux levels in the range 250–350 kW/m², the flame zone was optimized by controlling the air access, as well as limiting heat losses from the combustion zone. Based on the innovative and successful test concept, the performance of thermal insulation in conjunction with 16 mm, 12 mm, 6 mm and 3 mm thick steel walls was tested to check the influence of the significantly less heat sink for the thinner walls. Regardless of the tested steel plate thicknesses, about 10 minutes passed before a nearly linear steel temperature dependency versus time was observed for the exposed steel wall. Thereafter, the thinnest plates systematically showed a faster temperature increase than the thicker plates, confirming the wall heat sink effect. During these fire tests, shrinkage of the industrial thermal insulation was observed. For the most severe tests, significant destruction of the thermal insulation was evident, and there was a need for further in-depth studies of the thermal insulation behavior when exposed to high temperatures.

To study thermal insulation behavior when heated, 50 mm thermal insulation cubes were heat treated (30 min holding time) at temperatures up to 1100 °C, i.e. limited by the available muffle furnace. No clear sign of melting was observed, but sintering resulted in 25% shrinkage, i.e. thickness reduction, at 1100 °C. To study this further, thermogravimetric analysis (TGA) to 1300 °C was undertaken. The TGA revealed mass loss peaks due to anti-dusting material at 250 °C and Bakelite binder loss at 460 °C. No significant mass loss occurred above 1000 °C. Differential scanning calorimetry (DSC) to 1300 °C was also undertaken to try to shed more light on the possible degradation processes involved. The DSC analysis revealed endothermic processes related to the anti-dusting material and Bakelite mass losses at the same temperatures as for the TGA. It did, however, also reveal a conspicuous endothermic peak at 1220 °C. This peak is most likely due to melting.

The endothermic processes involved when heating the thermal insulation may to a large part explain the 10 min delay in steel plate temperature increase during fire testing. Overall, the tested thermal insulation also performed surprisingly well for protecting the thin steel plates through the 30 minute test period.

The results show that this test concept has great potential for low-cost fire testing of other configurations, and it may serve as a setup for product development. Further research is therefore recommended to exploit these possibilities. It may also be worthwhile to study the thermal insulation breakdown mechanisms and heat transfer properties below and at breakdown temperatures. This could possibly allow the utilization of thermal insulation as a means of passive fire protection (PFP) in areas where significant cost reduction when refurbishing old process plants and oil platforms could be achieved.

List of papers

1. J. S. Bjørge, M. M. Metallinou, T. Log and Ø. Frette, Method for Measuring Cooling Efficiency of Water Droplets Impinging onto Hot Metal Discs, *Applied Sciences*, **2018**, 8(6), 953; DOI: 10.3390/app8060953.
2. J. S. Bjørge, S. A. Bjørkheim, M. M. Metallinou, T. Log and Ø. Frette, Influence of Acetone and Sodium Chloride Additives on Cooling Efficiency of Water Droplets Impinging onto hot Metal Surfaces, *Energies*, **2019**, 12(12), 2358; DOI: 10.3390/en12122358.
3. J. S. Bjørge, M. M. Metallinou, A. Kraaijeveld and T. Log, Hydrocarbon Fire Test Concept, *Technologies*, **2017**, 5(4); 72; DOI: 10.3390/technologies5040072.
4. J. S. Bjørge, A. Gunnarshaug, T. Log and M. M. Metallinou, Study of Industrial Grade Thermal Insulation as Passive Fire Protection up to 1200 °C, *Safety*, **2018**, 4(3); 41; DOI: 10.3390/safety4030041.

Contents

| | |
|--|------------|
| Acknowledgements | I |
| Abstract | III |
| List of papers | VI |
| Abbreviations | 1 |
| 1. Introduction | 2 |
| 1.1 Background..... | 2 |
| 1.2 Water droplet cooling efficiency at hot surfaces | 4 |
| 1.3 Passive fire protection..... | 6 |
| 2. Regulations | 11 |
| 2.1 Case history and revision findings..... | 11 |
| 2.1.1 The Lillestrøm train collision..... | 11 |
| 2.1.2 Hydrocarbon leak on the Ula P installation | 12 |
| 2.2 Norwegian regulations..... | 12 |
| 2.2.1 The framework regulation..... | 12 |
| 2.2.2 Technical and operational regulations | 12 |
| 3. Barriers and Barrier Models | 15 |
| 3.1 The concept of risk | 15 |
| 3.2 Barriers and barrier models | 15 |
| 3.2.1 Active fire protection | 17 |
| 3.2.2 Passive fire protection and thermal insulation | 18 |
| 3.2.3 Other protective barriers | 19 |
| 4. Fire Dynamics and Fire Testing | 22 |
| 4.1 General definitions..... | 22 |
| 4.1.1 Gas release rate | 23 |
| 4.1.2 Basic fire dynamics..... | 24 |
| 4.2 History and background of fire testing | 24 |
| 4.3 Heat transfer..... | 27 |
| 4.3.1 Convection | 27 |
| 4.3.2 Radiation | 27 |

| | | |
|-----------|--|-----------|
| 4.3.3 | Conduction | 28 |
| 4.4 | Water droplet properties and physics | 29 |
| 4.4.1 | Droplet breakup..... | 30 |
| 4.4.2 | Water droplet impact velocity..... | 31 |
| 5. | Experimental Work..... | 33 |
| 5.1 | Water droplet cooling experiments..... | 33 |
| 5.1.1 | Experimental setup..... | 33 |
| 5.1.2 | Setting up and performing the experiment..... | 36 |
| 5.1.3 | Determining water droplet cooling efficiency | 37 |
| 5.1.4 | Influence of surfactants on droplet cooling efficiency..... | 37 |
| 5.1.5 | Main conclusion from the water droplet efficiency measurements | 38 |
| 5.2 | Fire resistance in thermal insulation | 38 |
| 5.2.1 | Experimental setup..... | 38 |
| 5.2.2 | Material properties | 40 |
| 5.2.3 | Setting up an experiment..... | 41 |
| 5.2.4 | Performing the experiments | 43 |
| 5.2.5 | Other experimental details | 43 |
| 5.2.6 | Main conclusions from the fire testing of industrial thermal insulation..... | 44 |
| 6. | Introduction to the Papers..... | 47 |
| 7. | Summary and Outlook..... | 51 |
| 7.1 | Recommended further studies | 52 |
| 8. | Scientific Results..... | 55 |

Abbreviations

| | |
|-------|--|
| ALARP | As Low As Reasonably Practicable |
| BLEVE | Boiling Liquid Expanding Vapor Explosion. |
| CFD | Computational Fluid Dynamics |
| CHF | Critical Heat Flux |
| CUI | Corrosion Under Insulation |
| DSC | Differential Scanning Calorimetry |
| DTG | Differential Thermogravimetry |
| ESD | Emergency ShutDown |
| FPE | Fire Protection Engineering |
| HC | Hydrocarbon |
| HCM | HydroCarbon Modified temperature curve |
| HVAC | Heating, Ventilation and Air Conditioning |
| ISC | Ignition Source Control |
| LPG | Liquefied Petroleum Gas |
| O&G | Oil and Gas industry |
| PFP | Passive Fire Protection |
| PSA | Norwegian Petroleum Safety Authority |
| PSM | Pipe Section Mat |
| PSV | Pressure Safety Valve |
| PT | Plate Thermometer |
| Ra | Arithmetical Mean Roughness in Micrometers |
| TGA | Thermogravimetric Analysis |

Chapter 1

Introduction

1.1 Background

The control and use of fire was a turning point in human evolution. Fire provided early humans with a heat source and was a revolutionary tool within hunting and cooking, as well as a means of protection. The pursuit of understanding fire has thus been part of the human experience since the first primitive human viewed the glow. Since these early observations, mankind has slowly developed the knowledge to use and understand fire in gradually more advanced ways, including the production of a number of products for their households, tools and weapons.

Combustible materials were abundant in the environment, as biomass. Fossil materials (oil from pitch in Mesopotamia) were first used as building materials in walls and streets, as well as to tar boats made of straw. The use of oil as fuel dates back thousands of years to ancient China, and the first known oil well was drilled as early as 347 AD [1]. The first coal mine dates to ca. 1600 AD in northern America, today's Canada [2], while the usage of highly flammable oil and gas followed the invention of the internal combustion engine and gave rise to the petrochemical industry. In 2019, fossil fuels contribute about 80% of the world's energy consumption. Of these, coal contributes 30%, oil 35% and natural gas 15%. The remaining 20% is comprised of nuclear energy (5%) and energy from renewable resources (15%) [3].

Now, approximately 50% of the world's energy supply is produced by the oil and gas (O&G) industry [4]. Petroleum products are an essential source of energy, as well as raw material for producing plastic items, and thereby an important part of the modern world. The hydrocarbon processing industry involves complex mechanical interventions, with extraction of oil and gas from wells, as well as processing, to produce the products called for in the market. For many decades, this industry has been, and still is, an essential part of the world economy. In several locations, the O&G industry is a mature industry. The lifetime of equipment and process plants must therefore steadily be extended by maintenance, upgrades and modifications. Processes at elevated pressure, combined with highly flammable materials, make this an industry with high accident potential, in relation to fires and explosions.

From the start of the O&G industry on the Norwegian continental shelf, safety standards have been established. NORSOK S-001 [5], together with ISO 13702 [6], defines the required standard to establish and maintain an adequate level of safety for personnel, environment and material assets. The aspect of maintaining an adequate level of safety throughout the facility's lifetime must take into account the challenges allocated with each operational phase. An example of this can be illustrated with the Bathtub Curve (Figure 1). When designing and starting up new equipment or process segments, there is a higher risk of malfunction (complex system, pressurized, etc.). This phase is referred to as phase A. When the process is in operation and runs normally, the failure rate is lower (not quite new equipment, stable processes, tested, etc.), illustrated by phase B. When the years pass and equipment ages, due to wear, tear, and corrosion, the failure rate again increases, Phase C, giving a failure rate illustration of a bathtub for the complete life cycle [7].

The illustration given in Figure 1 is representative of electrical equipment; the lifespan and deterioration of mechanical equipment are believed to differ somewhat.

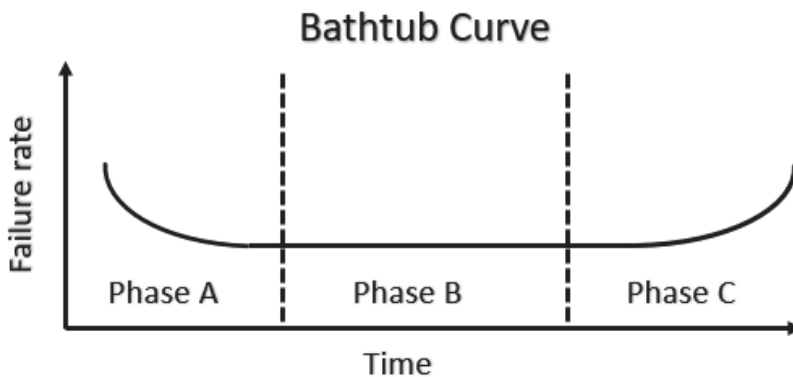


Figure 1 The bathtub curve [7].

During the last three to four decades, the international O&G industry has experienced several severe accidents [8-9]. Much effort is therefore put into limiting the fire and explosion risks associated with processing highly combustible hydrocarbon products. However, every year there are still severe fires in the hydrocarbon processing industry [9-10].

Some would say that almost every accident that has occurred in recent times could have been prevented, since similar accidents have occurred before, and the learnings from and accounts of these accident investigations are published.

Within safety engineering, the prevention and mitigation of fires and explosions is of the utmost importance. On- and offshore petroleum facilities process and handle large quantities of pressurized hydrocarbons in vessels and routed in pipes. Equipment and piping are often constructed in different steel alloys, which are vulnerable to fires. At elevated temperatures, the steel strength is reduced. In the O&G industry, carbon steel and stainless steel are most commonly used. Carbon steel is expected to lose 55% of its strength at 600 °C [11], while stainless steel is expected to have lost 30% of its strength at the same temperature. Fire-exposed

pressurized pipes and vessels may therefore rupture violently and release their combustible or poisonous contents, if weakened by overheating.

Jet fires can be defined as “pressurized releases of hydrocarbons that result in impinging flames with significant momentum” and quickly achieve high temperatures. The potential for a jet fire exists wherever storage, process equipment or pipework contains flammable petroleum gases at pressures approximately 1 bar or greater above ambient pressure. Another risk is pool fire, which is defined as “a diffusion flame where a layer of volatile liquid is evaporating and burning”. This is an important scenario to assess within safety engineering, due to the large amount of liquid fuels stored and handled. Research shows that, for those types of fires, temperatures up to 1200 °C and heat fluxes between 250 and 350 kW/m² may be received by an object at 20 °C engulfed in fire [12-15]. If the fire plume affects other process equipment, this may also rupture, increasing the severity of the incident. Active and passive fire protection measures could therefore prevent the violent escalation of industrial fires.

Considerable resources are used for designing and maintaining protective barriers, i.e. deluge systems, fire monitors, passive fire protection, etc. As an example, the NORSOK standard S-001 [5] devotes multiple pages to these risk-reducing measures. For process areas, the design criteria are standardized and general. The requirement for designing fire water systems is 10 L/m²min, i.e. 10 liters of water per minute per square meter of wetted surface. The deluge systems provide water droplets of various diameters, while the distance and orientation of impingement will vary according to the configuration and the shape of the protected equipment. Therefore, the literature on water droplets impinging on hot metal objects is relevant.

If 10 liters of water vaporize on 1 m² over 1 minute, is heated to 100 °C and evaporate at 100 °C, it will be able to remove 430 kW/m². This (or some similar type of) calculation may lie behind the NORSOK firewater requirement. However, water droplet cooling efficiency exhibits large variations, depending mainly on the temperature of the hot metal surface [16-17].

Time to rupture and escalation of pipes or other pressurized equipment is a complex and essential part of a risk assessment. Time to rupture of pipes of smaller dimension could be a few minutes when exposed to a jet fire. While automated firewater release is the norm at offshore facilities, manual activation is the norm at land-based facilities. In some cases, the time to initiate firewater could be longer, due to manual activation.

The author would mention that some text is copied from articles [13, 17-19], as they describe some essential background and experimental information.

1.2 Water droplet cooling efficiency at hot surfaces

The first part of the thesis was to develop a method for measuring the cooling efficiency of water droplets impinging onto hot metal discs in the temperature range of 80–400 °C. This temperature range covers the different boiling regimes that are associated with water droplets on hot metal substrates. When the method and setup was developed and verified, the goal was to study the effect of changing parameters, such as type of metal, surface roughness, additives, impingement velocity, etc.

Few studies regarding droplet cooling efficiency, covering the whole range from below the boiling point and all the way into the film boiling regime, were identified. The main task was to get a better understanding of these phenomena for the droplet cooling experiments. Numerous large-scale deluge experiments and studies were identified [20-22]. The same studies struggled to conclude, due to a lack of understanding of physical properties and how they affected the cooling processes. Many of the studies therefore concluded that the next step in droplet cooling efficiency studies should be conducted on a smaller scale.

We started the discussion of this issue during the fall of 2013, due to cost-saving issues in the O&G industry, with a single question: “What is the cooling efficiency for water droplets above the Leidenfrost point?” However, early on, these experiments indicated a limited cooling efficiency of water droplet impinging onto heated metal surfaces. The thesis was therefore changed to also include part two of the thesis, presented in Chapter 1.3.

Studies of the performance of active fire protection in scenarios in which equipment is exposed to a jet fire are scarce. For active fire protection, the analysis needs to cover all the involved boiling regimes, as illustrated in Figure 2.

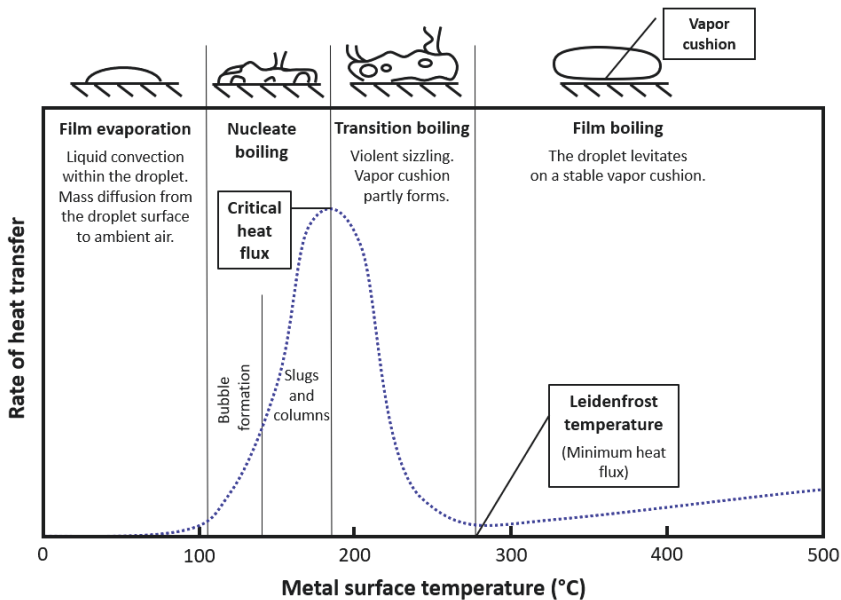


Figure 2 Droplet evaporation/boiling regimes for a fictitious metal surface.

The German theologian and physician, Johann Gottlob Leidenfrost, was the first scientist to study the phenomenon of water droplet evaporation on hot metal surfaces [23-24]. He noticed that, when the temperature of a particular metal object exceeded a certain value, the water droplets were moving about on the hot metal surface with a very low evaporation rate, i.e. a very low cooling rate. Since then, it has become common to call the temperature for the onset of this phenomenon the Leidenfrost temperature. Different parameters, e.g. the metal itself (thermal properties), surface roughness (depth of anomalies and pattern), as well as droplet size and deposition method used, exert influence on the observed Leidenfrost temperature [16].

Starting with placing water droplets on a metal surface (no impingement), we can distinguish the following regimes: (1) Evaporation at temperatures below the boiling point. (2) Nucleate boiling from temperatures a few degrees above the boiling point and up to a maximum heat flux, determined as the “boiling crisis”. For the typical temperature range of 104–124 °C, vapor pockets form inside the droplet and move upwards to the surface of the droplet. (3) Transition boiling for even higher temperatures, with partial lift-up of the droplet by vapor bubbles forming under it. As the contact area and/or contact time between the water droplet and the metal surface are reduced, so are the heat flux and cooling efficiency of the droplet. The minimum observed heat flux denotes the “Leidenfrost point”, with practically no direct contact between droplet and surface. (4) At even higher temperatures, the levitated droplet removes some more heat from the surface, due to the larger difference between the surface temperature and the evaporating droplet. The heat flow is still low, since the heat must flow through a gap of steam (vapor cushion) between surface and droplet.

The Leidenfrost temperature is not one clearly defined temperature but is affected by the type of metal (thermal properties), perhaps on the surface treatment, and on the way the droplets become in contact with the surface (carefully deposited, impinging, surface inclination etc.). A typical Leidenfrost temperature may be about 300 °C for stainless steel.

By achieving a better understanding of the actual effect of an active firefighting measure, installations and facilities could be built and operated with a higher safety level or at a lower cost. This statement was one of the main reasons for starting this research project, and the way of thinking is supported by the analyzed major accidents in [25].

1.3 Passive fire protection

In several hydrocarbon processes, thermal insulation is required to maintain the proper production temperatures. Distillation columns may serve as an example of process equipment where the temperature profiles are carefully designed to obtain good production efficiency and the right quality for the distilled products. Such process units, which may release huge quantities of flammable materials if ruptured in a fire, are normally also protected by mineral-based passive fire protection.

A distillation column is a basic separation equipment. It obtains the separation of hydrocarbons by boiling the liquid products to evaporate the more volatile components away from the low-volatile components. Typical dimensions of the steel structure may be 4 meters in diameter and 20–25 m in height. Because of the height, diameter and the operating pressures, the column walls are comparatively thick (typically 16 mm). Corrosion protection paint was typically applied to prevent external corrosion of the process equipment. Mineral-based thermal insulation was then put in direct contact with this paint.

Due to temperature differences in, e.g., a distillation column, humid air may entrain at lower levels. When heated, this humid air travels upwards and is pushed further upwards by new air entraining at lower levels, to locations where the column wall is below the entrained air dew point temperature. This results in condensed water gradually draining down through the insulation. In some cases, where units operate below the ambient air dew point, natural convection supplies humidity into the thermal insulation, which finally becomes soaked in

water. This ruins the insulation capacity, since only 4% moisture by volume can reduce the thermal efficiency by 70%, due to the high thermal conductivity of water [13, 26]. Soaked thermal insulation may finally destroy the corrosion protective paint, exposing the column steel to liquid water. Severe corrosion may be the consequence of this process, resulting in large maintenance costs or, in the worst case, severe hydrocarbons leaks.

Complete rehabilitation is therefore often required. In a time period of 15 years, over 130 corrosion-related accidents were reported to the Norwegian Petroleum Safety Authority (PSA). Among these 130 reported accidents, 60 incidents were due to corrosion under insulation (CUI), i.e. making it one of the costliest issues facing the O&G industry, especially for aging installations.

In order to achieve proper passive fire protection, high temperature resistant mineral-based insulation (typically 30–50 mm thickness, certified through ISO 22899 [27]) was provided outside the thermal insulation. Stainless steel cladding (typically 0.7 mm thickness) represented the outer surface, preventing ingress of rain and snow. The cladding would also serve as flame deflection in a fire scenario, protecting the passive fire protection and the thermal insulation from direct flame exposure.

During the fall of 2016, inspections at the Equinor Kårstø gas processing plant revealed extensive corrosion on distillation columns. Due to these corrosion findings, it was necessary to improve the thermal insulation (and passive fire protection) solution. The current best practice recommends adding an air gap (25 mm) at the wall to prevent contact between the wall material and the insulating material. However, given such an air gap, there was no space for Passive Fire Protection (PFP) without a significant effort, involving rearranging the structure, etc. Such a rearranging of structure would also require much hot work. Seeking other solutions was therefore assessed to be beneficial.

A simple question from the Kårstø ISO project to an Equinor advisor started the process of evaluating whether there was indeed a need for PFP for thick-walled thermally insulated distillation columns. Theoretical calculations revealed that testing was necessary to answer this question, since there was uncertainty regarding the behavior of the thermal insulation at elevated temperatures.

Testing was therefore decided on, with only regular thermal insulation, i.e. without any passive fire protection, as this setup might show sufficient slow-temperature development of the column wall during fire exposure. Due to the price of PFP there was also a significant material cost reduction. Less hot work in the area, fewer planning expenses, as well as a safety gain with respect to less hot work, were major drivers for investigating whether thermal insulation might provide sufficient fire protection.

The second goal was to investigate a concept for the small-scale testing of mockups resembling a part of a typical hydrocarbon distillation column, with thermal insulation in accordance with the modern requirements. The mockup was built according to relevant requirements and was exposed to a small-scale propane flame, where the flow rate and flame zone were optimized to limit heat losses and give high heat flux levels, e.g. in the range 250–350 kW/m². When the mockup was built and verified, further analysis of the effect of other thicknesses of stainless steel wall and degradation modes of the thermal insulation was conducted.

Today, an improved insulation methodology, where an air gap (typically 1 inch thick) is introduced as previously mentioned, prevents direct contact between the thermal insulation and the steel unit. The thermal insulation is kept at this distance by perforated metal plates (aluminum or stainless steel) that are electrically insulated from the steel wall by non-conducting spacers. This air gap has proven to be quite effective in preventing accumulation of water and thereby mitigating the probability of corrosion. However, given such an air gap, the necessary spacing increases. The new insulation method adds at least 52 mm to the equipment's total diameter. However, in some situations, there is not sufficient room available for this added spacing. Relocating structural elements would require much hot work, which should be avoided in live plants. Shutting down the plant for such work may not be realistic, due to the associated costs. The possibility of providing space by relocating structural elements is also very costly.

Thermal insulation could also be applied to serve other functions: personal protection, temperature control, humidity prevention or even to decrease noise emission. The implementation buildup for passive and thermal insulation is identical. The best practice, as indicated in Figure 3, consists of:

- 25 mm air gap between the protective object and the insulation for corrosion prevention.
- 0.7 mm perforated metal plate.
- 50 mm thermal insulation.
- 50 mm passive fire protection (where required).
- 0.7 mm stainless steel cladding.

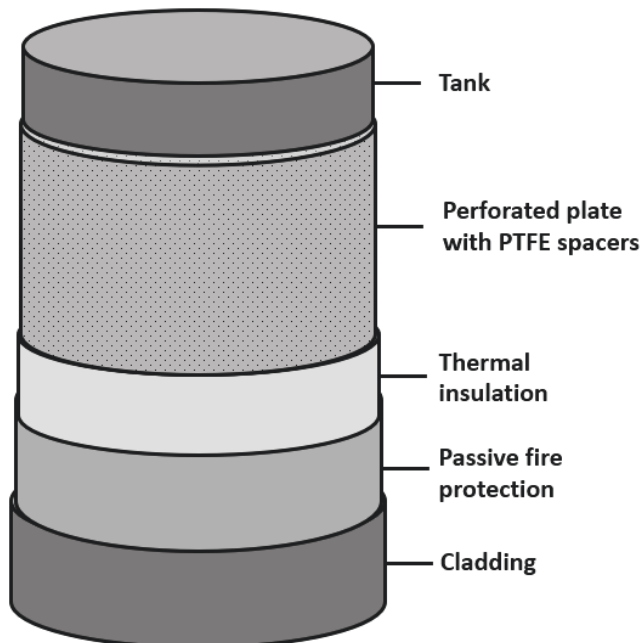


Figure 3 Example of insulated column [28].

Passive fire protection is quite similar to thermal insulation, although made of high temperature resistant materials. Passive fire protection typically displays 30% to 50% higher thermal

conductivity than thermal insulation, but it is verified that it retains its protective performance for extended periods even at temperatures up to 1200 °C.

The comparably thick distillation column walls represent a major heat sink when exposed to a heat source. It could therefore in principle be a possibility that the complete system, i.e. the wall, air gap, perforated metal plate, thermal insulation, and cladding, without additional passive fire protection, would result in a sufficiently slow column wall temperature increase in a fire scenario. This could also be valid for other equipment, such as pipes, tanks, separators, etc. To demonstrate this by large-scale testing is, however, costly. As an alternative, small-scale tests may give valuable information. It was therefore decided to develop a method for testing the new thermal insulation method in high heat loads. The risk of jet fire and escalation is well known. The performance of thermal insulation (without the high resistance PFP layer), in conjunction with steel walls of various thicknesses, is not known. The present thesis investigates the temperatures which the steel structure (of various thickness) will experience if insulated with only thermal insulation: stainless steel cladding exposed to the heat flux levels which are expected in a jet fire.

Thermal insulation could potentially prove to be an adequate fire safety barrier. This was the starting point for the second research question: What would be the consequence of omitting the high thermal resistance layer (PFP) for the temperatures a steel structure will experience if the equipment is exposed to a jet fire?

Although the melting temperature of steel is above 1300 °C, it starts to lose its structural integrity between 550 °C and 620 °C. If the steel is fully utilized, it may already lose 10% of its strength at 400 °C.

The critical steel temperature and the duration (time) to reach this temperature when exposed to a fire are the two main factors used in the design of the PFP solution. However, as the effect of a real fire scenario is virtually impossible to predict or model up front, certain defined fire scenarios with given temperatures and scales are used in the testing and certification of PFP solutions. [15].

Chapter 2

Regulations

The thesis addresses experimental aspects related to the efficiency of water as an active fire protection barrier and thermal insulation as a passive fire protection barrier. To address the importance of these barriers and knowledge in regard to mitigating effect, this chapter presents a brief introduction to both relevant Norwegian regulations for onshore installations and some incidents where active and passive fire protection played an essential role or had inadequate design.

2.1 Case history and revision findings

Major accidents often result in the revision of national regulation and international standards. One example is the Alexander Kielland accident, which led to numerous changes in the requirements for control against fatigue and redundancy of load-bearing structures, flow stability, emergency preparedness and safety equipment on platforms. Alexander Kielland was originally built as a semi-submersible drilling platform. It was later used as a flotel on the Ekofisk prospect in the North Sea. Due to fatigue failure, the platform lost one of its five legs and capsized on 27 March 1980. This resulted in the loss of 123 lives, and the incident is recognized as the largest industrial accident in Norway.

2.1.1 The Lillestrøm train collision

Two trains collided at Lillestrøm station in April 2000. One of the trains was transporting two propane tank wagons. In the collision, the tanks were damaged, propane leaked out and ignited shortly after collision. Approximately 2000 people were evacuated from within the 1000 meter safety zone [29].

The investigation committee concluded that the effort of the rescue service, due to good emergency preparedness, access to suitable equipment and a good water supply, prevented the accident from escalating into a catastrophic BLEVE (Boiling Liquid Expanding Vapor Explosion). CFD simulations showed that the margins to a BLEVE most likely were small. A minor change in parameters, such as stronger wind or higher temperature, could have led to a BLEVE, even before rescue personnel started cooling the tanks with water [29].

2.1.2 Hydrocarbon leak on the Ula P installation

The Ula production platform located in the Norwegian sector of the North Sea was in normal operation when a hydrocarbon leak occurred. At the time of the accident, only three people were located on Ula P, since an emergency shutdown (ESD) test was being prepared. They noticed that a substantial leak had occurred when multiple gas detectors were activated. The personnel quickly evacuated to the Ula drilling facility [30].

A production water seepage, with a high content of chlorides and a temperature of 120 °C, had exposed the stainless steel ESD valve bolts, which finally gave way, due to chloride stress corrosion [30].

The potential consequence of the accident was assessed to be an ignited hydrocarbon leak. The timing of the accident was also considered to be arbitrary, and people could have been present in the module. The investigation identified multiple nonconformities, such as inadequate passive fire protection and inadequate strategies and principles for designing, using and maintaining safety barriers, etc. [30].

2.2 Norwegian regulations

2.2.1 The framework regulation

The purpose of the Framework regulation [31], or “Regulations on health, environment and safety in the petroleum activities and on certain land facilities”, is to:

“Promote a high level of health, environment and safety in activities covered by these regulations and achieve systematic implementation of measures to meet the requirements and achieve the goals set in health, environment and safety legislation and to further develop and improve the level of health, environment and safety.”

A principle worth mentioning, and also part of Norwegian legislation and mentioned in the framework regulation, is the ALARP (As Low As Reasonably Practicable) principle. Its main objective is to reduce the risk, beyond stated requirements, to a level where further risk reduction can only be performed with unreasonable cost. The ALARP principle is to be applied when requirements have been complied with, and it means that identified risk-reducing measures, exceeding minimum standards, shall be implemented, provided the associated costs are not significantly disproportionate to the risk reduction achieved. An important issue in the ALARP process is that one has to argue when deciding not to implement a suggested risk-reducing measure. The Norwegian regulation has specified a practice in regard to continually assessing risk reduction in daily operations, as described in § 11 in [31].

2.2.2 Technical and operational regulations

Onshore O&G facilities in Norway are bounded by the requirement stated in the “Technical and Operational Regulations” (“Regulations on technical and operational conditions on land facilities in the petroleum activities”) issued by the PSA. The relevant paragraphs related to active and passive fire protection state:

Chapter V: Fire and explosion protection in the design of onshore facilities, section 36 [32]:

“Installation of fixed fire-fighting appliances shall be based on a risk assessment.

Facilities shall be equipped with sufficient manual fire-fighting and firefighter equipment to effectively combat fires and prevent escalation.”

Chapter V: Fire and explosion protection in the design of onshore facilities, section 30 [32]:

“Where passive fire protection is used, this shall be designed such that it provides relevant structures and equipment with sufficient fire resistance as regards load capacity, integrity and isolation properties during a design fire load.

When designing passive fire protection, the cooling effect from fire-fighting equipment shall not be considered.”

Chapter VIII: Planning, operation and control when performing activities, section 58 [32]:

“The responsible party shall ensure that onshore facilities and parts of them are kept intact, so that the required functions are maintained in all phases of the life span.”

Chapter 3

Barriers and Barrier Models

This chapter will give an introduction to the term “risk” and present different barriers and barrier models.

3.1 The concept of risk

Through history, the definition of risk has changed, and there are still some inconsistencies in how risk is defined. Some would define risk as a measure for future loss. Others would describe risk as the combination of probability and the extents of its consequence. On a daily basis, it is common to use risk in the sense of danger and as a potential or possible unwanted incident or loss. PSA defines risk as [33]:

“By risk is meant the consequences of the business with associated uncertainty.”

3.2 Barriers and barrier models

The use of safety barriers as a mitigating measure towards major accidents in the O&G industry has been an established practice for many decades. A barrier can be defined as a:

“system or action with the function to stop or prevent further development of a state (in a negative direction)” [34].

How to define a barrier would also depend on the context; therefore, barriers are divided into three categories:

- Technical barriers.
- Organizational barriers.
- Human and operational barriers.

Hydrocarbon products can create severe damage when handled incorrectly. Fire and explosion protection therefore represents an important part in risk management processes, in both design and operation at oil and gas processing plants. Risk-reducing measures and barrier strategies in

the O&G industry are often based on methods and philosophies to eliminate, prevent, mitigate or reduce the frequency of incidents or the hazard level of the system itself, by identifying the possible hazard, evaluating its risk and recommending appropriate safeguards. Typical safeguards used in the O&G industry could be leak detection, ignition source control, active and passive fire protection, layout, ventilation, spill control, overpressure protection, emergency depressurization, etc. [35].

Barriers can be probability reducing (preventive) or consequence reducing (reactive). There are several philosophies and methods developed on barrier concepts, which give graphic and illustrative overviews of the complex interactions between the different barriers [36]. Commonly used models are the Swiss cheese and the Bow Tie models [36]; see Figure 4 and Figure 5.

The Swiss cheese model consists of several layers stacked side by side, in which multiple layers need to fail, due to every layer representing a new barrier. This could be due to corrosion, malfunction, lack of handover, stressed workforce, etc. All these different circumstances make it possible for the initial hazard to escalate into an accident. This illustrates the principle of multiple barriers of defense lying between the risk and its escalation to an accident. A Swiss cheese barrier model illustration is given in Figure 4, where barrier degradation or malfunction modes are illustrated with black spots: “holes”.

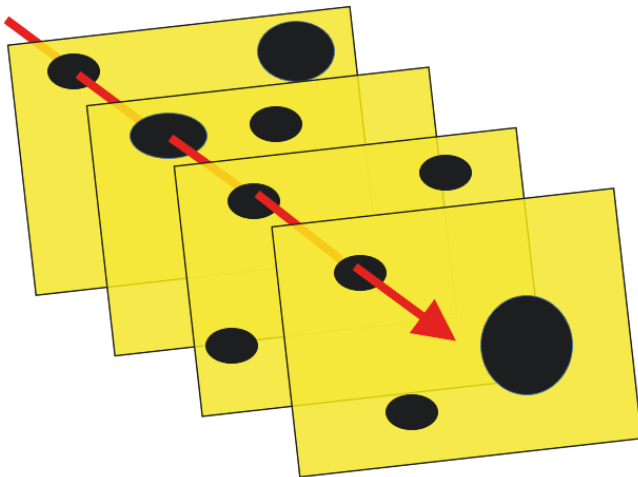


Figure 4 Illustration of a Swiss cheese model [36].

The Swiss cheese model only focuses on preventive barriers, which will mitigate the probability of the top event (accident). In the Bow Tie model, a top event is defined and probability-reducing barriers (on the left side) are implemented in the illustration to prevent the top event from occurring, which is illustrated in the same way as the Swiss cheese model. Consequence-reducing barriers are put on the right side. The top event is chosen based on relevant unwanted scenarios, for example: ignited gas leak or fire. An example of a Bow Tie diagram is given in Figure 5, where the different barriers are illustrated by “black obstructions”. These obstructions may have holes, as illustrated in the Swiss cheese model in Figure 4.

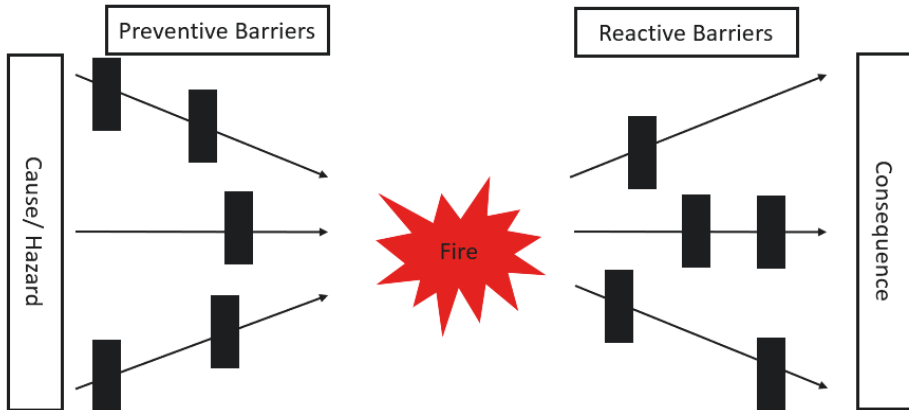


Figure 5 Illustration of a Bow Tie model with top event Fire [36].

NORSOK S-001 [5] defines the following technical barriers for the O&G industry:

- Fire and gas detection system.
- Emergency shutdown.
- Ignition source control.
- Alarm and communication system.
- Emergency power.
- Communication through signs and markings.
- Process safety.
- HVAC (Heating, Ventilation and Air Conditioning).
- Layout and arrangement.
- Active fire protection.
- Passive fire protection.

A given onshore petroleum processing plant shall have functional safety systems, which shall at all times be able to detect abnormal conditions, prevent abnormal conditions from developing into hazards and accident situations and limit the damage caused by possible accidents. The two most relevant barriers for this thesis are active (Chapter 3.2.1) and passive (Chapter 3.2.2) fire protection.

3.2.1 Active fire protection

A process plant has to be divided into fire areas to prevent a hazardous situation from escalating from one fire area to another. Active fire protection is regarded as a risk-reducing measure, which is expected to reduce the consequence by preventing escalation. After ignition, active fire protection systems are regarded as a first line of defense. Such systems, together with manual fire intervention (if considered safe for the firefighters), shall be able to handle the largest dimensioning fire scenario in each fire area.

Fire water is not recommended as an extinguishing media for low flash point liquids, but it is widely used throughout the O&G industry for fire control and exposure protection.

Foam systems are a more effective extinguishing media for low flash point substances and are mainly used against liquid fires. Foam systems can have a good extinguishing effect. Extinguishing with foam will cool the fire and form a coating, covering the fuel and preventing any ingress of oxygen, resulting in suppression of the combustion. However, the throw length is limited, due to foam composition and weather conditions, etc. On land sites, requiring considerable coverage, one must have large droplets (water without additives) to reach heat exposed areas, to cool any exposed equipment, load-bearing structures, etc.

The main purpose of active fire protection systems, such as deluge, foam and monitors, is to provide quick and reliable means for preventing/delaying further escalation, by reducing heat radiation, convection, etc. In addition, active fire protection systems may be used to mitigate explosion effects, as investigated in [37].

Deluge systems are normally considered the first choice of equipment and structural protection, compared to other active fire protection barriers. The central strategy of deluge systems is divided into two main principles: Fire extinguishment/suppression and cooling.

There are in principle four types of active fire protection [14]:

- Active fire protection designed to provide dedicated coverage and protection of critical equipment.
- Active fire protection designed to provide area protection to a non-specific coverage.
- Structural protection.
- Water/spray systems to reduce thermal radiation and smoke control.

Fire water monitors are often used if traditional deluge systems are not suitable. The monitors have a high-water flow capacity and high momentum, giving long throw lengths. Fire water monitors are often set in an oscillation mode. Thereby, the monitor coverage area is quite significant. Recently, most hydrocarbon processing plants in Norway have refurbished the fire water monitors to make them remotely operated.

3.2.2 Passive fire protection and thermal insulation

The purpose of passive fire protection is to ensure that relevant structures, piping and equipment components have adequate fire resistance, with regard to load-bearing properties, integrity and insulation properties during a dimensioning fire. However, the use of PFP could result in reduced inspection possibilities, which could lead to an increased leak frequency, due to unidentified corrosion under insulation (CUI) and congestion, as previously mentioned.

For fire protection of pipes and vessels, etc., numerous concepts for PFP can be used to ensure proper protection [38]:

- Mortar-based coating.
- Intumescent coating.
- Sublimation coating.
- Mineral fiber matting.
- Earth mounds.

PFM based on coating is normally sprayed onto the surface. A reinforcing glass fiber scrim or steel wire gauze is applied, to avoid cracking and peeling of the coating under fire exposure and to provide additional strength, in order to increase resistance to the impact of high-pressure jet fires. The fire protective coating is further safeguarded by a weather-protective top layer. The resistance performance of the coating is dependent on the thickness [38]. Fiber matting systems consist of fireproof mineral fiber, covered with a protective stainless steel cladding. The protective resistance of the system is provided by the low heat conductivity of the insulation mat.

Earth mounds are commonly used in the liquefied petroleum gas industry, where vessels are either fully or partially buried. The presence of the earth mound effectively prevents a fire from developing around the protected vessel [38]. It should also be mentioned that, for land sites, cables are generally laid down into sand-filled concrete-covered trenches and into the substations from below, thereby ensuring protection against fire, as well as providing mechanical protection.

After 20+ years of servicing of O&G installations, inspection has shown that it is necessary to perform maintenance and rehabilitation of process equipment [39]. The servicing of the O&G industry also gives valuable learnings in regard to the long-term effect of deterioration and weathering on passive fire protection. The study concluded that there was little change in fire resistance, as determined through both furnace and jet fire tests [39].

There are some general recommendations to avoid the use of PFM, if possible [14], due to reduced access possibilities for inspection and maintenance, increased weight, increased spacing, increased cost, etc.

These concerns highlight that PFM in some situations may lead to increased leak frequencies and increased congestion, which could result in increased fire and explosion risk.

3.2.3 Other protective barriers

NORSOK S-001 [5] and ISO 13702 [6] define the principles and requirements for the development of safety design and emergency preparedness, to establish and maintain an adequate level of safety for personnel, environment and material assets. Both standards describe different barriers, their roles, interfaces, required utilities, and functional and survivability requirements.

In addition to active and passive fire protection, other barriers, such as fire relief valves, depressurization, ignition source control and layout, are used. A depressurization system is installed in order to reduce the pressure and to vent its content to a safe location, if the system experiences a leak, is exposed to a fire or due to maintenance. Reducing the pressure will minimize the material stress, hence reducing the risk of rupture of the equipment when heated by a fire. The reduced pressure will also reduce the leak rate and the duration of a potential leak. This will also limit the consequence of fire, if the leak is ignited. Depressurization can also be used to reduce the pressure when conducting maintenance. The depressurization system is often designed in accordance with API Std 520, Part 1 [40] and API Std 521 [41], which implies that the depressurization should be able to reduce the pressure to 6.9 barg or to 50% of the design pressure, whichever is lowest, within 15 minutes. Normally, depressurization is therefore applied in combination with PFM, to avoid escalation of the jet or pool fire, before sufficient

depressurization is achieved. The combination of PFP and depressurization could be essential, due to the fact that the expected time to rupture, when fire-exposed, could be as low as a couple of minutes for smaller pipes and flanges. Time to rupture could, in many cases, be even before the depressurization is initiated.

Another effect during depressurization is the flow of gas/liquid, with the resulting cooling effect to the inside of the pipe/vessel, due to expansion and fluid transport. This effect may be accounted for in thermal calculations, but it will obviously not be present until the depressurization is activated [11]. Depressurization will either prevent a possible rupture or ensure less severe consequences.

Pressure safety valves (PSVs) are provided to protect against overpressure in the case of process upsets or fires. The PSV's job is to relieve the pressurized fluid during a fire, in the case of a blocked outlet or other scenarios which could lead to over-pressurizing the system. The purpose could also be to relief gas which is expanding due to heat input or relief the expanding liquid for a 100% liquid-filled system [11]. There are, however, some recorded incidents, where rupture of a pressure vessel or pipe occurred before the PSV opened. This is related to a situation where the heat transported into the gas is low compared to the heat transfer to the wall material, resulting in a high temperature increase in the wall material [14].

The most effective way of preventing fires and explosions is to avoid the development of flammable mixtures, i.e. to prevent loss of containment. Should combustible products be released, and flammable mixtures develop, the ignition probability should be minimized, rendering potential ignition sources harmless. This is the intended role of an ignition source control system (ISC). The layout of an O&G plant should be designed to reduce the probability and consequences of any accidents through, e.g., the location, separation and orientation of production areas, equipment and functions, should an ignition occur.

Chapter 4

Fire Dynamics and Fire Testing

This chapter will describe the motivation for the choice of fire scenarios and acceptance criteria, as well as general fire dynamics theory.

4.1 General definitions

Fire is a rapid oxidization of a material, in exothermal chemical processes, releasing heat, various soot, reaction products and light. Combustion is a complicated process, consisting of a series of chemical reactions. Free radicals and chain reactions between ions, atoms and molecules play a crucial role in the chemical reactions that take place inside the combustion zone of a fire. We call these chain reactions. In addition, there must be three other conditions present to get a fire; oxygen, fuel and heat. These four basic assumptions are referred to as a fire tetrahedron, which is illustrated in Figure 6.

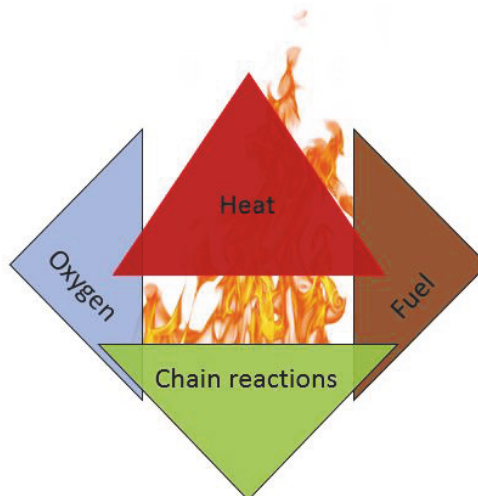


Figure 6 Fire tetrahedron [42].

In the case of a fire, the exothermic chain reaction sustains the fire and allows it to continue until at least one of the described conditions of the fire tetrahedron is removed.

Usually, hydrocarbon fires in the O&G industry are divided into two types:

- Pool fires (liquid).
- Jet fires (could be both gas and liquid).

A pool fire is defined as a combustion of flammable or combustible fluids spilled and retained on a surface, while a jet fire is defined as an ignited release of pressurized, flammable fluids [14]. A jet fire is characterized by its high erosive forces. The behavior of a jet fire depends on e.g. fuel composition, release conditions, leak rate, release geometry, direction of the release and ambient conditions such as wind. Low-velocity two-phase releases of condensate can produce “lazy”, wind-affected, buoyant, sooty and highly radiative flames. Sonic releases of natural gas can produce very high-velocity fire plumes that are initially less dominated by buoyancy, less sooty, with flames of a lower emissivity.

Due to their size and fire plume characteristics, industrial pool and jet fires usually give high convective and radiative heat flux levels. Typical heat flux levels in design accidental loads for industrial pool or jet fires are given in Table 1 [14].

Table 1 Incident heat flux levels for fuel-controlled fires

| | Jet fire | | Pool fire |
|--------------------------|--|--|-----------------------|
| | For leak rates $\dot{m} > 2 \text{ kg/s}$ | For leak rates $\dot{m} > 0.1 \text{ kg/s}$ | |
| Local peak heat load | 350 kW/m ² | 250 kW/m ² | 150 kW/m ² |
| Global average heat load | 100 kW/m ² | 0 kW/m ² | 100 kW/m ² |

The heat flux levels given in Table 1 are based on observed heat flux levels obtained from numerous experiments, as well as CFD simulations, and are defined as the heat flux levels transmitted to an object of 20 °C. The heat flux is expected to vary during the fire duration, and the values presented are used as average incident heat flux. No effect of active firefighting has been included in the heat flux values.

The local peak heat load, which is the highest heat flux level, is used for rupture calculations of the pressurized pipe or exposed equipment. The global heat load is typically used to calculate the effect on pressure development inside the exposed object, which gives valid information regarding dimensioning of PSVs.

4.1.1 Gas release rate

Usually the production pressures are at least two times the ambient pressure. The gas is then released at the sound of speed for the particular gas being released. Sonic gas release rates can be calculated as a function of pressure drop over a release opening, as given by Equations (1)-(3) [43].

$$q_s = C_d A_h \Psi \sqrt{\rho_0 P_0 \gamma (2/(\gamma + 1))^{\frac{\gamma+1}{\gamma-1}}} \text{ (kg/s)} \quad (1)$$

where

$$\gamma = C_p / C_v \text{ (-)} \quad (2)$$

where C_d (-) is the discharge coefficient, A_h (m²) is the opening cross-section area, Ψ (-) is the flow coefficient, ρ_0 (kg/m³) is the initial density, P_0 (N/m²) is the initial gas pressure, γ (-) is the specific heat ratio, C_p (J/kg K) is the specific heat at constant pressure, and C_v (J/kg K) is the specific heat at constant volume.

The release flow rate will be greatest at the beginning when the pressure is highest, i.e. highest gas density. A reduction in pressure and density will result in a decrease in mass flow.

$$P = P_0 \left(\frac{M}{M_0} \right)^\gamma \text{ (N/m}^2\text{)} \quad (3)$$

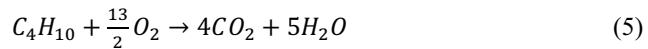
where M_0 (kg) is the initial mass and M (kg) the current mass.

$$\rho = P / (R_{gas} T) \text{ (kg/m}^3\text{)} \quad (4)$$

where R_{gas} (J/kg K) is the universal gas constant and T (K) is the temperature.

4.1.2 Basic fire dynamics

The equation for stoichiometric combustion of butane is given in Equation (5). Explosions are often most intense at/or right above the stoichiometric mixture (rich mixture) [44]. If a flammable gas mixture occurs and the fuel to air ratio is decreased or increased, then the composition will reach a composition where it is no longer able to propagate a flame. For butane, the lower flammability limit is 1.6 volume % and the upper flammability limit is 8.4 volume %. It is only between these limits that the butane gas can ignite at ambient temperatures.



The heat of combustion ΔH_c (kJ/mol) can be defined as: The heat evolved when 1 mol of a substance burns completely in oxygen at standard conditions. The heat of combustion for butane is given by Equation (6).

$$\Delta H_c = \sum \Delta H_f(p) - \sum \Delta H_f(r) \quad (6)$$

where ΔH_f (kJ/mol) is the heat of formation for products (p) and reactants (r). The heat of combustion for butane is -2755.5 kJ/mol.

4.2 History and background of fire testing

The development of the First Law of Thermodynamics and the discoveries of the "thermoelectric effect" led to the creation of apparatus for calorimetry, providing for the

measurement of temperatures and heat flux levels. The next revolution in measuring and understanding fire occurred in the early twentieth century, with worldwide recognition that scientifically and rule-based fire standards were needed to protect life and property [45]. During the same period, engineering innovation developed electromechanical equipment that could record data measured from fire experiments. This advancement in data logging allowed for more detailed studies of measured fire behavior. The third major advancement in fire testing occurred in the last half of the twentieth century, with the development of affordable data-logging equipment and computers that improved data analysis, as well as the development of empirically based predictive models [45]. Technology and computational methods have opened the theoretical world of fire science, which provides insight into the subtle features of fire dynamics and provides a means for developing a greater understanding of fire test method performance [45].

During the 1980s, it became apparent that the previously developed wood product fire tests were not appropriate. It was observed that jet fires exposed engulfed objects to much more severe heat flux levels. A jet fire test task group was assembled in March 1992, as it was shown that key conditions typical for large-scale jet fires could be reproduced at a smaller scale [12].

The task group's objectives were to examine the available industrial data regarding jet fires and to work with the industry to develop a standard jet fire procedure for certification of passive fire protection materials. The report produced by this group was published in 1995 [12]. In general, the selected solutions were demonstrated to give sufficient resistance to hydrocarbon pool fires [12, 39].

The traditional jet fire test is presented in ISO 22899 [27], which describes a method for testing passive fire protection materials exposed to a jet fire. The test aims to simulate the thermal and mechanical exposure towards the passive fire protection material under a large-scale jet fire, resulting from high-pressure propane gas releases. Propane is used as fuel, due to its high propensity to form soot, compared to natural gas, and therefore to produce a flame of higher luminosity, i.e. higher emissivity. The nozzle is aligned horizontally and aimed at the test specimen at a distance of 1 m, i.e. additionally exposing the specimen to high erosive forces. The jet fire test consists of a jet fire with a rate of 0.3 kg/s propane gas, corresponding to an approximately 14 MW sonic release of gas, aimed into a shallow chamber, with the object of producing a fireball with an extended tail. The flame thickness is thereby increased, hence increasing the heat radiation to the test specimen.

To gain a better understanding of the risk-reducing effect of safety measures, different standards and standardized test concepts are used. For instance, fire testing is usually done in standardized furnaces that are fired according to a given temperature time curve. An example is structural building elements, tested in furnaces fired in accordance with the ISO 834 temperature time curve [46]:

$$T = 20 + 345 \cdot \log_{10}(8 \cdot t + 1) \text{ (}^\circ\text{C)} \quad (7)$$

where t (minutes) is the exposure time. Oil and gas fires are expected to quickly result in very high flame temperatures. The standardized hydrocarbon (HC) test curve developed by the Norwegian Petroleum Directorate is therefore different from the ISO 834 temperature time curve and is given by [47]:

$$T = 20 + 1080 \cdot (1 - 0.325 \cdot e^{-0.167 \cdot t} - 0.675 \cdot e^{-2.5 \cdot t}) \text{ (}^\circ\text{C)} \quad (8)$$

It should be noted that there are also other temperature time curves for less severe fire exposure situations, e.g. façade fire exposure and more severe hydrocarbon fire exposure, such as the French HydroCarbon Modified (HCM) curve. The latter one was developed as a result of several full-scale fire tests, where temperatures well in excess of 1100 °C were recorded. The HCM curve is given by [48]:

$$T = 20 + 1280 \cdot (1 - 0.325 \cdot e^{-0.167 \cdot t} - 0.675 \cdot e^{-2.5 \cdot t}) \text{ (}^\circ\text{C)} \quad (9)$$

The three standard temperature time curves are shown in Figure 7.

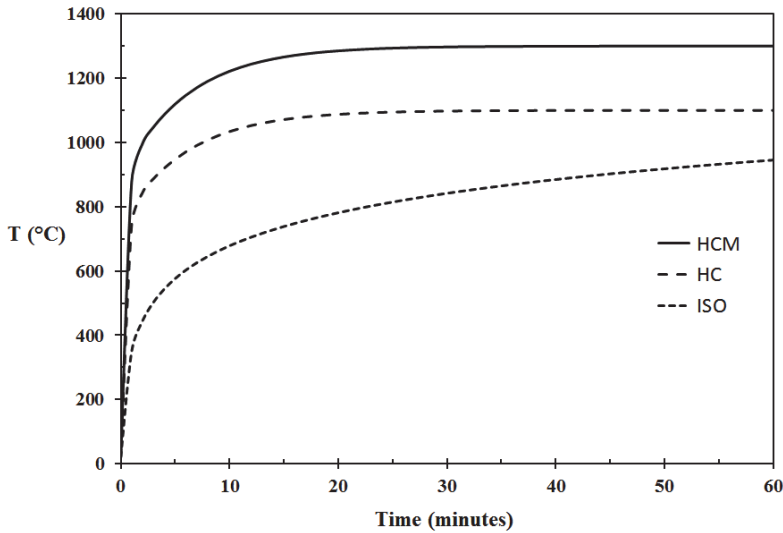


Figure 7 Fire testing temperature time curves.

The reason for jet fires giving more severe heat exposure is due to the higher speed of the combustion products, giving a higher convective heat transfer coefficient, as well as the increased turbulence level, resulting in cleaner burning and higher flame temperatures. Jet fires are also in general more erosive.

NORSOK S-001 [5] argues that, in heat exposure calculations, the total heat flux level should be set to 250 kW/m² for pool fires and 350 kW/m² for jet fires; ref. Table 1. The oil and gas companies have therefore recently started specifying 250 kW/m² for pool fires and 350 kW/m² for jet fires, e.g. the Equinor requirements for new installations, TR2237 [49]. For heat transfer calculations, this technical requirement recommends a convective heat transfer coefficient of 100 W/m² K, flame emissivity unity and steel emissivity 0.85. Flame temperatures of 1050 °C and 1200 °C then correspond, respectively, to 250 kW/m² and 350 kW/m² for an object at 20 °C.

The radiant heat flux that is absorbed by an exposed object is a function of the temperature and emissivity of the receiving surface, as well as the emissivity and temperature of the flames. The net heat flux received by an object fully engulfed in flames is given by:

$$\dot{Q}_{net}'' = h(T_f - T_s) + \varepsilon_f \sigma T_f^4 - \varepsilon_s \sigma T_s^4 \text{ (W/m}^2\text{)} \quad (10)$$

where h (W/m K) is the convective heat transfer coefficient, T_f (K) is the flame temperature, T_s (K) is the temperature of the exposed surface, ε_f is the emissivity of the flames, ε_s is the emissivity of the solid and σ ($5.67 \cdot 10^{-8}$ W/m² K⁴) is the Stefan-Boltzmann constant. The emissivity of the flames is given by:

$$\varepsilon_f = 1 - \exp(-KL) \quad (11)$$

where K (1/m) is the extinction coefficient and L (m) is the optical flame thickness. Due to the potential size of fires in the oil and gas industry, it is common to assume that the flames are optically thick, i.e. the emissivity is unity.

4.3 Heat transfer

Due to its relevance to this thesis, basic theory regarding heat transfer will be presented in this chapter. Heat transfer is basically the transport, exchange and redistribution of thermal energy. There are three forms of heat transfer: convection, radiation and conduction. For the relevance of this thesis, the dominant heat transfer mechanisms are radiation and convection.

4.3.1 Convection

Heat transfer by convection occurs when a flame or hot combustion products come into contact with other objects. Convection can be described as heat transfer to or from a body by the motion of a fluid, as given by Equation (12):

$$q'' = h\Delta T \text{ (W/m}^2\text{)} \quad (12)$$

where h (W/m K) is the convective heat transfer coefficient and ΔT (°C) the temperature difference.

4.3.2 Radiation

All objects with a temperature above absolute zero, i.e. temperatures above 0 K, emit heat radiation, as described by Equation (13):

$$q = A\varepsilon\sigma T^4 \text{ (W)} \quad (13)$$

where σ ($5.67 \cdot 10^{-8}$ W/m² K⁴) is the Stefan-Boltzmann constant, A (m²) is the area of the emitting body and ε the emissivity (-). Examples of emissivities are given in Table 2 [50].

Table 2 Emissivity of different materials [50]

| Material | Emissivity (-) | Temperature (°C) |
|--------------------------|----------------|------------------|
| Aluminum highly polished | 0.04–0.05 | 1 |
| Wood beech | 0.91 | 70 |
| Steel plate rough | 0.94–0.97 | 40–540 |
| Steel polished | 0.07 | 40 |

4.3.3 Conduction

Conduction occurs by atoms and molecules with different kinetic energy influencing each other. Heat transfer in form of conduction occurs when heat flows from the higher temperature region to the colder temperature region. The heat flux is given by:

$$q'' = k \frac{\Delta T}{\Delta x} \text{ (W/m}^2\text{)} \quad (14)$$

where k (W/m K) is the thermal conductivity and $\frac{\Delta T}{\Delta x}$ (K/m) is the temperature gradient. Materials with high thermal conductivity conduct heat well, while materials with low thermal conductivity are poor heat conductors. Some examples of thermal conductivities are given in Table 3.

Table 3 Examples of thermal conductivities for different materials [51]

| Materials | Thermal conductivity (W/m K) |
|--------------------|------------------------------|
| Aluminum | 170 |
| Stainless steel | 15 |
| Air | 0.026 |
| Thermal insulation | 0.041 |

The thermal diffusivity is defined as the ratio between thermal conductivity and volumetric heat capacity.

$$\alpha = \frac{k}{\rho c_p} \text{ (m}^2\text{s}^{-1}\text{)} \quad (15)$$

Large thermal diffusivity means that a temperature wave distributes quickly within the given material. Some examples of thermal diffusivities for common substances are given in Table 4.

Table 4 Examples of thermal diffusivity for some selected materials [52]

| Materials | Thermal diffusivity (m ² /s) |
|---------------------------|---|
| Aluminum | $9.7 \cdot 10^{-5}$ |
| Stainless steel, AISI 310 | $3.35 \cdot 10^{-6}$ |
| Air 27 °C | $1.9 \cdot 10^{-5}$ |

Specific heat is the amount of heat required to raise the temperature per unit mass. The specific heat of aluminum and stainless steel (AISI 316) is given in Figure 8.

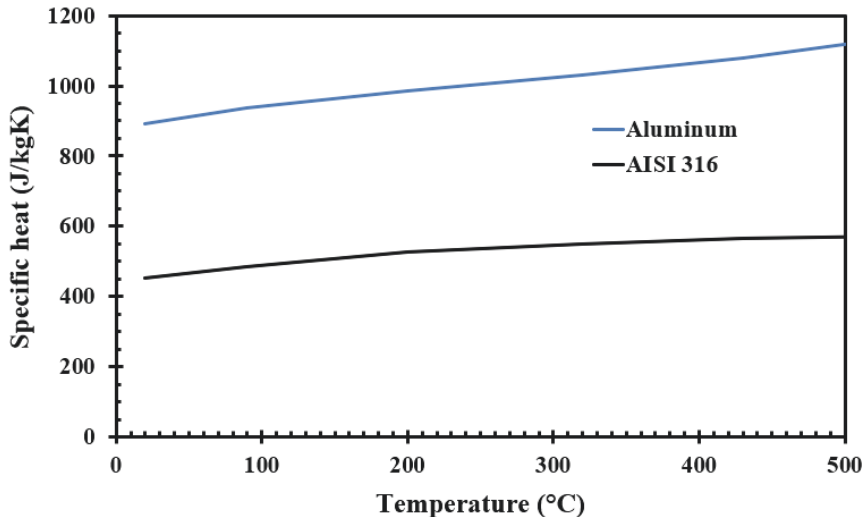


Figure 8 Specific heat [53].

4.4 Water droplet properties and physics

Evaporation processes are of interest in numerous areas, such as agricultural [54], industrial [55], and academic [56] communities, as well as for individuals [57]. When evaporating at room temperature, the substrate material plays an important role in the evaporation process, as does the ambient air relative humidity [58]. However, the ambient air relative humidity is less important when droplets evaporate on substrates at elevated temperatures [59]. In a recent study of a wide range of water droplet sizes in the transition regime of a boiling crisis, Misyura [60] demonstrated that several material parameters are important when water droplets hit objects, wet the surface in different ways, and then start evaporating. Droplet contact angles play a role [61] and may depend on impurities, additives, etc. Additives may therefore be used to reduce surface tension and thus improve performance [62-63]. Some researchers have studied the behavior of different droplet parameters, such as size, impinging velocity [64], water droplet velocity, wall material [65-66] temperature below the Leidenfrost temperature [67], and the influence of solid-liquid contact time [68]. A review concerning droplets impinging onto hot metals was conducted by Liang and Mudawar [16] for all the involved boiling regimes for water droplets on metal surfaces. A literature review on the Leidenfrost temperature for water on different heated materials is given by Bernardin and Mudawar [69]. Water droplet cooling efficiency for droplets hitting Teflon-covered copper was recorded by Sawyer et al. [70], who reported a cooling efficiency in the range of 50% to 90% at temperatures up to those associated with a boiling crisis, i.e. the temperature at which heat transfer to the evaporating droplet is at the maximum.

The boiling regimes for water as a function of substrate temperature are shown in Figure 2. At ambient pressure, relative humidity below 100%, and temperatures below the boiling point,

water droplets evaporate by mass diffusion [58]. Boiling starts when the surface temperature is just above 100 °C, i.e. typically 104 °C [71]. At this temperature, bubble formation within the saturated fluid starts and results in very slow boiling. The involved mechanism is called nucleate boiling. For a metal surface at 104 °C, the heat flux to a sessile water droplet is limited. Increasing the metal surface temperature increases the heat flux until it reaches a maximum, i.e. the critical heat flux (CHF), also called boiling crisis, as shown in Figure 2. Beyond this temperature, increasing the surface temperature reduces the heat flux, due to a vapor film partially forming below the droplet. This boiling regime is called transition boiling and is characterized by violent sizzling and droplet breakup. Further increasing the temperature induces a stable vapor film below the droplet. Thereafter, the heat flux from the hot surface to the levitated droplet increases slightly with increasing surface temperature, due to the increasing temperature difference between the hot surface and the levitated droplet. The starting temperature for this final boiling regime is called the Leidenfrost temperature [23-24].

4.4.1 Droplet breakup

How a falling water droplet is affected by the air is traditionally analyzed by the dimensionless Weber number. The Weber number relates the surface tension of the droplet to the aerodynamic forces exerted by the ambient gas. The Weber number is given by [72]:

$$We = \frac{\rho_a v^2 D}{\sigma} (-) \quad (16)$$

where ρ_a (kg/m³) is the droplet density, v (m/s) the droplet impinging speed and σ (N/m) the surface tension.

Much work has been done on this topic, and it is shown that different breakup regimes have been characterized in the Weber number range in which they occur. There is, however, a lack of consistency in the available research, as shown by the review conducted in [73], presented in Figure 9.

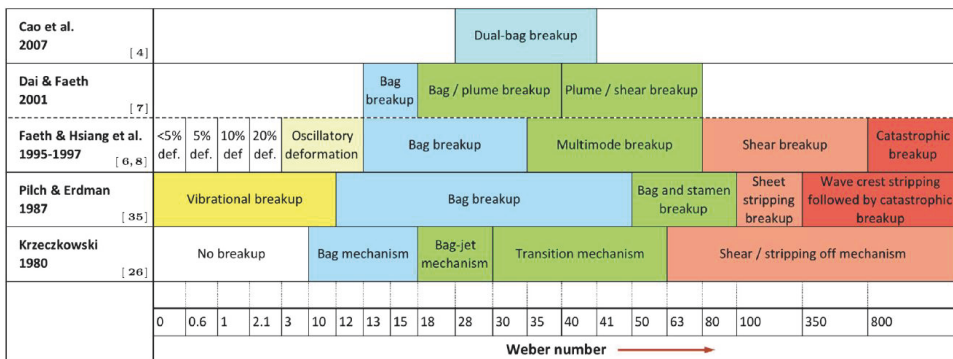


Figure 9 Breakup modes in terms of the Weber number according to different sources [73].

It has been suggested [72] that fluid viscosity can affect droplet breakup. The dimensionless Ohnesorge number (Oh) includes the viscosity:

$$Oh = \frac{\mu_d}{\sqrt{D\rho_d\sigma}} (-) \quad (17)$$

where μ_d (Pa s) is the viscosity.

4.4.2 Water droplet impact velocity

For water droplets released at zero speed, the impact velocity for the cooling efficiency experiment, the impingement velocity, is calculated by:

$$v = \sqrt{v_0^2 - 2g\Delta h} \text{ (m/s)} \quad (18)$$

where v_0 (m/s) is the initial velocity, Δh (m) is the fall height and g (m^2/s) is the acceleration of gravity. In the present study, the initial velocity was zero.

At an increasing fall height, the impinging droplet will approach a constant velocity, i.e. the terminal velocity. The terminal velocity was not met in any of the droplet experiments in the present study.

Chapter 5

Experimental Work

In this chapter the experimental work is presented. The first part presents the water cooling experiments and the second part presents the small-scale jet fire tests.

5.1 Water droplet cooling experiments

Verification and presentation of the setup and experimental work on water droplet cooling are outlined in detail in [17].

5.1.1 Experimental setup

Stainless steel (AISI 316) and aluminum (EN AW-6082) were the selected metals to verify the experimental setup. These metals have room temperature thermal conductivities of about 15 W/m K and 170 W/m K, respectively. The arithmetical mean roughness (Ra) used for both discs was Ra 0.4 (polished/smooth surface) and Ra 3, as defined by [74]. Discs of 50 mm diameter and 10 mm thickness (Figure 10) resulted in convenient cooling rates, with and without water cooling. The disc surface emissivity was stabilized by successive complete measurement cycles prior to the measurements reported in the present work. This treatment ensured no influence of this parameter within a measurement series.

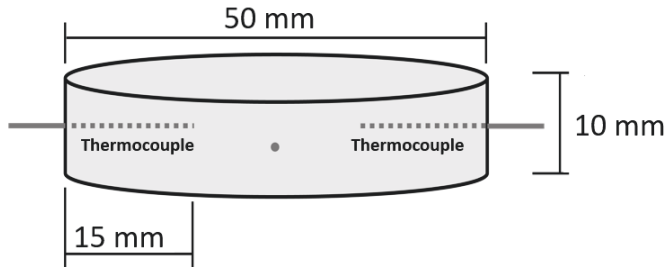


Figure 10 Sketch of metal disc with four inserted type K mantle thermocouples (with 1.6 mm diameter) at 90° horizontal separation.

Ideally, there should be as few heat losses as possible to a fixture keeping the disc in position. Thin metal rods for supporting the disc were considered. This led to the decision to combine disc support with temperature recordings, i.e. to suspend the disc by four standard 1.6 mm diameter type K (chromel–alumel) mantle thermocouples, as shown in Figure 10. This solution minimized contact between the disc and neighboring objects. It was decided to have a disc diameter that could be quite evenly preheated by a Bunsen burner prior to the experiments, without introducing major temperature gradients. If temperature gradients did result from the preheating, they should have time to spatially even out between the preheating and the start of the experiments. A diameter of 50 mm was found to be convenient in this respect.

The measurements of the disc cooling without, and with, water droplet cooling relied on exhausting the heat stored in the disc after the preheating. The disc thickness therefore had to be selected such that it allowed for a convenient time period for temperature recordings in both these cases. By trial and error, it was found that a disc thickness of 10 mm resulted in a proper cooling time, both without and with droplets impacting onto the disc.

The disc was aligned to the desired angle with a leveler and heated to about 430 °C prior to the measurements, as shown in Figure 11. The heater was then removed, and the disc was allowed to cool to 410 °C, ensuring time for the internal temperature gradients to spatially equilibrate prior to each measurement. The disc temperatures were recorded at a frequency of 1 s⁻¹ by a data logger (National instruments NI cDAG-9184, Austin, TX, USA).

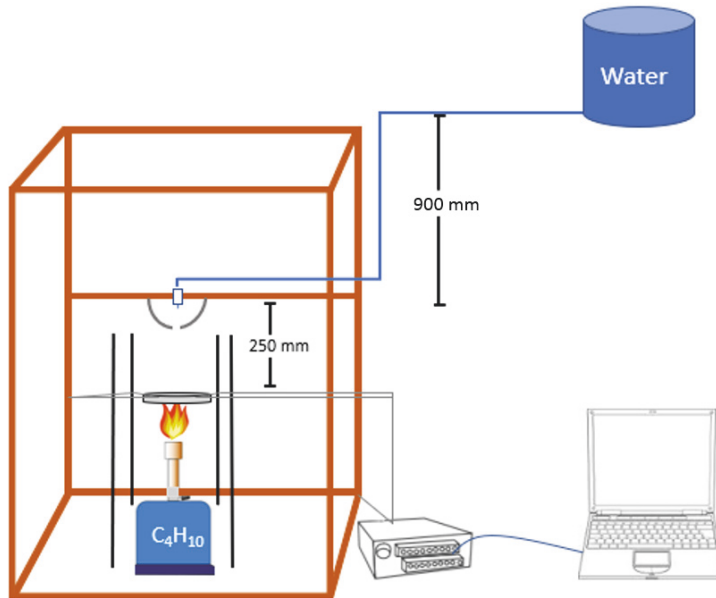


Figure 11 Sketch of the experimental setup (not to scale).

Water droplets were formed at the tip of medical stainless steel hypodermic infusion needles. The arrangement included flow regulation, thereby allowing the droplet rate to be regulated to obtain a particular flow rate. This simple injection needle system performed well and represented an ultimate low-cost droplet generator, which has also been used by other researchers [67]. The water droplets detached due to gravity.

Prior to and after each water-cooling measurement, 20 droplets were generated from the arrangement and collected in a small laboratory dish. The mass of the 20 droplets was determined using a balance (AG204DR METTLER TOLEDO, Columbus, Ohio, USA). Thus, the mass of the individual droplets was determined. The droplet diameter was calculated based on the assumption of a spherical droplet shape. Very low variation was observed in the collective mass of the succeeding 20 new droplets that were weighed when checking for reproducibility.

In laboratories, the ventilation currents may disturb experiments significantly. Inspired by Log and Heskestad [75], who studied small-scale fire plumes, the influence of air ventilation was minimized, as well as the influence of personnel movements. This was done by making an open wood frame, 1.1 m × 0.55 m × 1.55 m height, and covering it with a fine mesh screen. A simple roll-up door was made to give access to the interior for setting up experiments, heating the discs, etc. The principal setup is shown in Figure 11.

For more information regarding the experimental setup and verification, see [17].

5.1.2 Setting up and performing the experiment

Prior to every experiment, the metal disc was cleansed with acetone, positioned in the test rig and leveled. The temperature and humidity of the laboratory atmosphere were recorded before and after each measurement series.

For the baseline experiments, the Bunsen burner was placed under the disc and used to heat the disc to approximately 430 °C. The measurement, as such, started when the disc had cooled to 410 °C and continued to disc temperatures of about 80 °C. The experimental setup is shown in Figure 11.

In addition to use both aluminum (EN AW-6082) and stainless steel (AISI 316) metal for the discs, Figure 12 presents the altered parameters for the droplet cooling experiments.

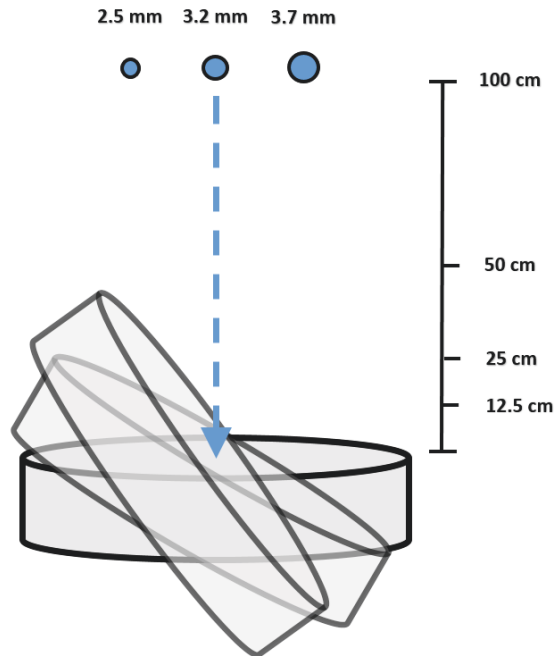


Figure 12 Altered parameters for the water droplet cooling experiments.

The droplet interval was monitored throughout the droplet experiment, and the mass flow was checked prior to and after each experiment. All excess water was removed after each experiment. A photo of the experimental setup is given in Figure 13.

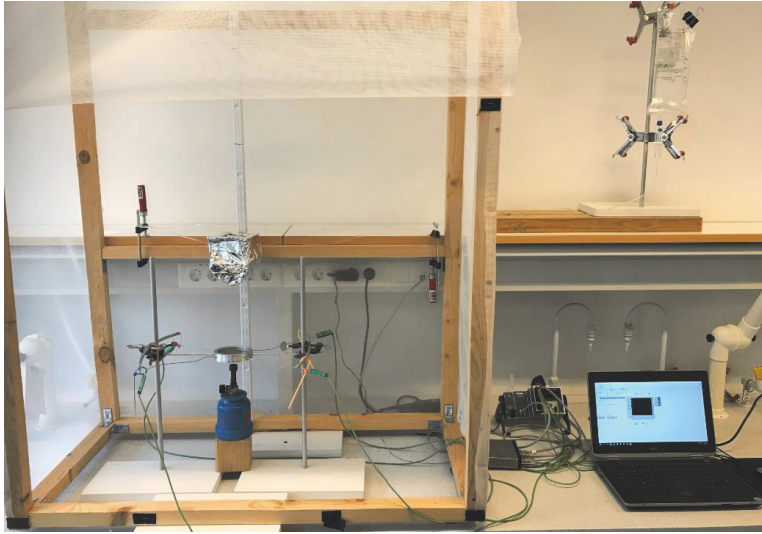


Figure 13 Experimental setup for droplet cooling experiments.

5.1.3 Determining water droplet cooling efficiency

The temperature versus time during disc cooling, with and without impinging water droplets, was recorded for disc temperatures in the range 85–400 °C. Based on the differences in cooling rates between dry- and wet-cooling, disc mass, and specific heat, the heat flow to the impinging water droplets was calculated.

Subtracting the respective temperature versus time derivatives for the given temperature gives the net water droplet disc cooling rate, i.e. $\left\{\frac{dT}{dt}\right\}_{\text{Net}}$ (K/s). Knowing the mass, m (kg), and the specific heat, $C_P(T)$ (J/kg K), of the disc as a function of temperature, the water droplet cooling heat flow may be calculated by:

$$\dot{Q}_{\text{Drops}}(T) = m_{\text{Disc}} \cdot C_P(T) \cdot \left\{\frac{dT}{dt}\right\}_{\text{Net}} \quad (\text{W}) \quad (19)$$

The heat flow that is needed to evaporate the droplets at a rate of \dot{m}_{Drops} (kg/s) is given by:

$$\dot{Q}_{\text{Max}} = \dot{m}_{\text{Drops}} \cdot \Delta H_{\text{vap}} \quad (\text{W}) \quad (20)$$

where ΔH_{vap} (2571 kJ/kg) represents the enthalpy needed to heat water droplets to 100 °C and water vaporization at 100 °C. The relative droplet cooling efficiency was then calculated by:

$$\xi = \dot{Q}_{\text{Drops}} / \dot{Q}_{\text{Max}} \quad (21)$$

5.1.4 Influence of surfactants on droplet cooling efficiency

The influence of additives and inclination was studied in the fourth paper. An aluminum disc with smooth surfaces (Ra 0.4) was used for the water droplet experiments with additives. The

choice of a material with high thermal conductivity was made, in order to obtain results with less scattering [17]. When assessing surface roughness, the expected steam layer thickness, keeping the droplets levitated at temperatures above the Leidenfrost temperature, is an essential parameter. Using computational methods, Chatzikiyriakou et al. [76] showed through their research, for a sessile water drop, that the vapor layer exhibits oscillatory behavior. However, it eventually settles to a thickness between 20 and 40 μm , which is supported by the theoretical value of 28.9 μm obtained by Wachters et al. [77] for similar drop conditions. It was further shown in [16, 60] that there is some contradiction in regard to surface roughness effect on heat transfer for the transition and film boiling regime.

This contradiction may be related to the fact that some heat transfer dependencies are valid in a certain temperature range. Additionally, surface patterns giving similar Ra values may influence the flow conditions below the droplet differently. The choice of a smooth surface (Ra 0.4) was made based on the discrepancies in the literature as to the effect of surface roughness on cooling efficiency. Focusing on smooth surfaces (Ra 0.4) when studying the influence of additives eliminated such issues.

Further details are given in papers [17, 19].

5.1.5 Main conclusion from the water droplet efficiency measurements

The reported low film boiling regime cooling efficiency for pure water, as well as for 35 g/kg NaCl solution, 300 ppm and 700 ppm acetone solutions, demonstrates the importance of activating fire water deluge or monitors early, in the case of an industrial fire. Otherwise, it may be very difficult to cool exposed pipes, equipment and structural members. Due to the low cooling efficiency, late activation of fire water will have a limited effect on metal temperatures at and above the respective metal's Leidenfrost temperatures. Overall, the additives only marginally improved the water droplet cooling efficiency.

It may therefore be concluded that the standard industrial water application rate (i.e., 10 L/min·m²) is insufficient, compared to the heat fluxes expected in industrial pool and jet fires.

5.2 Fire resistance in thermal insulation

Verification and presentation of the experimental work for the small-scale jet fire testing and the experimental mockup are given in detail in [13].

5.2.1 Experimental setup

An experimental test was assessed as the most appropriate method for verifying the fire resistance of the representative industrial thermal insulation. Due to the number of parameters exerting influence on the test's severity, it is not sufficient to, e.g., define 1100 °C recorded by a thermocouple as the target of the flame temperature. Test configuration, heat losses, etc. also need to be considered. Testing in a situation that is similar to the real fire is appealing, i.e. where a fire exposes the equipment to be tested.

Distillation columns are often quite large structures, i.e. diameter 4 m and height 20–25 m. When considering a wall thickness that is only a small fraction of the column diameter, i.e. 16 mm to 4000 mm, the heat flow into the system may be considered one-dimensional. The small-scale testing could therefore also be one-dimensional with respect to the direction of the heat flow, i.e. the vertical (z) orientation in the test configuration. Regarding the horizontal direction during testing, a radial configuration is very convenient, given a cylindrical burner located at radius zero. Arranging the cylindrical propane fire source vertically, i.e. in positive z -direction, and exposing a horizontal mockup, the heat flow would be one-dimensional through the thermal insulation, as long as the size of the mockup is not very large when compared to the deflected flame. The heat exposure should be as independent of the radius as possible. Selecting a convenient test specimen diameter was therefore important.

On the other hand, a very low diameter mockup would be more influenced by edge effects due to limited size. It was therefore decided to use steel plate dimension where the diameter was 20 times the thickness, i.e. diameter 320 mm. This represented a sufficiently small-scale and convenient test plate mass for manual handling, i.e. about 10 kg for the 16 mm thickness. The principal concept chosen for the present study is shown in Figure 14, in which it can be seen that thermocouples were also arranged at three diameters in both steel plates to verify that no significant radial temperature gradients developed during fire testing.

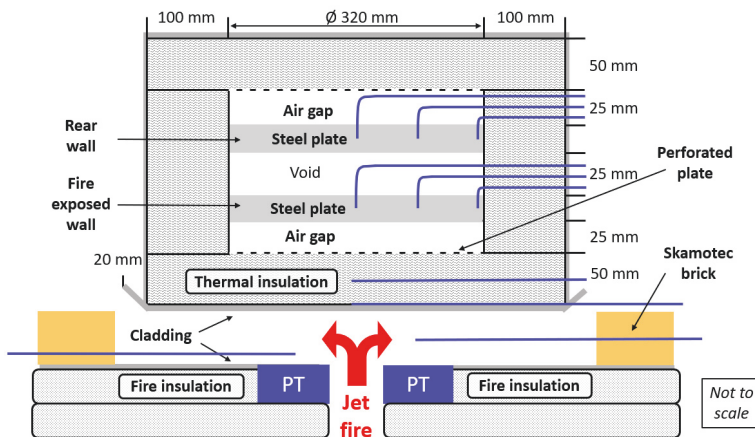


Figure 14 Sketch of mockup, including flame zone, type K mantle thermocouples (blue lines), flush mounted plate thermometers (marked PT) and Skamotec bricks.

In high temperature tests like these, one may introduce water-cooled total flux meters to record the heat flux levels of the test object. The heat flux meter would, however, in this small-scale setting, not fit in without severely interfering with the heat flux that is received by the test object. Given a combustion chamber propane flame thickness of about 50 mm, the radiation from the exposed solid surfaces quickly dominates the heat flux levels. The best way to ensure proper heat flux levels is then to record the cladding temperatures. This may be done by fixating a thermocouple to the inner cladding surface. Alternatively, introducing a plate thermocouple directly viewing the exposed cladding adds much information about the system heat flux levels. Two 100 mm by 100 mm by 20 mm thickness type K plate thermometers (100 mm PT, article number 5928050-001, Pentronic AB, Västervik, Sweden), whose function is explained in [78–81], were therefore introduced flush with the fire insulation below the flame zone, viewing

directly upwards, as shown in Figure 14. It should be noted that this is the opposite of the orientation intended for such plate thermometers. In horizontal orientation, the PTs were mostly exposed to the heat radiation that they could view from the mockup cladding, in addition to convective heat that is received from the propane flame. Facing upwards and aligned flush with the fire insulation cladding, they had virtually no influence on heat transfer within the flame zone. When purchased, the surfaces of the PTs had already been blasted and heat treated to obtain an emissivity of about 0.9, i.e. about the same value as the emissivity suggested by the TR2237 [49]. During the fire, it is believed that all the surfaces approach at least emissivity of 0.9, due to oxidation processes.

The stainless steel plate, which is the active part of the plate thermometer, had a thickness of 0.7 mm, which is the same as that of the cladding used in the industry. The flush-mounted plate thermometers allowed for a very compact flame volume, when exposing the mockup during testing.

To prevent the mockup being exposed to excessive heat, it was covered by cladding on the radial surface as well as on the top surface. The cladding directly exposed to fire continued 3 cm outside the radius of the mockup and was folded and bent 45°, to guide excess flames away from the mockup, as illustrated in Figure 14, thus reducing the heat stresses. This allowed this part of the mockup to be used for repeated testing.

The propane burner given in Figure 15 (Sievert 346051 Turboroofer, 60 mm titanium power burner and a 500 mm neck tube) was used as the flame source. The specified maximum output was 114 kW at the recommended working pressure of 4 bar. The fuel used in the present tests was the recommended fuel, i.e. propane. The propane supply tube was carefully bent to about 90° at a local plumber's workshop, to allow for vertical upward oriented premixed propane jet exposing the downward facing test unit cladding. The setup was arranged symmetrically along the test unit at radius zero, i.e. the center of the jet flame was aligned in the center of the test unit. The mockup and the validation activities are presented in detail in [13].



Figure 15 Burner: Sievert 346051 Turboroofer (original, without 90° bend) [82].

5.2.2 Material properties

The thermal insulation tested was Pipe Section Mat (PSM). Details of the thermal insulation (Rockwool) used are shown in Table 5.

Table 5 Information Rockwool Pipe Section Mat (PSM, Thermal insulation)

| Name | Description |
|-----------------|---------------|
| Material | Stone wool |
| Operating range | -40 to 700 °C |

| Name | Performance | | | | | | | | Norms |
|----------------------------------|----------------------------------|-------|-------|-------|-------|-------|-------|-------|-------------|
| Thermal conductivity | Tm°C | 50 | 100 | 150 | 200 | 250 | 300 | 350 | EN ISO 8497 |
| | W/mk | 0.041 | 0.046 | 0.054 | 0.064 | 0.075 | 0.088 | 0.106 | |
| Maximum service temperature | 700 °C | | | | | | | | EN 14706 |
| Reaction to fire | Euroclass A1 | | | | | | | | EN 13501-1 |
| Nominal density | 140 kg/m ³ | | | | | | | | EN 1602 |
| Water absorption | ≤ 1 kg/m ² | | | | | | | | EN 1609 |
| | ≤ 20 kg/m ³ | | | | | | | | BP 172 |
| Water vapor diffusion resistance | s _d > 200m | | | | | | | | EN 12086 |
| Air flow resistivity | ≥ 60 kPa.s/m ² | | | | | | | | |
| Designation code | MW EN 14303-T4-ST(+)-700-WS1-MV2 | | | | | | | | EN 14303 |

The cladding, distance calling, and perforated plate were made of stainless steel, AISI 316 / EN 14404.

5.2.3 Setting up an experiment

Prior to every experiment, a new set of cladding and thermal insulation was mounted on the exposed side of the mockup. The lower part of the mockup, consisting of cladding, thermal insulation, perforated plate and threaded rods to keep the mockup assembled, is shown in Figure 16.

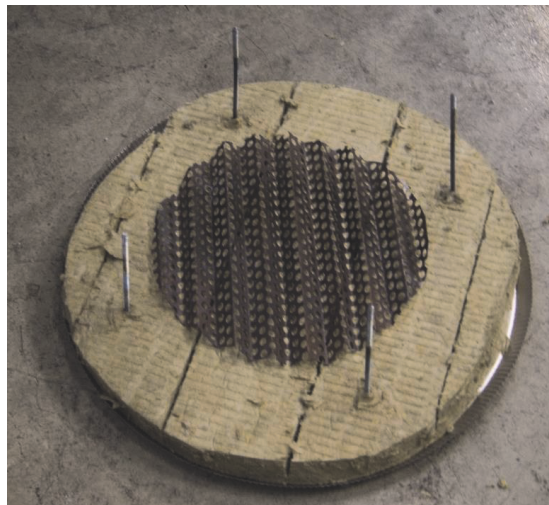


Figure 16 Mockup mounting: cladding, thermal insulation and perforated plate.

When the bottom was assembled, as shown in Figure 16, the two plates indicating the front and back walls of the distillation column were assembled on separate threaded rods. They were then placed on top of the bottom part, consisting of cladding, thermal insulation and perforated plate. Industrial thermal insulation was then placed vertically around and on top of the plates, to minimize heat loss. The final step was to also place cladding around the periphery and top of the mockup, finalizing the assembly process which is shown in Figure 17.

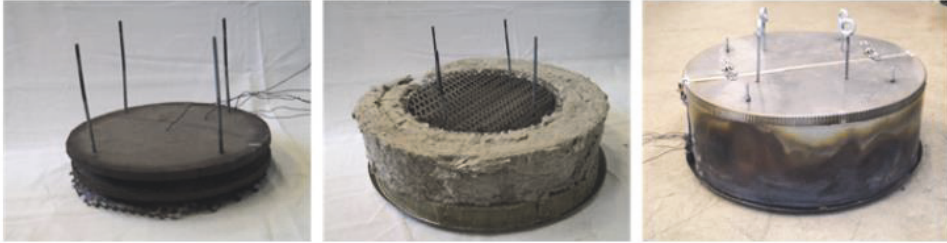


Figure 17 Mockup mounting.

Before the mockup was put in place, the burner was leveled, to ensure vertical burner orientation. The mockup was suspended from a table frame, as illustrated in Figure 18, and leveled in a horizontal position 50 mm above the burner and adjusted to get the burner at radius zero.

The last preparation before testing was to shield the flame zone with lightweight concrete bricks (Skamotec 225, Skamol A/, 100 mm × 100 mm × 50 mm bricks). This minimized the ingress of unwanted air in the flame zone, as well as preventing radiative heat losses from the flame zone. It was also necessary to perform some trial and error testing to optimize the air access to the combustion zone. The mockup ready for an experiment is shown in Figure 18.

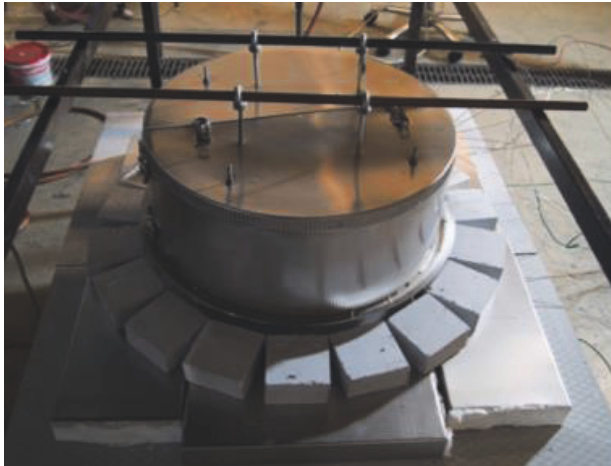


Figure 18 Fire zone shielding and mockup.

5.2.4 Performing the experiments

When the mockup was in position and the safety and operational procedures had been followed, propane at the given rate of 0.6 g/s was released and ignited with an ignition rod. This gave a heat release rate of about 25 kW. For safety reasons, the experiments were conducted by two persons, who were present throughout each fire test. One supervised the gas flow and the other evaluated the temperature recordings and overall fire test development. The fire tests lasted for 30–40 minutes, depending on the exposed wall temperature. An ongoing experiment is shown in Figure 19.



Figure 19 Ongoing experiment.

5.2.5 Other experimental details

It should be noted that the presented test method is not a fully rated test according to any international standard. It simulated full-scale fire testing. It represents a test scenario recognized as being more severe than can be expected in large pool fires. The testing severity is similar to the heat flux levels that may be expected in full-scale jet fire testing. The vibrations etc. expected in such jet-fires would, however, probably give further disintegration of the thermal insulation.

The validity of the experiments can be addressed through two general remarks:

1. The experiments were conducted horizontally, while the insulation was mounted/installed on a vertical column.
2. The experiment was conducted on a scaled model.

In the industrial-scale horizontal distillation column configuration, an increase in convective air cooling will be expected:

- Between the cladding and the thermal insulation (both in the troughs and peaks), cold air will rise, due to buoyancy when heated, and thereby cool the inner surface of the cladding.
- When the thermal insulation starts degrading, there will be increased room for cold air convection, cooling the remaining thermal insulation.
- When the perforated plate and/or the steel wall on the fire-exposed side gets warm, cold ambient air will rise in the 25 mm spacing, due to buoyancy when heated, and thereby cool these surfaces.
- The column steel wall will also be cooled by internal convection (and radiation) inside the distillation column.

Together, these mechanisms will reduce the rate of temperature increase significantly, compared to the horizontal test configuration used in the present study.

It is therefore reasonable to assume that the fire resistance will be better in a real-scale vertical distillation column orientation than in the horizontal non-convective cooling test approach. The horizontal test setup is therefore assessed as conservative, due to a lower degree of convective heat transfer, compared to vertical orientation in a real distillation column; i.e., the scaled model represented conservative testing. It should also be noted that the PT temperatures during fire testing were for long periods well above the target temperature of 1200 °C.

The present thesis also aimed to investigate the passive fire protection performance of the industrial thermal insulation protecting steel walls of 16 mm, 12 mm, 6 mm and 3 mm thickness during 350 kW/m² jet fire exposure. This was done to evaluate how the thermal insulation would behave when backed by steel plates representing gradually less heat sink.

In order to study the breakdown of the thermal insulation with temperature, 50 mm cubes of the thermal insulation were heat treated, i.e., 30 min holding time, at varying temperatures up to 1100 °C in a muffle furnace. To further shed light on the thermal insulation behavior at elevated temperatures, thermogravimetric analysis was performed at temperatures up to 1300 °C to reveal mass loss at elevated temperatures. Differential scanning calorimetry to 1300 °C was performed to investigate the high temperature performance of the thermal insulation, with respect to identifying any potential melting below 1300 °C.

Further details are given in [13, 18]. Recommendations for further studies are summarized in Chapter 7.1, and in [18].

5.2.6 Main conclusions from the fire testing of industrial thermal insulation

The fire testing of industrial thermal insulation showed that fire protection performance was better for the thicker steel plates. This confirms the importance of the higher thermal capacity of the thicker steel plates. A 10 min delay in temperature increase was, however, revealed for all the plate thicknesses. After this time delay, the temperature increased systematically faster for the thinner plates, due to their lower thermal capacity. The heat flux to the plates as a function of time turned out to be almost similar, regardless of the steel plate thickness. This result may be interpreted as better passive fire protection of the thinner steel plates than previously anticipated and represented a positive surprise in the present study.

Testing 5 cm cubic thermal insulation test specimens showed that there was about 25% thickness shrinkage after holding the thermal insulation for 30 min at 1100 °C, indicating sintering effects. There were, however, no signs indicating that the thermal insulation started to melt at this temperature.

Thermogravimetric analysis (TGA) and differential thermogravimetry (DTG) showed mass loss, consistent with degradation of the dust binder (oil) and Bakelite binder at temperatures below 700 °C. There was, however, no indication of any mass loss above 1100 °C. Differential scanning calorimetry (DSC) revealed a major endothermic reaction, peaking at just above 1200 °C. It was also evident that the sample had melted in the platinum crucible after TGA/DSC to 1300 °C. The endothermic peak at about 1200 °C is therefore most likely due to melting of the mineral-based thermal insulation.

Chapter 6

Introduction to the Papers

Paper I: Method for Measuring Cooling Efficiency of Water Droplets Impinging onto Hot Metal Discs

This paper presents a method for measuring the cooling efficiency of water droplets impinging onto hot metal discs in the temperature range of 85 °C to 400 °C, i.e. covering the boiling regimes experienced when applying water to objects heated in fires. Stainless steel and aluminum test discs (with 50 mm diameter, 10 mm thickness, and a surface roughness of Ra 0.4 or Ra 3.0) were suspended horizontally by four thermocouples that were simultaneously used to record disc temperatures. The discs were heated by a laboratory burner prior to the experiments and left to cool with and without applying water droplets to the discs. Based on the recorded rate of the temperature change, as well as disc mass and disc specific heat, the absolute droplet cooling effect and the cooling efficiency relative to complete droplet evaporation were obtained. At 100% efficiency, the NORSOK spray application flux of 10 L/min·m² [5] would be able to withdraw about 430 kW/m² from the fire-exposed surface. In this study, cooling efficiency above the Leidenfrost temperature was generally recorded to be below 10%. Given the NORSOK spray application flux, this corresponds to a cooling flux of only 43 kW/m². This is much lower than the heat flux that may be expected in industrial fires. Dependent on the fire scenario, an object may experience net heat flux levels in the range 200–350 kW/m². The low cooling efficiency experienced above the Leidenfrost temperature explains why it is very important to activate deluge systems early, in order to cool fire-exposed pressurized pipes and process equipment, to keep the temperature development under control. This simple and straightforward technique was well suited for assessing the cooling efficiency of water droplets impinging onto heated metal objects. The test rig also worked well for demonstrating droplet boiling regimes and water droplet cooling efficiency to fire safety engineering students.

For this paper, Torgrim Log conceived the concept. Maria-Monika Metallinou and I designed the experimental setup. I performed the experiments. Torgrim Log and I analyzed the data. Maria-Monika Metallinou contributed materials and equipment, and Øyvind Frette contributed as an advisor throughout. Maria-Monika Metallinou, Torgrim Log and I wrote the paper.

Paper II: Influence of Acetone and Sodium Chloride Additives on Cooling Efficiency of Water Droplets Impinging onto Hot Metal Surfaces

In this study, we investigated the cooling efficiency of water droplets falling/impinging onto hot aluminum and/or stainless steel discs from 12.5 cm, 25 cm, 50 cm and 100 cm fall height, corresponding to droplet impact speeds of 1.5 m/s, 2.2 m/s, 3.1 m/s and 4.4 m/s, respectively. Based on the temperature decay during free cooling of the metal discs (50 mm diameter and 10 mm thickness), with and without droplet cooling, the droplet cooling efficiency was obtained. The discs were aligned at 0° (horizontal), 30° and 60° inclinations. The water application rate was 0.022 g/s and the droplet diameters studied were 2.5 mm, 3.2 mm and 3.7 mm. Acetone solutions (300 ppm and 700 ppm) were tested, to evaluate the influence of an active surfactant on the recorded cooling efficiency, as well as NaCl (35 g/kg) solution, emulating seawater. The temperature range studied in the present work covered all droplet cooling regimes. Overall, the additives only marginally changed the water droplet cooling efficiency. The standard industrial water application rate, i.e. 10 liter/minute·m², is insufficient compared to the heat fluxes expected in pool and jet fires.

Parts of this work were presented as a poster at the Interflam Conference, London, UK, 1-3 July 2019.

For this paper, Torgrim Log conceived the concept. Maria-Monika Metallinou and I designed the experimental setup. Svein Arne Bjørkheim and I performed the experiments. I analyzed the data. Maria-Monika Metallinou, Torgrim Log and I wrote the article; Øyvind Frette contributed as an advisor throughout.

Paper III: Small Scale Hydrocarbon Fire Test Concept

In this paper, we present the development and validation of a test concept for testing the fire resistance of equipment protected with only airgap and thermal insulation, i.e. without fire-protective insulation. The study demonstrates a conceptual methodology for small-scale fire testing of mockups resembling a section of a distillation column. The mockups were exposed to a small-scale propane flame in a test configuration, in which the flow rate and the flame zone were optimized for high heat loads. Results are presented for a mockup resembling a 16 mm-thick distillation column steel wall. The results show that this methodology has great potential for low-cost fire testing of other configurations, and it may serve as a setup for product development. The main purpose of the study was to develop the test concept and demonstrate its applicability to small-scale fire testing. It was somewhat surprising to the authors that the thermal insulation worked as well as it did.

For this paper, Torgrim Log conceived the project idea and performed the first calculations and sketches. Arjen Kraaijeveld and I arranged the propane burner and flow control unit and made the basic test rig. I mounted the mockup for each test and carried out the preliminary testing, as well as Test 1 and Test 2, together with Arjen Kraaijeveld. Maria-Monika Metallinou introduced the plate thermocouples and wrote the paper, together with Torgrim Log and me.

Paper VI: Study of Industrial Grade Thermal Insulation as Passive Fire Protection up to 1200 °C

In this study, we investigated the passive fire protection performance of the industrial thermal insulation protecting steel walls of 3 mm, 6 mm, 12 mm and 16 mm thickness during 350 kW/m²

jet fire exposure. Steel wall temperature versus time was recorded, and it was assumed that the thinner steel walls would obtain higher temperatures early, which could severely influence the thermal insulation degradation processes. A 10 min delay in the exposed steel wall temperature increase was, however, revealed for all the plate thicknesses. After this time delay, the temperature increased systematically faster for the thinner plates, due to their lower thermal capacity. The heat flux to the plates as a function of time turned out to be almost similar, regardless of the steel plate thickness. In order to study the breakdown of the thermal insulation with temperature, 50 mm cubes of the thermal insulation were heat treated, i.e. 30 min holding time, at varying temperatures up to 1100 °C in a muffle furnace. No clear sign of melting was observed, but sintering resulted in 25% shrinkage in thickness at 1100 °C. To further shed light on the thermal insulation behavior at elevated temperatures, thermogravimetric analysis was performed at temperatures up to 1300 °C, to reveal mass loss at elevated temperatures. The thermogravimetric analysis revealed mass loss peaks due to anti-dusting material at 250 °C and Bakelite binder at 460 °C. Differential scanning calorimetry to 1300 °C was performed to investigate the high temperature performance of the thermal insulation, with respect to identifying any potential melting below 1300 °C. Differential scanning revealed endothermic processes related to the anti-dusting material and Bakelite mass losses, as well as a conspicuous endothermic peak at 1220 °C, most likely due to melting.

For this paper, Torgrim Log conceived the project idea. Amalie Gunnarshaug and I mounted the mockup for each small-scale jet fire test and performed the experiments. Amalie Gunnarshaug performed the muffle oven experiments under my guidance. Torgrim Log, Maria-Monika Metallinou and Amalie Gunnarshaug and I analyzed the results. Maria-Monika Metallinou, Torgrim Log and I wrote the paper.

Chapter 7

Summary and Outlook

This PhD thesis consists of two parts.

The first part was to study the cooling efficiency of water droplets impinging onto heated metal substrates. As part of the study, a new innovative method for measuring the cooling efficiency of droplets impinging onto hot metal discs was developed. The method involved a minimum of experimental equipment, and measurements could be performed at a low cost. The developed method worked well, and measurements were performed in the temperature range from 85 °C to 400 °C, i.e. covering the boiling regimes experienced when applying water to heated objects in fires. Distilled water droplets were tested for cooling both aluminum and stainless steel. Acetone solution (300 ppm and 700 ppm) water droplets were tested for cooling aluminum discs, to evaluate the influence of an active surfactant. NaCl (35 g/kg) solution was also tested to determine the cooling efficiency of emulated seawater.

There were significant differences in the cooling efficiency as a function of temperature for the two metals investigated. For each metal, there was, however, no statistically significant difference, with respect to whether the surface roughness was Ra 0.4 or Ra 3.0. The droplets of higher impact speed resulted in lower cooling efficiency, especially at disc temperatures above the Leidenfrost temperature, likely due to more vigorous droplets bouncing. Larger inclination did, as expected, result in lower cooling efficiency. At temperatures associated with nucleate boiling, the water droplets with NaCl conspicuously displayed higher cooling efficiency at about 110 °C. This may be explained by the formation of small salt deposits at the disc surface, thus improving the cooling efficiency. At temperatures between 120 °C and the Leidenfrost temperature, acetone and NaCl additives did not significantly alter the cooling efficiency of the water droplets. Above the Leidenfrost temperature, a minor increase in cooling efficiency was observed for the acetone solutions. Overall, the additives only marginally changed the water droplet cooling efficiency. Generally, the cooling efficiency was below 10% at temperatures above the Leidenfrost temperature.

A NORSOK spray application rate of 10 L/min·m² [1] would be able to withdraw 43 kW/m² from the fire exposed surface, given a cooling efficiency of 10%. This is much lower than the heat flux levels expected in industrial fires. The low cooling efficiency experienced above the Leidenfrost temperature explains why it is very important to activate active fire protection systems early, in order to cool pressurized pipes and process equipment, to prevent

hot spot formation. It is important to keep the temperature development under control, in order to prevent further escalation of a fire scenario.

The second part was to develop an innovative low-cost concept for small-scale testing of industrial thermal insulation exposed to heat release rates expected in industrial fires. A setup was built, in which mockups resembling a part of a typical hydrocarbon distillation column, with thermal insulation according to the modern requirements, could be fire-exposed. The mockups were exposed to a small-scale propane flame in a test configuration, where the flow rate and the flame zone were optimized to give heat flux levels in the range 250–350 kW/m². The study investigates the performance of thermal insulation in conjunction with 3 mm, 6 mm, 12 mm and 16 mm thick steel walls, when exposed to 350 kW/m² heat load. Regardless of the tested steel plate thicknesses, about 10 min passed before a nearly linear steel temperature increase versus time was observed. Thereafter, the thinnest plates systematically showed a faster temperature increase than the thicker plates, confirming the wall heat sink effect.

The endothermic processes involved when heating the thermal insulation may to a large part explain the 10 min delay in steel plate temperature increase during fire testing. Overall, the tested thermal insulation also performed surprisingly well for protecting the thin steel plates through the test period of 30 minutes.

Heat treatment of the thermal insulation for 30 minutes at 1100 °C revealed 25% shrinkage in thickness due to sintering. Differential scanning calorimetry revealed melting of the thermal insulation at about 1220 °C. The limited sintering and the high melting point may explain why the thermal insulation performed surprisingly well during the fire testing.

The results show that this methodology has great potential for low-cost fire testing of other configurations, and it may serve as a setup for product development. Further research is therefore recommended.

7.1 Recommended further studies

With respect to water droplet cooling efficiency, one may seek other additives influencing the surface tension more than, e.g., acetone. It may also be beneficial to build an apparatus for studying the cooling efficiency of water droplets on, e.g., electrically heated metal surfaces exposed to medium-scale water sprays. It is, however, quite likely that the Leidenfrost temperature can only be slightly changed and that the cooling efficiency may be low, regardless of the conditions when metal objects are exposed to fires. The solution would probably always be to apply water early or to flood the metal with water application rates much higher than those in the NORSOK S-001 recommendation [5].

It would be very beneficial if muffle furnace testing of the thermal insulation could be done at holding temperatures of, or even higher than, 1200 °C. This would cover the range of interest for jet fire testing and could give valuable information about breakdown temperatures and possible breakdown mechanisms. With more knowledge, it may be possible to adjust the thermal insulation mineral composition, to gain even better high-temperature heat protection.

Differential scanning calorimetry (DSC) measurements revealing absolute values, e.g. W/g, would be very beneficial for potential future modelling of the fire protection performance of

thermal insulation. When the other information about an oil and gas process area is known, such as fire detection time delays, blowdown times, etc., one may consider whether the thermal insulation could be sufficient for fire protection of the involved pipes and equipment. This could potentially reduce cost when designing new, or refurbishing older, plants and oil platforms. Currently, there is therefore a need for more knowledge about the high-temperature performance of industrial thermal insulation in this industry.

The fire testing in the present work was done in a way that is representative of fire exposure. That was worthwhile for demonstrating the performance of the thermal insulation. For future testing, some sort of guarded hot plate setup [83-84], for heat exposure of the thermal insulation, may be considered. At lower temperatures, this was done for developing pipeline thermal insulation by Li et al. [85], who also investigated new low-temperature thermal insulation properties by DSC. A guarded hot plate approach, simulating the fire exposure, may allow for more controlled heat exposure and more detailed analysis of thermal insulation behavior during heat exposure.

Passive fire protection material mats, i.e. quite similar to thermal insulation but made of high-temperature resistant materials, generally show higher thermal conductivity than the thermal insulation. They do, however, not break down at 1200 °C. Placing a rather thin layer of fire insulation mat at the fire-exposed side of the thermal insulation may therefore be considered. The thickness of this layer could then be designed such that the temperatures of the thermal insulation for a prolonged period could be kept below, e.g., 1100 °C, ensuring that the thermal insulation would not sinter too severely or break down/melt as fast as in the present study. The system could then potentially protect the steel for a very long period of fire exposure. It would be interesting to test this concept in a future study.

Chapter 8

Scientific Results

Concept Paper

Method for Measuring Cooling Efficiency of Water Droplets Impinging onto Hot Metal Discs

Joachim Søreng Bjørge ^{1,2,*}, Maria-Monika Metallinou ³, Torgrim Log ³  and Øyvind Frette ²

¹ Q Rådgivning AS/PDS Protek, Øvregata 126, 5527 Haugesund, Norway

² Department of Physics and Technology, University of Bergen, 5020 Bergen, Norway; oyvind.frette@uib.no

³ Faculty of Engineering and Science, Western Norway University of Applied Sciences, 5528 Haugesund, Norway; monika.metallinou@hvl.no (M.-M.M.); torgrim.log@hvl.no (T.L.)

* Correspondence: jsb@q-rad.no; Tel.: +47-9098-1051

Received: 18 May 2018; Accepted: 7 June 2018; Published: 9 June 2018



Abstract: The present work outlines a method for measuring the cooling efficiency of droplets impinging onto hot metal discs in the temperature range of 85 °C to 400 °C, i.e., covering the boiling regimes experienced when applying water to heated objects in fires. Stainless steel and aluminum test discs (with 50-mm diameter, 10-mm thickness, and a surface roughness of Ra 0.4 or Ra 3) were suspended horizontally by four thermocouples that were used to record disc temperatures. The discs were heated by a laboratory burner prior to the experiments, and left to cool with and without applying 2.4-mm diameter water droplets to the discs while the disc temperatures were recorded. The droplets were generated by the acceleration of gravity from a hypodermic injection needle, and hit the disc center at a speed of 2.2 m/s and a rate of 0.02 g/s, i.e., about three droplets per second. Based on the recorded rate of the temperature change, as well as disc mass and disc heat capacity, the absolute droplet cooling effect and the relative cooling efficiency relative to complete droplet evaporation were obtained. There were significant differences in the cooling efficiency as a function of temperature for the two metals investigated, but there was no statistically significant difference with respect to whether the surface roughness was Ra 0.4 or Ra 3. Aluminum showed a higher cooling efficiency in the temperature range of 110 °C to 140 °C, and a lower cooling efficiency in the temperature range of 180 °C to 300 °C compared to stainless steel. Both metals gave a maximum cooling efficiency in the range of 75% to 85%. A minimum of 5% cooling efficiency was experienced for the aluminum disc at 235 °C, i.e., the observed Leidenfrost point. However, stainless steel did not give a clear minimum in cooling efficiency, which was about 12–14% for disc temperatures above 300 °C. This simple and straightforward technique is well suited for assessing the cooling efficiency of water droplets impinging onto heated metal objects. The test rig also worked well for demonstrating droplet boiling regimes and water droplet cooling efficiency to fire safety engineering students.

Keywords: hot metals; water droplet cooling; heat transfer

1. Introduction

Evaporation processes are of interest in numerous areas such as agricultural [1], industrial [2], and academic [3] communities, as well as for individuals [4]. When evaporating at room temperature, the substrate material plays an important role in the evaporation process, as does the ambient air relative humidity [5]. However, the ambient air relative humidity is less important when droplets evaporate on substrates at elevated temperatures [6]. In a recent study of a wide range of water droplets sizes in the transition regime of a boiling crisis, Misyura [7] demonstrated that several material parameters are important when water droplets hit objects, wet the surface in different ways, and then start evaporating. Droplet contact angles play a role [8], and may depend on impurities, additives, etc.

Additives may therefore be used to reduce surface tension and thus improve performance [9,10]. Some researchers have studied the behavior of different droplet parameters such as size, impinging velocity [11], wall material [12,13], temperature below the Leidenfrost point [14], and the influence of solid–liquid contact time [15]. A review concerning droplets impinging onto hot metals was conducted by Liang and Mudawar [16] for all of the involved boiling regimes for water droplets on metal surfaces. A literature review on the Leidenfrost temperature for water on different heated materials is given by Bernardin and Mudawar [17]. Water droplet cooling efficiency for droplets hitting Teflon-covered copper was recorded by Sawyer et al. [18], who reported a cooling efficiency in the range of 50% to 90% at temperatures up to the temperatures associated with a boiling crisis. However, no studies were identified as covering the whole range from below the boiling point and all the way into the film-boiling regime.

In the process industry, fire-exposed pressurized pipes and vessels may rupture violently and release their combustible or poisonous contents if weakened by overheating. Considerable resources are therefore used for designing and maintaining active fire protection systems, i.e., deluge systems, fire monitors, etc. The NORSOK standard S-001 [19] devotes multiple pages to active fire protection. For process areas, the design criteria is $10 \text{ L}/\text{min}\cdot\text{m}^2$. However, studies of the performance of these systems are scarce, and would need to cover all of the involved boiling regimes. Full-scale experiments were performed by Kazemi [20] and Drange [21] in standardized $0.3 \text{ kg}/\text{s}$ jet fire scenarios. Deluge and fire monitors in large-scale jet fires were studied by Opstad [22]. None of these studies reported water droplet cooling efficiency.

The purpose of the present study was to develop a method for measuring the cooling efficiency of water droplets impinging onto hot stainless steel and aluminum in the temperature range of 80–400 °C. This temperature range covers the different boiling regimes that are associated with water droplets on metal substrates. These water droplet boiling regimes are presented in Section 2. The apparatus that was developed for the study is presented in Section 3. The theory and calculative method to reveal the cooling efficiency based on temperature versus time measurements with and without water cooling is outlined in Section 4. Statistical analysis in order to reveal the differences in cooling efficiency as a factor of surface roughness is described in Section 5, and the overall results are discussed in Section 6. The possibility for using the test rig for teaching purposes regarding water droplet boiling regimes and water droplet efficiency is also discussed.

2. Water Droplet Boiling Regimes

At ambient pressure, relative humidity below 100%, and temperatures below the boiling point, water droplets evaporate by mass diffusion [5]. Boiling starts when the surface temperature is just above 100 °C, i.e., typically 104 °C [23]. At this temperature, bubble formation within the saturated fluid starts and results in very slow boiling. The involved mechanism is called nucleate boiling. For a metal surface at 104 °C, the heat flux to a sessile water droplet is limited. Increasing the metal surface temperature increases the heat flux until it reaches a maximum, i.e., the critical heat flux, as shown in Figure 1. Beyond this temperature, increasing the surface temperature reduces the heat flux due to a vapor film partially forming below the droplet. This boiling regime is called transition boiling, and is characterized by violent sizzling and droplet breakup. Further increasing the temperature induces a stable vapor film below the droplet. Thereafter, heat flux from the hot surface to the levitated droplet increases slightly with increasing surface temperature due to the increasing temperature difference between the hot surface and the levitated droplet. The starting temperature for this final boiling regime is called the Leidenfrost temperature [24,25]. The boiling regimes are summarized in Figure 1.

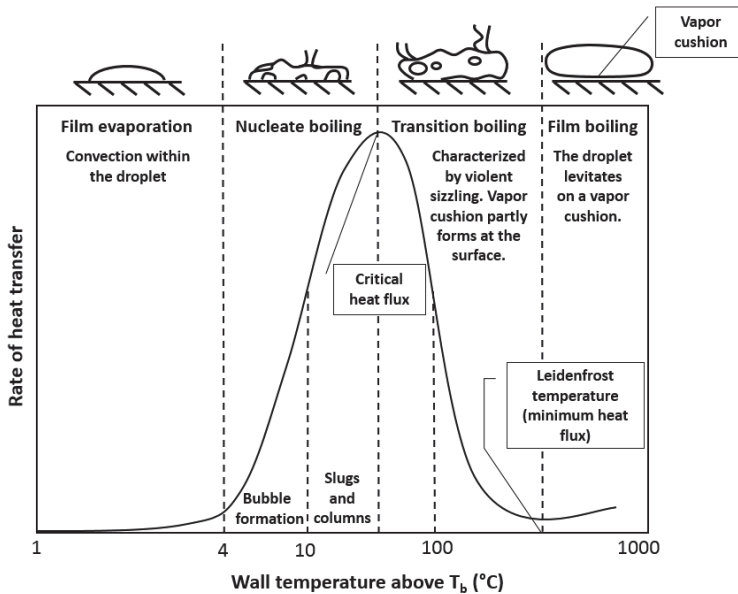


Figure 1. Droplet evaporation/boiling regimes: film evaporation, nucleate boiling, transition boiling, and film boiling. Adapted from [16,17,26].

3. Experimental Setup

3.1. The Discs

Stainless steel (AISI 316) and aluminum were the selected metals in the present study, with room temperature thermal conductivities of about $15 \text{ W/m}\cdot\text{K}$ and $150 \text{ W/m}\cdot\text{K}$, respectively. The arithmetical mean roughness (R_a) used for both discs were $R_a 0.4$ (polished/smooth surface) and $R_a 3$, as defined by [27]. Disc sizes of 50-mm diameter and 10-mm thickness (Figure 2) resulted in convenient cooling rates, with and without water cooling. The disc surface color (emissivity) was stabilized by successive complete measurement cycles (explained later in the present chapter) prior to the measurements reported in the present work.

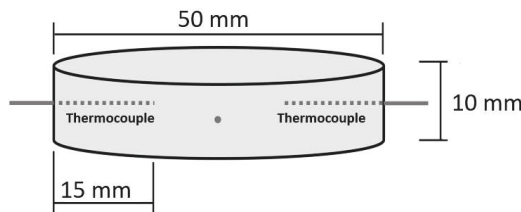


Figure 2. Sketch of metal disc with four inserted type K mantle thermocouples (with 1.6-mm diameter) at 90° horizontal separation.

3.2. Disc Positioning and Temperature Measurements

Ideally, there should be as few heat losses as possible to a fixture, keeping the disc in position. Thin metal rods for supporting the disc were considered. This led to the decision to combine disc support with temperature recordings, i.e., suspend the disc by four standard 1.6-mm diameter type K

(chromel–alumel) mantel thermocouples, as shown in Figure 2. This solution minimized contact between the disc and neighbor objects. The disc was aligned horizontally with a leveler, and heated to about 430 °C prior to the measurements, as shown in Figure 3. The heater was then removed and the disc was let to cool to 410 °C, ensuring time for the internal temperature gradients to spatially equilibrate prior to each measurement. The experiment as such started when the disc had cooled to temperatures below 410 °C. The disc temperatures were recorded at a frequency of 1 s⁻¹ by a data logger (National instruments NI cDAG-9184, Austin, TX, USA).

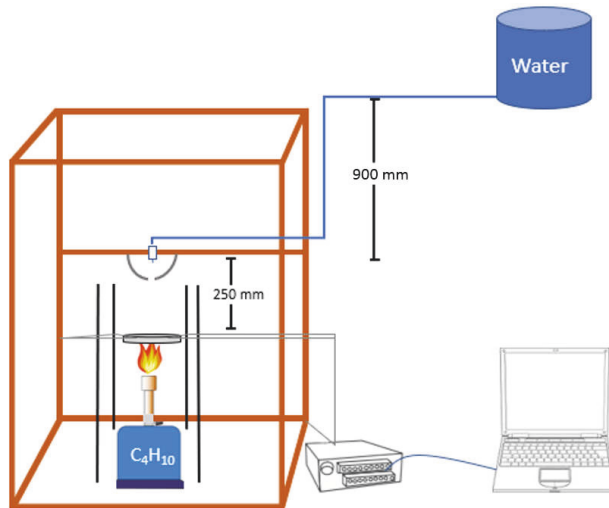


Figure 3. Sketch of the experimental setup (not to scale).

3.3. Droplet Generation

Droplets of distilled water were formed at the tip of a medical infusion hypodermic stainless steel needle (25G*1). The arrangement allowed the droplet rate to be regulated in order to obtain a particular flow rate. This simple injection needle system performed well, and represented an ultimate low-cost droplet generator, which has also been used by other researchers [14]. The water droplets detached due to gravity. The chosen impingement height was 25 cm, resulting in an impact velocity of 2.2 m/s.

Prior to and after each water-cooling measurement, 20 droplets were generated from the arrangement and collected in a small laboratory dish. The mass of the 20 droplets was determined using a balance (AG204DR METTLER TOLEDO, Columbus, OH, USA). Thus, the mass of the individual droplet was determined. Very low variation was observed in the collective mass of succeeding 20 new droplets that were weighed when checking for the reproducibility. Assuming that the droplets were spherical, the droplet diameter was calculated to be 2.4 mm. The mass flow was 0.02 g/s, i.e., about three droplets/s.

3.4. Shielding the Setup from Air Currents

In laboratories, the ventilation currents may disturb experiments significantly. Inspired by Log and Heskestad [28], who studied small-scale fire plumes, the influence of air ventilation was minimized, as well as the influence of personnel movements. This was done by making an open wood frame, 1.1 m × 0.55 m × 1.55 m height, and covering this frame with a fine mesh screen. A simple roll-up door was made to give access to the interior for setting up experiments, heating the discs, etc. The principle setup is shown in Figure 3.

3.5. Metal Disc Dimensions

It was decided to have a disc diameter that could be quite evenly preheated by a Bunsen burner prior to the experiments without introducing major temperature gradients. If temperature gradients did result from the preheating, they should have time to spatially even out between the preheating and the start of the experiments. A diameter of 50 mm was found to be convenient in this respect.

The measurements of the disc cooling without, and with, water droplet cooling, relied on exhausting the heat stored in the disc after the preheating. The disc thickness therefore had to be selected such that it allowed for a convenient time period for temperature recordings in both these cases. By trial and error, it was found that a disc thickness of 10 mm resulted in a proper cooling time both without and with droplets impacting onto the disc.

4. Determining Cooling Efficiency

The temperature versus time during disc cooling, with and without impinging water droplets, was recorded for disc temperatures between 85–400 °C. In order to explain the procedure, data from a preliminary aluminum disc cooling experiment is used. The same calculative procedure was used for the final tests presented in Section 6.

4.1. Water Droplet Cooling Efficiency

Data from the two reference measurements without applying water droplets, sandwiching the water droplet experiment, were used to calculate the average reference cooling curve. The heat losses were in these cases mainly associated with heat radiation and convective heat losses, with some minor heat loss through the four thermocouples suspending the disc. Between these reference measurements, the droplet-cooling test was done with water droplets applied to the hot metal discs at a constant rate. Typical temperature versus time curves are shown in Figure 4. The respective cooling rates (dT/dt) versus temperature are shown in Figure 5. It is clearly seen that at certain temperatures, the cooling rate is more significant when water droplets were applied to cool the disc. Based on the differences in cooling rates, disc mass, and specific heat, the heat flow to the impinging water droplets was calculated.

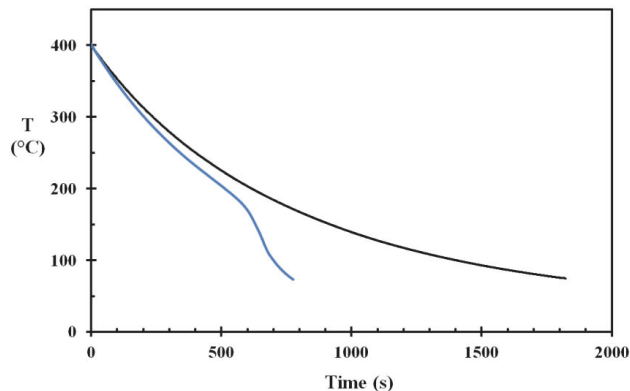


Figure 4. Temperatures of a representative aluminum disc (**blue**) with 2.4-mm diameter droplets and an application rate of 0.02 g/s, with the reference temperatures recorded prior to and after the droplet measurements (**black**).

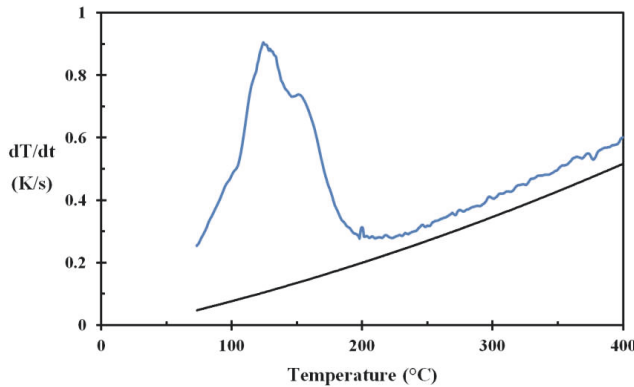


Figure 5. Cooling rate, dT/dt , for droplet application (blue) and reference recordings (black) based on temperature data from Figure 4.

Subtracting the temperature versus time derivatives presented in Figure 5 gives the net water droplets’ disc-cooling rate, i.e., $\left\{ \frac{dT}{dt} \right\}_{Net}$ (K/s). Knowing the mass, m (kg), of the disc, which is in this case 52.9 g, and the specific heat of aluminum as a function of temperature, $C_P(T)$ (J/kg K), the water droplet cooling heat flow can be calculated by:

$$\dot{Q}_{Drops}(T) = m_{Disc} \cdot C_P(T) \cdot \left\{ \frac{dT}{dt} \right\}_{Net} \quad (W), \tag{1}$$

where the specific heat as a function of temperature is given by the NIST-JANAF Thermochemical Tables [29] as:

$$C_P(T) = A + B \cdot \tau + C \cdot \tau^2 + D \cdot \tau^3 + E / \tau^2 \quad (J/kg K), \tag{2}$$

where $A = 28.08920$, $B = -5.414849$, $C = 8.560423$, $D = 3.427370$, $E = -0.277375$ and $\tau = T(K)/1000$. Ignoring the heat flow that is needed to heat the water droplets to 100 °C and possibly heating the steam above 100 °C, the heat flow that is needed to evaporate the droplets at a rate of \dot{m}_{Drops} (kg/s) is given by:

$$\dot{Q}_{Max} = \dot{m}_{Drops} \cdot \Delta H_{vap} \quad (W), \tag{3}$$

where the heat of vaporization at 100 °C, ΔH_{vap} , is 2571 kJ/kg.

The droplet cooling rate as a function of temperature and the droplet cooling potential, \dot{Q}_{Max} , for the test presented in Figure 4 are shown in Figure 6. The temperature of the highest droplet cooling rate, i.e., 124 °C, which corresponds to the critical heat flux, is marked in the figure. It is clearly seen that the cooling capacity does not reach \dot{Q}_{Max} . This was simply caused by some droplets being lost from the disc before evaporating completely.

The relative droplet cooling efficiency, i.e., $\dot{Q}_{Drops}(T) / \dot{Q}_{Max}$, is shown in Figure 7. The cooling efficiency relative to heating the steam to the disc temperature is also shown in the figure.

It should be noted that the cooling efficiency at disc temperatures below 100 °C is quite high. This is a result of droplet wetting, i.e., the remains of previous droplets spread out to make a quite substantial total wet surface area for film evaporation. This was also observed by Pasandideh-Fard et al. [14] in their study of droplets impinging onto metal surfaces at temperatures between 50–120 °C.

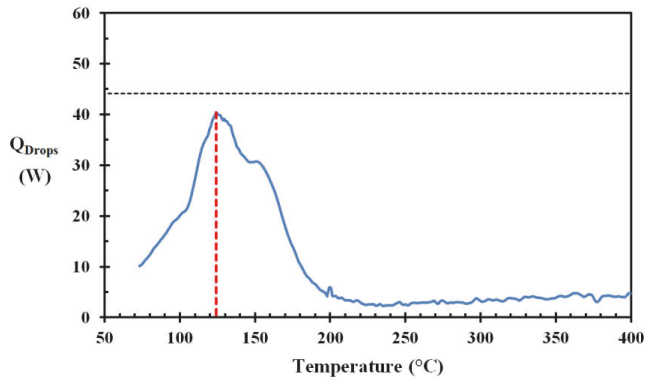


Figure 6. Droplet cooling rate (blue) and heat absorption potential (black dashed line) as a function of temperature. The temperature at the maximum cooling rate is marked (red).

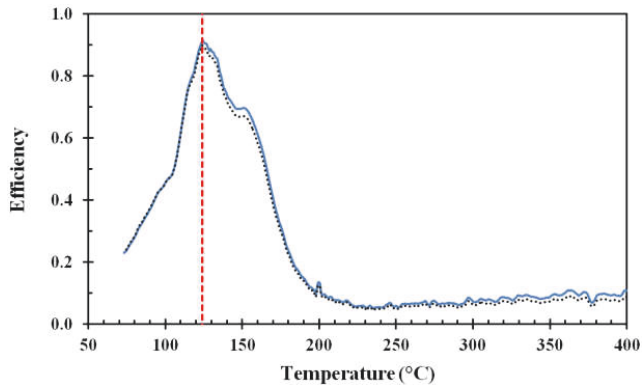


Figure 7. Dimensionless cooling efficiency (blue) and dimensionless cooling efficiency related to the disc temperature (black dashed line). The temperature of the maximum cooling efficiency is marked (red). Data from Figure 6.

4.2. Confirming Droplet Evaporation Regimes

When studying Figure 6 in detail, it may be seen that at about 104 °C, there is an abrupt change in the water cooling efficiency versus temperature. This abrupt change corresponds to the transfer from film evaporation below 104 °C to nucleate boiling above 104 °C. The nucleate boiling regime in this case continued up to about 124 °C, which may be identified as the temperature of critical heat flux, which is also named the boiling crisis [7]. Above about 124 °C, the regime of transition boiling prevails to about 235 °C. Above 235 °C, the droplets experienced film boiling, i.e., the Leidenfrost temperature for the aluminum discs was in this case about 235 °C. This result corresponds well with results reported by other researchers, e.g., the literature review conducted by Bernardin and Mudawar [17] with a reported Leidenfrost temperature for aluminum in the range of 235–265 °C.

4.3. Classroom Demonstrations

The setup, without the wood frame and the fine mesh screen, was moved to a classroom for demonstrating water droplet behavior and cooling efficiency for BSc and MSc students in fire safety engineering. Placed centrally in the room, it allowed for visual and audial observations while the droplets hit the metal plate and cooled the disc. This allowed the students to observe the droplet cooling development through the different evaporation regimes.

It was not within the scope of the present work to formally interview students during the demonstrations. However, they did express increased understanding of water droplet evaporation regimes as a function of metal surface temperature. The potential of very low water cooling efficiency in fire scenarios for temperatures above the Leidenfrost temperature was noted; therefore, it looks like this simple setup may serve both scientific and educational purposes.

5. Results for Stainless Steel and Aluminum with a Surface Roughness of Ra 0.4 and Ra 3

Water droplets impinging onto stainless steel and aluminum discs with a surface roughness of Ra 0.4 and Ra 3 were studied in the present work to demonstrate the method for recording water droplet cooling efficiency. A series of five tests with water droplet application, which were sandwiched by two reference measurements as explained earlier, were needed due to the stochastic variations observed, especially close to the temperatures associated with critical boiling.

5.1. Results of the Stainless Steel Surface Roughness Measurements

For testing the droplet cooling efficiency for the stainless steel disc, a water application rate of 0.02 g/s and droplet size of 2.4 mm, giving a droplet frequency of 3 s^{-1} , were targeted. The droplet speed, which was calculated through the fall height and acceleration of gravity, was 2.2 m/s. According to Pasandideh-Fard et al. [14], this corresponds well to the droplet speed obtained by photographic methods for similar sized droplets and similar fall heights. The results obtained for surface roughnesses of Ra 0.4 and Ra 3, are shown in Figures 8 and 9, respectively.

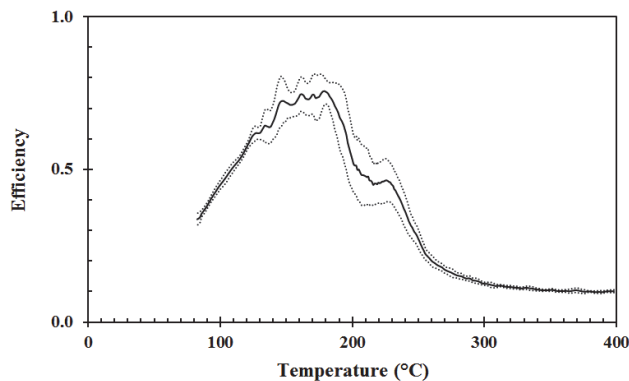


Figure 8. Average cooling efficiency for water droplets impinging onto the stainless steel disc with a surface roughness of Ra 0.4 as a function of temperature (black). The dotted lines represent \pm one standard deviation, respectively.

The standard deviation of the efficiency recorded for the surface roughnesses studied, i.e., Ra 0.4 and Ra 3, is shown in Figure 10 as a function of temperature. The average results for the stainless steel discs with surface roughnesses of Ra 0.4 and Ra 3 are compared in Figure 11.

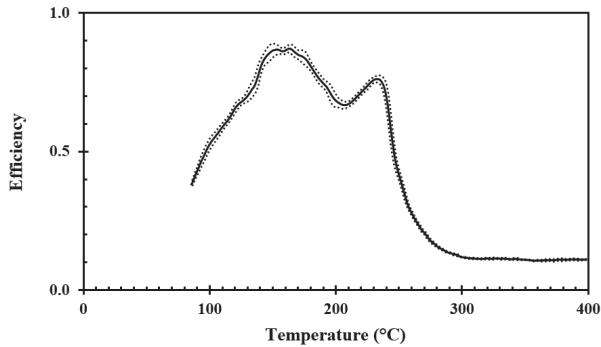


Figure 9. Average cooling efficiency for water droplets impinging onto the stainless steel disc with a surface roughness of Ra 3 as a function of temperature (black). The dotted lines represent \pm one standard deviation, respectively.

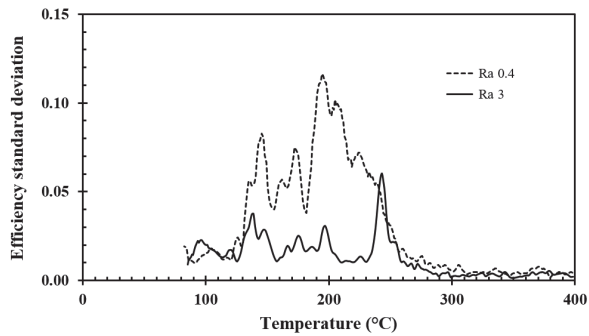


Figure 10. Cooling efficiency standard deviation for water droplets impinging onto the stainless steel disc with surface roughnesses of Ra 0.4 and Ra 3 (marked on the figure).

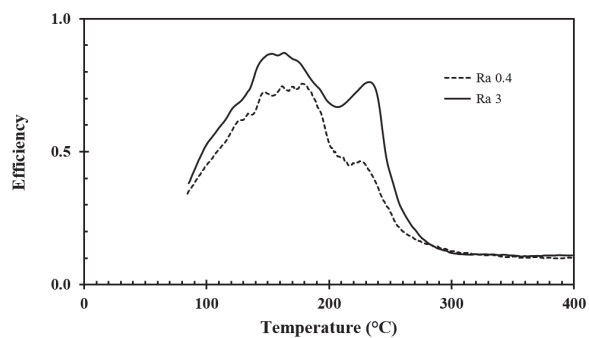


Figure 11. Average cooling efficiency for water droplets impinging onto the stainless steel disc with surface roughnesses of Ra 0.4 and Ra 3 (marked on the figure).

A Student's *t*-test was used to evaluate whether the efficiency recorded for the stainless steel discs with surface roughnesses of Ra 0.4 and Ra 0.3 were significantly different. Checking through the whole temperature range from 85 °C to 400 °C and requiring an alpha <0.05 indicated that the difference in efficiency as presented in Figure 11 was not statistically valid.

5.2. Results of the Aluminum Surface Roughness Measurements

For recording the droplet cooling efficiency of the aluminum discs, similar water application rates, droplet sizes, droplet frequencies, and droplet speeds as for the stainless steel tests were used, i.e., respectively 0.02 g/s, 2.4 mm, 3 s⁻¹, and 2.2 m/s. The results obtained for surface roughnesses of Ra 0.4 and Ra 3 are shown in Figures 12 and 13, respectively.

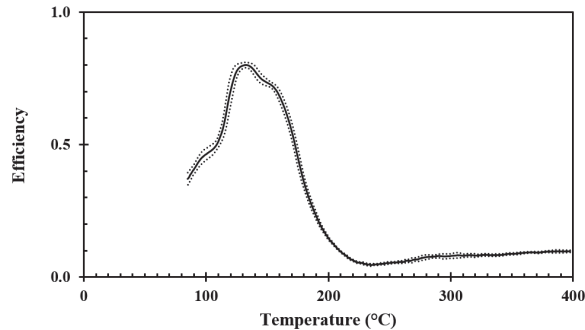


Figure 12. Average cooling efficiency for water droplets impinging onto the aluminum disc with a surface roughness of Ra 0.4 as a function of temperature (black). The dotted lines represent \pm one standard deviation, respectively.

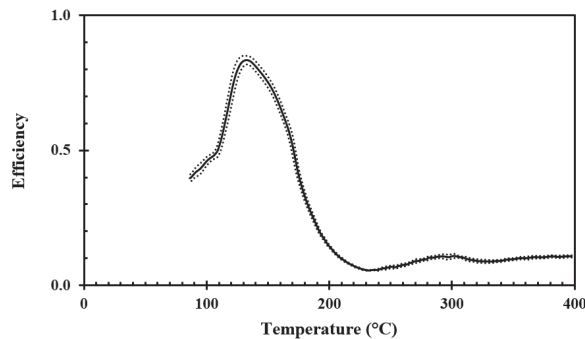


Figure 13. Average cooling efficiency for water droplets impinging onto the aluminum disc with a surface roughness of Ra 3 as a function of temperature (black). The dotted lines represent \pm one standard deviation, respectively.

The standard deviation of the efficiency recorded for the surface roughnesses studied, i.e., Ra 0.4 and Ra 3, is shown in Figure 14 as a function of temperature. The average results for the aluminum discs with surface roughnesses of Ra 0.4 and Ra 3 are compared in Figure 15.

The average results for the aluminum discs with surface roughnesses of Ra 0.4 and Ra 3 are compared in Figure 15.

For aluminum, the Student's *t*-test ($\alpha < 0.05$) showed that the recorded difference in efficiency for surface roughnesses of Ra 0.4 and Ra 3 was significant only for temperatures between 220–310 °C.

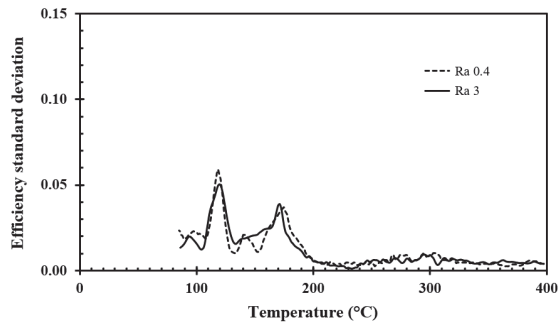


Figure 14. Cooling efficiency standard deviation for water droplets impinging onto the aluminum disc with surface roughnesses of Ra 0.4 and Ra 3 (marked on the figure).

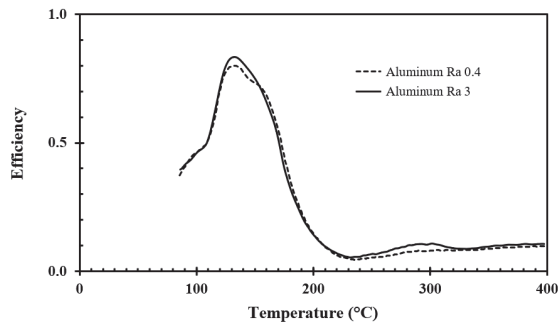


Figure 15. Average cooling efficiency for water droplets impinging onto the aluminum disc with surface roughnesses of Ra 0.4 and Ra 3 (marked on the figure).

5.3. Comparing the Results for Stainless Steel and Aluminum

The results for droplets impinging onto the stainless steel and aluminum discs with surface roughnesses of Ra 0.4 and Ra 3 are compared in Figures 16 and 17, respectively. It is clearly seen from these figures that there are quite significant differences in the water droplet efficiency between the respective metals. However, for both of these metals, quite low droplet cooling efficiencies were recorded at temperatures above 300 °C.

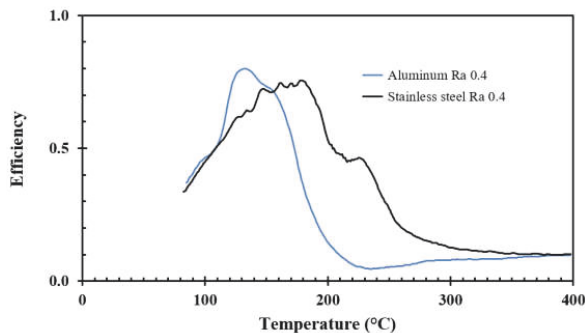


Figure 16. Average cooling efficiency for water droplets impinging onto the stainless steel and aluminum disc (marked on the figure) with a surface roughness of Ra 0.4.

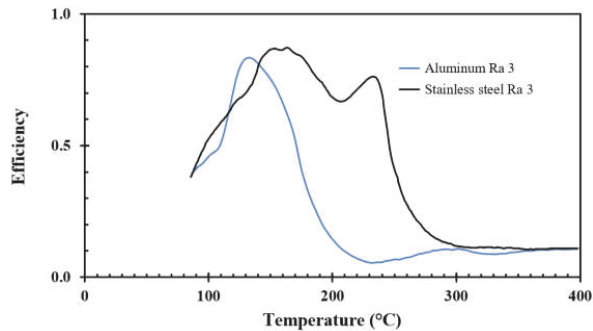


Figure 17. Average cooling efficiency for water droplets impinging onto the stainless steel and aluminum disc (marked on the figure) with a surface roughness of Ra 3.

5.4. NORSOK Requirements versus Spray Efficiency

Applying a certain spray flux \dot{m}'' ($\text{kg}/\text{s}\cdot\text{m}^2$) with a cooling efficiency of ζ to a hot surface above the boiling point of the liquid, the cooling potential is given by:

$$\dot{Q}_{Cool} = \zeta \cdot \dot{m}'' \cdot \Delta H_{vap} \quad (\text{W}/\text{m}^2) \quad (4)$$

Assuming that at e.g., 400 °C the cooling efficiency is about 0.10, a NORSOK [19] spray application rate of 10 L/min·m², i.e., 0.167 kg/s·m², would be able to withdraw 43 kW/m² from the fire exposed surface. This is much lower than the heat flux from an industrial fire to an exposed object at 400 °C. Dependent on the fire scenario, this object may experience net heat flux levels between 200–350 kW/m².

The low cooling efficiency experienced above the Leidenfrost temperature explains why it is very important to activate deluge systems early in order to cool pressurized pipes and process equipment in order to keep the temperature development under control. If not, the water spray may have limited effects, and may not be able to prevent hot spot formation and a possible loss of containment, possibly resulting in a severely increased fire scenario.

5.5. Error Analysis

It was not possible to get exactly the same water application rate and exactly the same droplet diameters for each measurement series with the current setup. However, the standard deviation was within 2% for the water application rate and within $\pm 1\%$ for the droplet diameter. The 25.0-cm elevation for droplet acceleration was measured to be within 1 mm, i.e., representing less than 1% error in the droplet speed. Given the rather large standard deviations observed for the stainless steel discs, the droplet diameter, application rate, and droplet speed can be considered sufficiently constant for comparing the results from the different measurement series.

The discs were aligned horizontally to within 0.5° before each measurement series. However, there may be some slight misalignment during the heating and cooling cycles. This may to some extent influence the results. However, misalignment larger than 1° after the completion of each measurement series was not discovered. It is therefore reasonable to assume that the differences recorded in the water droplet cooling efficiencies were due to the different metals used, and for some temperature regions, the surface roughness.

The reason for the larger standard deviation in the recorded efficiency for stainless steel compared with aluminum may be due to the lower thermal conductivity/diffusivity of the stainless steel. When two consecutive droplets hit exactly the same spot, which ideally was the goal, the stainless steel surface did not recover thermally as much between each droplet impact as was the case for the aluminum discs. If a droplet then hit just off the impact point of the previous droplets, it would be

partly exposed to a higher surface temperature. The one order of magnitude higher heat transport properties of aluminum better evened out the cooling impacts by the previous droplets. When the temperature gradients for aluminum were less steep, it did not make much difference whether the subsequent droplets hit the same location, or were slightly off from that location. Therefore, it was expected that the standard deviations experienced for the droplets impacting onto the aluminum discs would be lower than for the stainless steel discs.

6. Discussion

A method for measuring the cooling efficiency of water droplets impinging onto hot metal surfaces was developed. The test apparatus was described, measurements were performed on stainless steel and aluminum discs, and the recordings were processed to reveal the cooling efficiency in the temperature range between 85–400 °C. It was also investigated whether the method can reveal any differences in the cooling efficiency as a function of the surface roughness. Therefore, the 50-mm diameter and 10-mm thick metal discs tested were prepared with roughnesses of Ra 0.4 and Ra 3 for both materials. The test setup was validated by droplets (with a 2.4-mm diameter) generated by the acceleration of gravity from a hypodermic injection needle impacting onto the disc center at a speed of 2.2 m/s and a rate of 0.02 g/s, i.e., about three droplets per second.

The horizontally aligned disc was suspended by four thermocouples penetrating the disc 15-mm radially, along the horizontal symmetry plan. This solution minimized contact between the disc and other objects, and allowed for recording the disc temperature during the cooling phase with and without cooling the disc by water droplets. Several researchers placed a thermocouple junction either flush with or 0.5 mm below the droplets' impact point [11,14]. This allowed them to record the surface temperature at the impact point. The thermocouple then induces a disturbance in the metal exactly at the point where the droplets hit the surface. The present method aimed at recording the temperature within the metal disc, with four symmetrically located thermocouples giving minimal disturbances to the droplet impact point. This gave a better representation of the water-cooling process of metallic objects, as such, during the cooling process. The tradeoff by losing information about the impact point surface temperature was thus outweighed by the possibility for better determining the water droplet cooling efficiency.

For the aluminum discs, the water droplet cooling efficiency associated with the critical heat flux, i.e., at about 125 °C, was in the range of 80% to 85%. The lowest water droplet cooling efficiency, i.e., in the range of 6% to 10%, was observed at a disc temperature of about 230 °C. Since this temperature was associated with a minimum in the cooling efficiency, it may be defined as the Leidenfrost temperature. The cooling efficiency then slightly increased with increasing temperature up to 400 °C due to the increasing temperature difference between the disc surface and the evaporating levitated droplet.

For stainless steel discs, at the recorded temperatures associated with the critical heat flux, i.e., about 150 °C to 180 °C, the droplet cooling efficiency was found to be in the range of 70% to 80%. The reason for this slightly lower maximum cooling efficiency compared to aluminum is likely due to the differences in thermal properties, i.e., a thermal conductivity of 150 W/mK for aluminum versus 15 W/mK for stainless steel.

For aluminum, the surface temperatures recovered more between each droplet impact compared to stainless steel, i.e., the impingement point was more thermally disturbed by the time the next droplet hit the stainless steel surface. Small variations in droplet impact point and droplet movements just after impact likely explained the higher standard deviations in the recorded efficiency for the stainless steel discs. Large standard deviations in measurements from the temperature regions near the temperature associated with the critical heat flux are also reported in other studies [16], although those researchers did not focus on droplet cooling efficiency.

Clear differences in cooling efficiency were demonstrated between aluminum and stainless steel (same roughness for both metal disc surfaces). It was more challenging to reveal the differences in cooling efficiency within the same material, i.e., for the two different roughnesses studied (Ra 0.4

and Ra 3). The Student's *t*-test ($\alpha < 0.05$) was applied to indicate whether there were statistically significant differences between the water droplet cooling efficiency obtained for Ra 0.4 and Ra 3. The observed water droplet cooling efficiency differences for Ra 0.4 and Ra 3 were for the aluminum discs significant ($\alpha > 0.05$) only for temperatures between 220–310 °C, where the higher surface roughness (Ra 3) gave a slightly higher cooling efficiency. This may be explained by the better possibilities for the water vapor generated to escape through the crevices below the droplet, i.e., resulting in less distance between the droplet and the aluminum surface peaks.

Due to the larger standard deviation in cooling efficiency observed for the stainless steel discs, any observed differences between the surface roughnesses of Ra 0.4 and Ra 3 were not statistically significant, i.e., Student's *t*-test $\alpha > 0.05$. Indeed, for temperatures above 265 °C, the cooling efficiency was practically equal for stainless steel surface roughnesses of Ra 0.4 and Ra 3. It is more difficult to explain this observation. However, many parameters do control the heat and mass transfer in the film boiling regime [7]. For stainless steel, the influence of crevices and peaks may be less prominent due to the heat transfer capacity being 10 times lower than that of similar peaks on the aluminum surface.

The results indicate that the application of fire water early in a fire scenario is very important, i.e., while the water cooling will likely be most efficient and thereby may prevent further temperature increase past the temperature associated with a boiling crisis. Upon reaching the film boiling regime, the cooling efficiency of the stainless steel discs was shown to become as low as about 12% to 14% due to the stable vapor film below the droplet. Even with application of the recommended 10 L/min·m², i.e., 0.167 kg/s·m² recommended by NORSOK [19], the spray would only be able to withdraw 50–60 kW/m² from the fire exposed surface. This is significantly lower than the heat flux that objects may be exposed to in industrial fires, i.e., 250 kW/m² to 350 kW/m². This is a paradox for fire safety engineering.

The literature study did not reveal research papers investigating the absolute cooling efficiency of water droplets applied to hot metal surfaces of e.g., 10-mm wall thickness. Therefore, the present work may be the first to attempt quantifying this for objects of representative wall thicknesses. However, it should be noted that a variety of metal qualities are used in process plants, and that the present study is limited to horizontally aligned stainless steel discs of 10-mm thickness. In the process industry, equipment and pipe work may also be thermally insulated and shielded by stainless steel cladding. Such cladding, with thicknesses of 0.5 mm or 0.7 mm, is unfortunately too thin to be analyzed by the presented setup.

Omitting the fine mesh screen and moving the core setup to the classroom for demonstrating water droplet behavior and cooling efficiency worked well for demonstrating the mentioned physical phenomena to BSc and MSc students in fire safety engineering. The students expressed an increased understanding of water droplets' cooling efficiency as a function of substrate temperature. The potential of very low water cooling efficiency in fire scenarios was noted. Therefore, it can be concluded that this simple setup serves both scientific and educational purposes.

Author Contributions: T.L. conceived the concept. J.S.B. and M.-M.M. designed the experimental setup. J.S.B. performed the experiments; J.S.B. and T.L. analyzed the data; M.-M.M. contributed materials and equipment and Ø.F. contributed as an advisor throughout; J.S.B., M.-M.M. and T.L. wrote the paper.

Funding: J.S.B. was supported by the Norwegian Research Council, Grant No. 257901 and Gassco Inc., Norway, Grant No. PO 4500024195.

Acknowledgments: The authors would like to acknowledge technical support from G. Kleppe. Support in realizing the project from Gunnar Birkeland, Uni Research Polytec, and Terje Øverland and Kjell Erik Kleveland, PDS Protek is also appreciated. The suggestions from the anonymous reviewers for improving the manuscript are highly appreciated.

Conflicts of Interest: The authors declare no conflict of interest.

References

1. Chegini, G.R.; Ghobadian, B. Spray Dryer Parameters for Fruit Juice Drying. *World J. Agric. Sci.* **2007**, *3*, 230–236.
2. Dugas, V.; Broutin, J.; Souteyrand, E. Droplet evaporation study applied to DNA chip manufacturing. *Langmuir* **2005**, *21*, 9130–9136. [[CrossRef](#)] [[PubMed](#)]
3. Deegan, R.D.; Bakajin, O.; Dupont, T.F.; Huber, G.; Nagel, S.R.; Witten, T.A. Capillary flow as the cause of ring stains from dried liquid drops. *Nature* **1997**, *389*, 827–829. [[CrossRef](#)]
4. Lopes, M.-C.; Bonaccorso, E.; Gambaryan-Roisman, T.; Stephan, P. Influence of the substrate thermal properties on sessile droplet evaporation: Effect of transient heat transport. *Colloids Surf. A Physicochem. Eng. Asp.* **2013**, *432*, 64–70. [[CrossRef](#)]
5. Log, T. Water Droplets Evaporating on Horizontal Semi-infinite Solids at Room Temperature. *Appl. Therm. Eng.* **2016**, *93*, 214–222. [[CrossRef](#)]
6. Girard, F.; Antoni, M.; Faure, S.; Steinchen, A. Influence of heating temperature and relative humidity in the evaporation of pinned droplets. *Colloids Surf. A Physicochem. Eng. Asp.* **2008**, *323*, 36–49. [[CrossRef](#)]
7. Misyura, S.Y. The effect of weber number, droplet sizes and wall roughness on crisis of droplet boiling. *Exp. Therm. Fluid Sci.* **2017**, *84*, 190–198. [[CrossRef](#)]
8. Nguyen, T.; Nguyen, A.; Hampton, M.; Xu, Z.; Huang, L.; Rudolph, V. Theoretical and experimental analysis of droplet evaporation on solid surfaces. *Chem. Eng. Sci.* **2013**, *69*, 522–529. [[CrossRef](#)]
9. Zhou, X.; Zhou, B.; Jin, X. Study of fire-extinguishing performance of portable water-mist fire extinguisher in historical buildings. *J. Cult. Herit.* **2010**, *11*, 392–397.
10. Bhatt, N.H.; Pati, A.R.; Kumar, A.; Behera, A.; Munshi, B.; Mohapatra, S.S. High mass flux spray cooling with additives of low specific heat and surface tension: A novel process to enhance the heat removal rate. *Appl. Therm. Eng.* **2017**, *120*, 537–548. [[CrossRef](#)]
11. Fukuda, S.; Kohno, M.; Tagashira, K.; Ishihara, N.; Hidaka, S.; Takata, Y. Behavior of small droplet impinging on a hot surface. *Heat Transf. Eng.* **2014**, *35*, 204–211. [[CrossRef](#)]
12. Lee, C.H.; Kim, D.Y.; Kim, H.D.; Kim, K.C. Dynamic behavior and micro-explosion characteristics of impinging droplets on a high-temperature surface. *J. Vis.* **2015**, *18*, 59–70. [[CrossRef](#)]
13. Gradeck, M.; Seiler, N.; Ruyer, P.; Maillat, D. Heat Transfer for Leidenfrost drops bouncing onto a hot surface. *Exp. Therm. Fluid Sci.* **2013**, *47*, 14–25. [[CrossRef](#)]
14. Pasandideh-Fard, M.; Aziz, S.D.; Chandra, S.; Mostaghimi, J. Cooling effectiveness of a water droplet impinging on a hot surface. *Int. J. Heat Fluid Flow* **2001**, *22*, 201–210. [[CrossRef](#)]
15. Birdi, K.S.; Vu, D.T.; Winter, A. A study of the evaporation rates of small water drop placed on a solid surface. *J. Phys. Chem.* **1989**, *93*, 3702–3703. [[CrossRef](#)]
16. Liang, G.; Mudawar, I. Review of drop impact on heated walls. *Int. J. Heat Mass Transf.* **2017**, *106*, 103–126. [[CrossRef](#)]
17. Bernardin, J.D.; Mudawar, I. The Leidenfrost point: Experimental Study and Assessment of Existing Models. *J. Heat Transf.* **1999**, *121*, 894–903. [[CrossRef](#)]
18. Sawyer, M.L.; Jeter, M.S.; Abdel-Khalik, S.I. A critical heat flux correlation for droplet impact cooling. *Int. J. Heat Mass Transf.* **1997**, *40*, 2123–2131. [[CrossRef](#)]
19. Norsk Standard. *Technical Safety, NORSOK Standard*, 4th ed.; Standard no. S-001; Norsk Standard: Lysaker, Norway, 2008; 62p.
20. Kazemi, Z. Droplet Impaction on Solid Surfaces Exposed to Impinging Jet Fires. Ph.D. Dissertation, Norwegian University of Science and Technology, Trondheim, Norway, 2006.
21. Drange, L.A. A Study of Selected Problems Related to Accidental Process Fires. Ph.D. Dissertation, University of Bergen, Bergen, Norway, 2011.
22. Opstad, S.A.; Wighus, R. *Droplet Sizes from Deluge Nozzles*; NBL F09117; SINTEF Report: Trondheim, Norway, 2009.
23. Chang, H. The myth of the boiling point. *Sci. Prog.* **2008**, *91*, 219–240. [[CrossRef](#)] [[PubMed](#)]
24. Leidenfrost, J.G. *De Aquae Communes Nonnullis Qualitatibus Tractatus*; Okenius: Duisburg, Germany, 1756.
25. Leidenfrost, J.G. On the Fixation of Water in Diverse Fire. *Int. J. Heat Mass Transf.* **1966**, *9*, 1153–1166. [[CrossRef](#)]

26. Faghri, A.; Zhang, Y.; Howell, J.R. *Advanced Heat and Mass Transfer*; Global Digital Press: Columbia, MO, USA, 2010; ISBN 978-0-9842760-0-4.
27. International Standard. *Geometrical Product Specifications (GPS)—Surface Texture: Profile Method—Terms, Definitions and Surface Texture Parameters*; ISO 4287; ISO: Geneva, Switzerland, 1997; 25p.
28. Log, T.; Heskestad, G. Temperatures of Restricted Turbulent Fire Plumes. *Fire Saf. J.* **1998**, *31*, 101–115. [[CrossRef](#)]
29. Chase, M.W. *NIST-JANAF Thermochemical Tables*, 4th ed.; American Institute of Physics: College Park, MA, USA, 1998. Available online: <https://srdata.nist.gov/JPCRD/jpcrdM9.pdf> (accessed on 5 February 2017).




© 2018 by the authors. Licensee MDPI, Basel, Switzerland. This article is an open access article distributed under the terms and conditions of the Creative Commons Attribution (CC BY) license (<http://creativecommons.org/licenses/by/4.0/>).

II

Article

Influence of Acetone and Sodium Chloride Additives on Cooling Efficiency of Water Droplets Impinging onto Hot Metal Surfaces

Joachim Søreng Bjørge ^{1,2}, Svein Arne Bjørkheim ³, Maria-Monika Metallinou ^{4,*},
Torggrim Log ⁴  and Øyvind Frette ²

¹ Q Rådgivning AS/PDS Protek, Øvregata 126, 5527 Haugesund, Norway; jsb@q-rad.no

² Department of Physics and Technology, University of Bergen, 5020 Bergen, Norway; Oyvind.Frette@ift.uib.no

³ Omega Areal AS, Kvassanesvegen 4, 5582 Ølensvåg, Norway; sveinarne@omega.no

⁴ Western Norway University of Applied Sciences, Fire Disaster Research Group, 5528 Haugesund, Norway; torggrim.log@hvl.no

* Correspondence: monika.metallinou@hvl.no; Tel.: +47-9882-5104

Received: 19 May 2019; Accepted: 17 June 2019; Published: 19 June 2019



Abstract: In the present work, the cooling efficiency of water droplets falling onto hot aluminum and stainless steel discs from heights of 12.5 cm, 25 cm, 50 cm and 100 cm, corresponding to speeds of 1.5 m/s, 2.2 m/s, 3.1 m/s and 4.4 m/s, respectively, were studied. The discs were aligned at 0° (horizontal), 30° and 60° inclination. The water application rate was 0.022 g/s and the droplet diameters studied were 2.5 mm, 3.2 mm and 3.7 mm. Acetone solutions (300 ppm and 700 ppm) as well as a NaCl (35 g/kg) solution, emulating seawater, were tested to evaluate the influence of an active surfactant on the recorded cooling efficiency. The droplets with higher impact speed resulted in lower cooling efficiency, especially at disc temperatures above the Leidenfrost temperature, likely due to more vigorous droplets bouncing. Larger inclination did, as expected, result in lower cooling efficiency. At temperatures associated with nucleate boiling, the water droplets with NaCl conspicuously displayed higher cooling efficiency at about 110 °C. However, at temperatures between 120 °C and the Leidenfrost temperature, acetone and NaCl additives did not significantly alter the cooling efficiency of the water droplets. Above the Leidenfrost temperature, a minor increase in cooling efficiency was observed for the acetone solutions. Overall, the additives only marginally changed the water droplet cooling efficiency. The standard industrial water application rate (i.e., 10 L/min·m²) is shown to be insufficient compared to the heat fluxes expected in pool and jet fires (i.e., 250 kW/m² and 350 kW/m², respectively).

Keywords: hot metals; water droplet cooling efficiency; acetone; NaCl

1. Introduction

From the start of the oil and gas industry (O&G industry) on the Norwegian continental shelf, safety standards have been established and developed. These national standards and guidelines regulate several industrial safety aspects. This applies both to design and operation of facilities and installations on land and at sea. The industry must operate and maintain its facilities and equipment so that accidents, such as fires and explosions, are prevented.

During the last 3–4 decades, the international O&G industry has experienced several major accidents [1,2]. Much work is therefore undertaken to limit the fire and explosion risks associated with processing highly combustible hydrocarbon products. However, severe fires in this industry still occur [2,3]. Equipment and piping is often constructed of different steel alloys, being especially

vulnerable to impinging jet fires (i.e., the release of hydrocarbon gases under pressure resulting in well mixed high temperature flames of significant momentum). The weakening of exposed pressurized piping, equipment and load bearing constructions when heated may result in escalation of the fire scenario.

In the unfortunate scenario of an industrial fire, active fire protection is very important to prevent escalation of the incident. Among active fire protection measures, fire water systems prevail as outdoor fire protection, with the aim to cool fire exposed objects as well as to cool the flame zone to reduce heat exposure and prevent escalation. The NORSOK S-001 standard devotes a whole section to active fire protection [4]. For process areas, the design criteria are known to be standardized and general (e.g., 10 L/min·m²). However, very few studies document cooling efficiency as a function of exposed metal temperature for representative water droplet sizes, which also includes all the relevant droplet cooling/evaporation regimes. The few studies found in the literature are generally devoted to horizontal objects [5].

Water droplets impinging onto hot surfaces display different boiling regimes, depending mainly on the surface temperature. The German theologian and physician Johann Gottlob Leidenfrost was the first scientist to study this phenomenon [6]. He noticed that when the temperature of a particular metal object exceeded a certain value, the water droplets were moving about at the hot metal surface with a very low evaporation rate (i.e., a very low cooling rate). Since then, it has become common to call the temperature for the onset of this phenomenon as the Leidenfrost temperature. Different parameters, like the metal itself (thermal properties) or surface roughness (depth of anomalies and pattern), as well as droplet size and deposition method used, exert influence on the observed Leidenfrost temperature. With increasing temperature, the cooling rates of hot metal objects impacted by water droplets go through a maximum in the nucleate boiling regime (i.e., where the critical heat flux is observed) and then decline rapidly in the transition boiling regime as vapor cushions develop below the droplets. At high temperatures, this process results in inefficient cooling, reaching a minimum value at the Leidenfrost temperature for the particular material. The Leidenfrost temperature is not fixed, as the droplet application mode also seems to exert a few K of influence. The importance of surface roughness appears ambiguous [7].

Bernardin and Mudawar [8] presented a review on Leidenfrost temperatures for water on heated materials. Liang and Mudawar [7] conducted a review concerning droplets impinging onto hot metals for all involved boiling regimes. Some researchers studied the behavior of different droplet parameters such as size, impingement velocity [9], wall material [10,11], temperature below the Leidenfrost point [12], influence of solid–liquid contact time [13], and evaporation of layers of aqueous salt solution [14]. Additives may also be used to reduce surface tension and thus enhance heat transfer [15,16]. Benedetto et al. [17] studied the phenomenon called combustion induced rapid phase transition (cRPT), and the effect different mixtures of CH₄/O₂/N₂ have on this behavior. They found cRPT to be most conspicuous at O₂ concentrations above 21 mole%. Bjørge et al. [5] presented a simple and straightforward method for obtaining the cooling efficiency of droplets impinging onto hot metal discs in the temperature range of 85 °C to 410 °C, covering all the boiling regimes experienced when water droplets are applied to hot metal objects.

The present study aims at analyzing: (a) The cooling efficiency of water droplets with various impingement speed and diameter falling on heated stainless steel discs with varied inclination, and (b) the effect of additives reducing surface tension on water droplet cooling efficiency. Experiments with acetone (additive, two different concentrations) were performed on aluminum discs for different impingement speeds at horizontal disc surface, as well as different surface inclinations for one selected impingement speed. The effect of adding NaCl at concentrations emulating seawater was also studied. The temperature range for all experiments was 85 °C to 410 °C, covering all water-droplet boiling regimes. The recorded droplet cooling efficiency for these different conditions is discussed.

2. Experimental Setup and Data Processing

2.1. Experiments on Stainless Steel Discs

Discs (diameter: 50 mm, thickness: 10 mm, surface roughness Ra 3, pattern: concentric circles) were fabricated in Stainless steel AISI 316 (room temperature thermal conductivity approximately 15 W/m·K). The discs were suspended by four horizontal type K thermocouples (1.6 mm stainless steel mantle), as shown in Figure 1, thereby minimizing unnecessary heat losses. The thermocouples penetrated the disc radially at a 90° angle, until 10 mm from the centre, and symmetrically as to the disc's thickness. The temperatures of the four thermocouples were recorded by a data logger (National Instruments NI cDAG-9184, Austin, TX, USA) at a frequency of 1 s⁻¹. Their average temperature was recognized as the disc temperature.

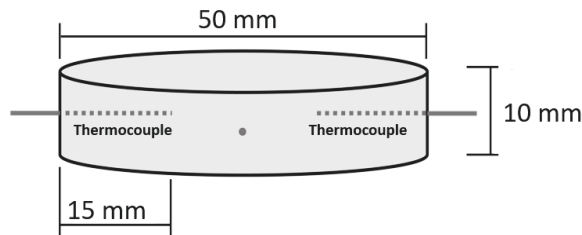


Figure 1. Sketch of metal disc with inserted thermocouples at 90° horizontal separation [5].

The experimental setup and method is described in detail in [5] and the principal setup is shown in Figure 2.

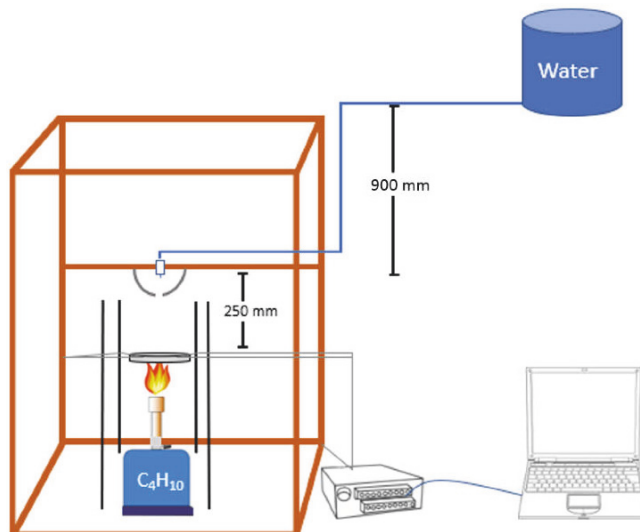


Figure 2. Sketch of the experimental setup. (The heater and the disc can be seen in the lower part of the air draft limiting frame).

The experimental procedure was as follows: The metal disc was first heated by a butane burner to about 430 °C. Next, the burner was removed and the disc left to “air-cool” to 85 °C, thus establishing the baseline temperature decay for the dry-cooling (i.e., free cooling). During this period, the setup frame was covered by a fine mesh screen to prevent any air drafts influencing the measurements.

Dry-cooling was also recorded after a series of droplet cooling experiments, with no more than 5 droplet (wet-cooling) experiments before a new dry-cooling temperature decay was recorded. This procedure ensured that any changes in ambient conditions in the laboratory would similarly affect both dry and wet-cooling recordings.

During the wet-cooling, droplets of distilled water with a flow rate of 0.022 g/s (giving 2 to 3 droplets per second, depending on the droplet sizes) were supplied to the hot discs. The studied parameters were: droplet diameter (2.5 mm, 3.2 mm and 3.7 mm), impingement height (25 cm, 50 cm, 100 cm, and surface inclination (0° (horizontal), 30° and 60°). Prior to the measurements, the discs were aligned using a leveler, and heated by the burner to about 430°C (see Figure 2). The burner was then removed and the discs were cooled to 410°C , ensuring time for any internal temperature gradients to spatially equilibrate prior to water droplet application. The experiment as such (i.e., supply of water droplets) started when the disc had cooled beyond 410°C . The measurement range used for the data analysis was from 400°C to 85°C , covering the principal droplet cooling regimes.

2.2. Experiments on Aluminum Discs with NaCl and Acetone Additives

To study droplet cooling efficiency with acetone and NaCl (salt) additives, aluminum (EN AW-6082) discs of 50 mm diameter and 10 mm thickness, surface roughness Ra 0.4 and thermal conductivities of about $170\text{ W/m}\cdot\text{K}$ were used. The choice of a material with much higher thermal conductivity than stainless steel was made to obtain results with less scattering [5]. The choice of a smooth surface (Ra 0.4) was made based on discrepancies in the literature as to the effect of surface roughness on cooling efficiency. Acetone solutions, as in the study by Bhatt et al. [16] (300 ppm (vol/vol) and 700 ppm (vol/vol) in distilled water) were used in the experiments, written as ppm throughout the article.

Droplets with a 2.5 mm diameter were released from heights of 0.125 m, 0.25 m and 0.50 m, resulting in impingement speeds of 1.5 m/s, 2.2 m/s and 3.1 m/s, respectively [5]. This represents a variation in impact Weber number from 150 to 500 for the 300 ppm acetone solution, 160 to 550 for the 700 ppm acetone solution and 80 to 320 for the NaCl solution. The surface tension for the acetone solution supplied by [16] was used for the Weber number calculations. Because of the lowered surface tension when adding acetone, no larger droplet diameters were studied since any attempt to generate larger droplets with our injection needle technique [5] resulted in a continuous flow of water rather than droplets.

The aluminum surfaces were aligned at 0° (horizontal), 30° and 60° for a 25 cm droplet fall height. At droplet fall heights of 12.5 cm and 50 cm, only the horizontal configuration was studied. The NaCl was mixed into distilled water at room temperature to a concentration of 35 g NaCl pr. kg, emulating representative seawater which is often used for fire control in the O & G industry. The same test configuration and parameters as for the acetone tests were chosen for the droplet cooling experiments involving NaCl.

Based on the differences in cooling rate with and without applying water droplets, disc mass and disc specific heat, the absolute cooling (in W) of the applied water droplets was determined. Droplet cooling was normalized by the water application rate and water evaporation heat to obtain the dimensionless cooling efficiency as a function of disc temperature, as briefly explained in Section 3.

The temperature range studied in the present work covered all droplet evaporation regimes. This included mass diffusion below 104°C [18], nucleate boiling and increasing cooling efficiency at temperatures above 104°C [19] until the critical temperature associated with maximum cooling efficiency followed by decreasing cooling efficiency to the Leidenfrost temperature, as well as film boiling at temperatures above the Leidenfrost temperature [6].

3. Theory: Determining Cooling Efficiency

Droplet impact point and principal convective air flows for upward facing disc surfaces in both horizontal and inclined disc positions are shown in Figure 3.

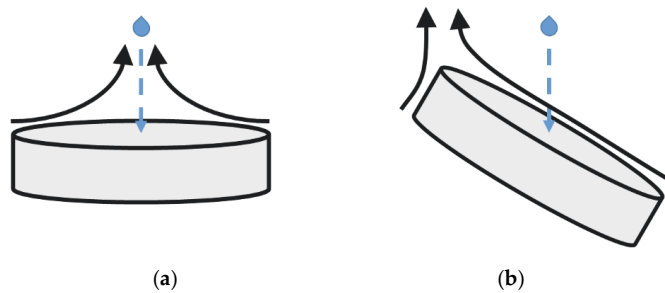


Figure 3. Sketch of the droplet impact point (blue lines) and convective air cooling flow for the upward facing disc surfaces (black lines) in both horizontal (a) and inclined surfaces (b).

Based on differences in cooling rates between dry- and wet-cooling, mass and specific heat of the disc for each orientation, the heat flow to the impinging water droplets can be calculated. Subtracting the respective temperature versus time derivatives for the given disc temperature gives the net water droplets cooling rate, $\left\{\frac{dT}{dt}(T)\right\}_{\text{Net}}$ (K/s). Based on the mass, m (kg), and the specific heat, $C_p(T)$ (J/kg K), of the disc as a function of temperature, the water droplet cooling heat flow is given by:

$$\dot{Q}_{\text{Drops}}(T) = m_{\text{Disc}} \cdot C_p(T) \cdot \left\{\frac{dT}{dt}(T)\right\}_{\text{Net}} \quad (\text{W}), \quad (1)$$

In the present work, the specific heat data for stainless steel and aluminum given by [5] were used in Equation (1). Ignoring the enthalpy needed to heat the water to 100 °C and heat the steam above 100 °C, the heat required to evaporate droplets at a rate, \dot{m}_{Drops} (kg/s), is given by:

$$\dot{Q}_{\text{Max}} = \dot{m}_{\text{Drops}} \cdot \Delta H_{\text{vap}} \quad (\text{W}). \quad (2)$$

Representative recordings of temperature versus time for dry-cooling and wet-cooling (by applying water droplets) are shown in Figure 4. The respective heat losses are shown in Figure 5. It can be seen from Figures 4 and 5 that dry-cooling was faster for the inclined orientation than for the horizontal orientation. Prior to, and after a measurement series, the free-cooling temperature versus time history was therefore always obtained. It should also be noted that the discs loose heat by thermal radiation, which was assumed independent on inclination.

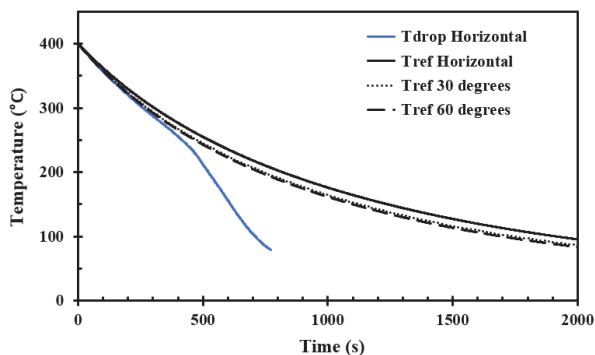


Figure 4. Temperature versus time for a representative stainless steel disc with 2.4 mm diameter droplets and 25 cm impingement height, including reference (dry-cooling) recordings for horizontal, 30° and 60°.

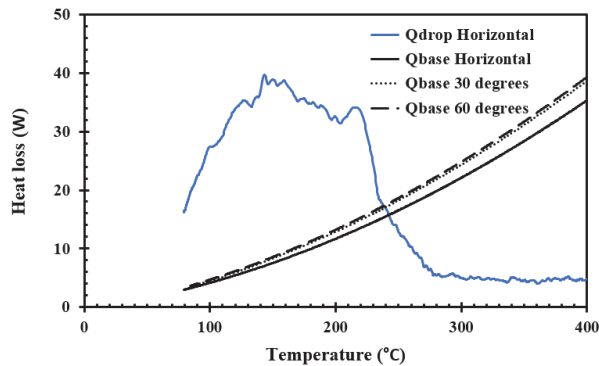


Figure 5. Heat loss to the water droplets in a representative test for droplets impinging a horizontal stainless steel disc, the corresponding dry-cooling (reference) heat loss for the horizontal disc and similar dry-cooling heat losses for 30° and 60° inclined discs.

The relative droplet cooling efficiency can then be calculated by:

$$\xi = \dot{Q}_{\text{Drops}}(T) / \dot{Q}_{\text{Max}} \quad (3)$$

4. Cooling Efficiency Results

4.1. Pure Water Droplets on Hot Stainless Steel Discs

4.1.1. Effect of Inclination on Cooling Efficiency at 25 cm Impingement Height, for Various Droplet Diameters

The results obtained for the selected droplet diameters at 0° (horizontal) 30° and 60° orientation are presented in Figures 6–8, respectively. Each curve represents the average of 5 measurement series with identical conditions.

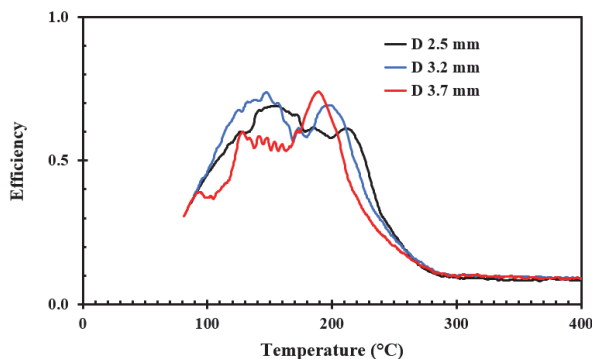


Figure 6. Cooling efficiency for pure water droplets with 25 cm impingement height for horizontal orientation and various droplet diameters. Droplet speed 2.2 m/s.

The results indicate highest cooling efficiency for the horizontal discs. This may be due to droplets remaining on the surface for a longer period. For the most inclined surface, 60°, the effect of the droplet size is limited. However, the results indicate that the smallest droplets display the lowest cooling efficiency. Similar results were also obtained for impingement height 50 cm and 100 cm (results not included).

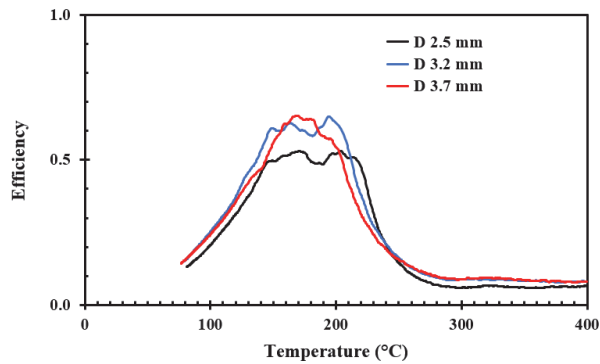


Figure 7. Cooling efficiency for pure water droplets with 25 cm impingement height for 30° inclination and various droplet diameters. Droplet speed 2.2 m/s.

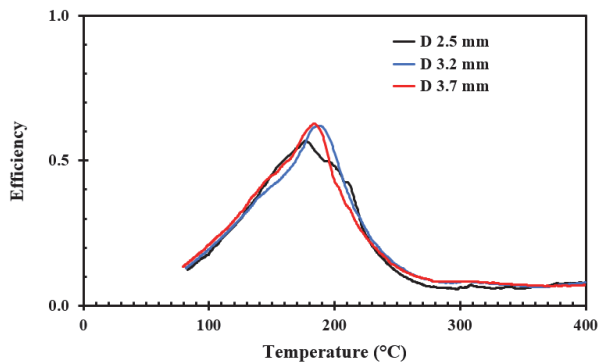


Figure 8. Cooling efficiency for pure water droplets with 25 cm impingement height for 60° inclination and various droplet diameters. Droplet speed 2.2 m/s.

4.1.2. Effect of Inclination on Cooling Efficiency for Droplet Diameter 2.5 mm for Various Impact Speeds

The results obtained for 25 cm, 50 cm and 100 cm impingement heights for 0° (horizontal), 30° and 60° inclination are presented in Figures 9–11, respectively.

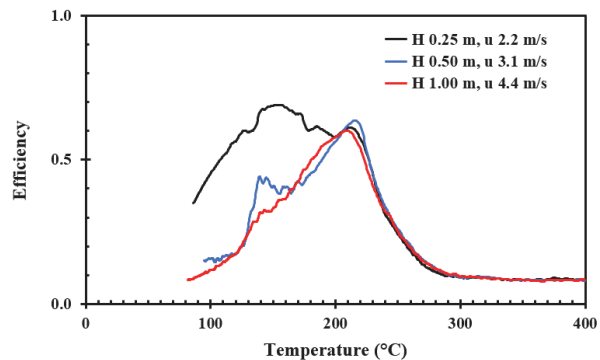


Figure 9. Cooling efficiency for pure water droplets at horizontal disc orientation, droplet diameter 2.5 mm. Impingement heights and speeds are given in the figure label.

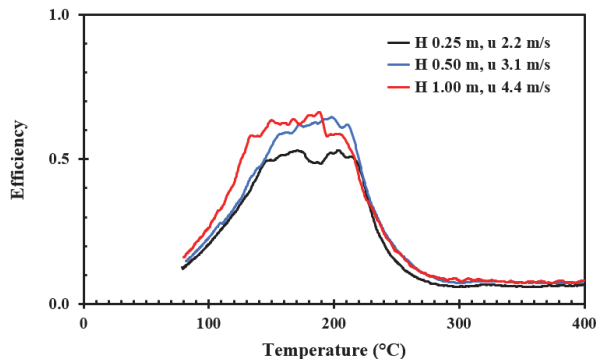


Figure 10. Cooling efficiency for pure water droplets at 30° disc inclination, droplet diameter 2.5 mm. Impingement heights and speeds are given in the figure label.

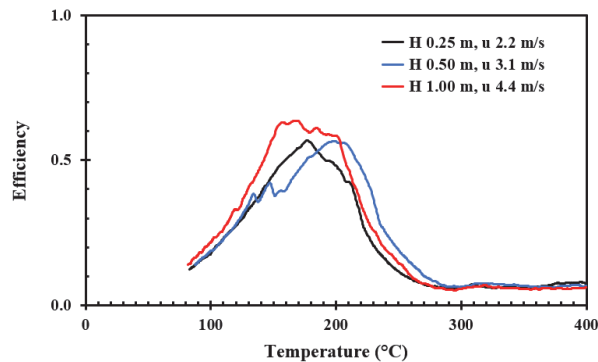


Figure 11. Cooling efficiency for pure water droplets at 60° disc inclination, droplet diameter 2.5 mm. Impingement heights and speeds are given in the figure label.

For impingement height 25 cm, the results indicate that horizontal orientation gave the highest cooling efficiency at temperatures of about 150 °C. This may be due to droplets remaining on the surface for a longer period. For inclined surfaces, increasing impingement height seems to increase cooling efficiency, though the cooling efficiency curves cross for parts of the investigated temperature range. Similar results were obtained for droplet diameter 3.2 mm and 3.7 mm (results not included).

The effect of inclination when both droplet diameter and impingement height were fixed is summarized in Figure 12. The three curves are previously presented in Figure 9 (black curve in Figure 12), Figure 10 (blue curve in Figure 12) and Figure 11 (red curve in Figure 12).

4.2. Cooling Efficiency of Water Droplets with Additives

4.2.1. Cooling Efficiency for Horizontal Orientation and Varying Impact Speeds

The results obtained for the water droplets with acetone and NaCl additives compared to the results for pure water droplets are shown in Figures 13 and 14 for 12.5 and 25 cm impingement height, respectively.

As presented in Figures 13 and 14, the 700 ppm acetone in water gave the highest cooling efficiency in the transition boiling regime and highest cooling efficiency at boiling crisis; the cooling efficiency increased from 80% to 90% at boiling crisis. For the NaCl additive, it is interesting to notice that the cooling efficiency was conspicuously increased at about 110 °C compared to the other experiments. The

nucleate boiling regime is clearly in a narrower temperature range, and the Leidenfrost temperature is slightly increased.

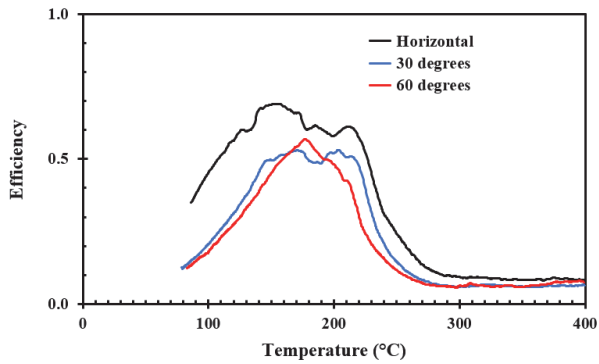


Figure 12. Cooling efficiency for pure water droplets with diameter 2.5 mm, various orientations at impingement height 25 cm and speed 2.2 m/s.

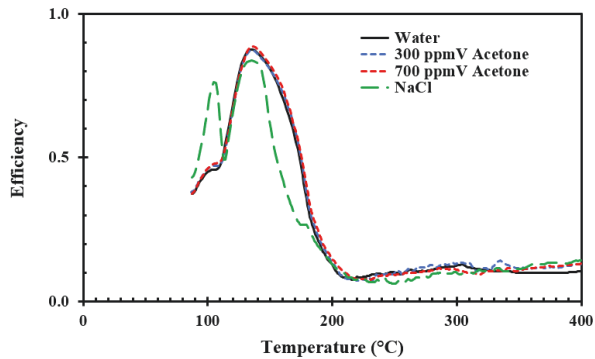


Figure 13. Cooling efficiency for water droplets with and without additives for droplet diameter 2.5 mm, horizontal orientation at impingement height 12.5 cm (speed 1.5 m/s).

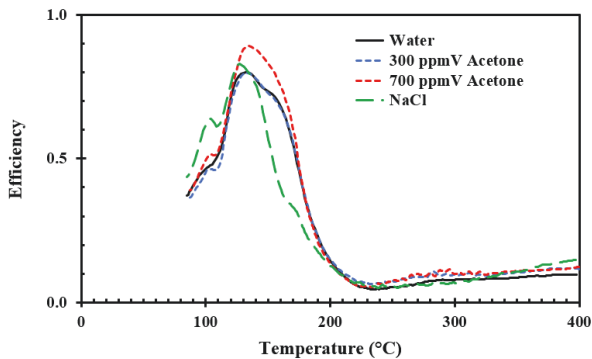


Figure 14. Cooling efficiency for water droplets with and without additives for droplet diameter 2.5 mm, horizontal orientation at impingement height 25 cm (speed 2.2 m/s).

The addition of 300 ppm acetone had a limited effect compared to pure water. This contradicts to the findings of Bhatt et al. [16]. However, they observed foam-formation from the given mixture

applied to their hot disc in form of a spray. The foam was believed to develop due to the combination of low surface tension of the mixture combined with the sprays' high mass flux (described to be in the range of 45.6–125.4 kg/m²·s) which is considerably larger than that used in our experiments, where no foam was observed. However, for temperatures above the Leidenfrost point (Figure 13), our results confirm the results of Bhatt et al. [16], where the 300 ppm acetone solution achieved slightly higher cooling efficiency than 700 ppm solution for the 12.5 cm impingement height.

4.2.2. Effect of Inclination on Cooling Efficiency

The results obtained for various disc orientations are presented in Figures 15–17 for 300 ppm and 700 ppm acetone solutions and 35 g/kg NaCl solution, respectively.

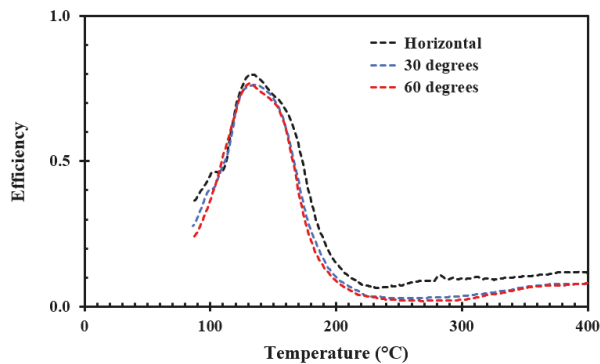


Figure 15. Cooling efficiency for 300 ppm acetone water solution for droplet diameter 2.5 mm, and various orientations at impingement height 25 cm (speed 2.2 m/s).

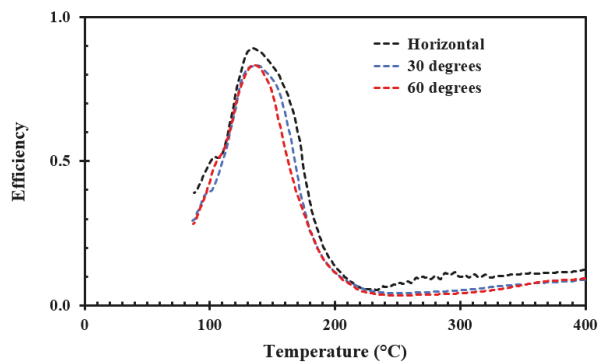


Figure 16. Cooling efficiency for 700 ppm acetone water solution for droplet diameter 2.5 mm, and various orientations at impingement height 25 cm (speed 2.2 m/s).

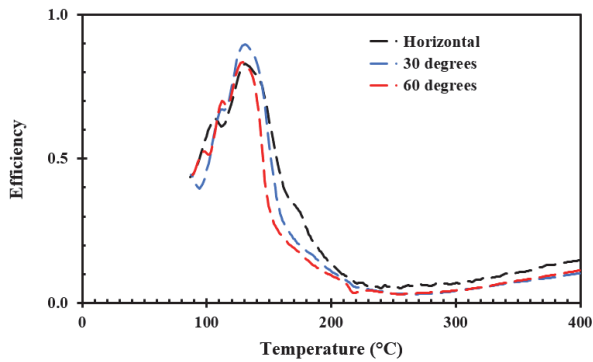


Figure 17. Cooling efficiency for 35 g/kg NaCl water solution for droplet diameter 2.5 mm, and various orientations at impingement height 25 cm (speed 2.2 m/s).

4.2.3. Effect of Impact Speed on Cooling Efficiency

The results obtained for variation in impinging heights are presented in Figures 18–20 for 300 ppm and 700 ppm acetone solutions and 35 g/kg NaCl solution, respectively.

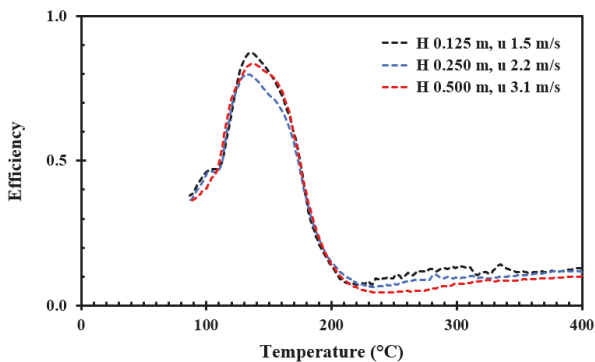


Figure 18. Cooling efficiency for 300 ppm acetone solution for droplet diameter 2.5 mm, horizontal orientation. Impingement heights and speeds are given in the figure label.

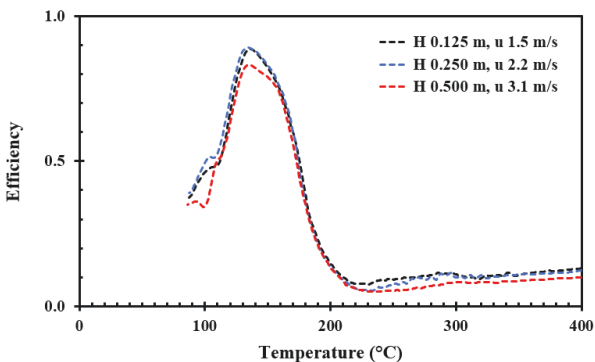


Figure 19. Cooling efficiency for 700 ppm acetone solution for droplet diameter 2.5 mm, horizontal orientation. Impingement heights and speeds are given in the figure label.

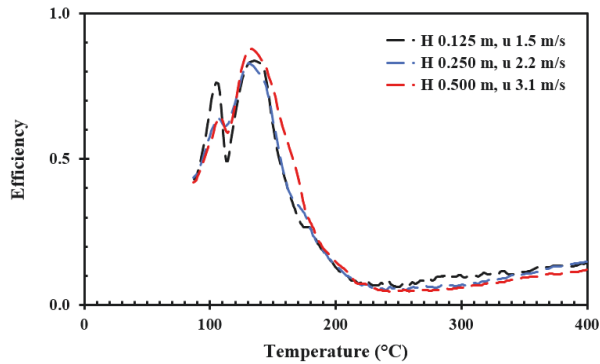


Figure 20. Cooling efficiency for 35 g/kg NaCl solution for droplet diameter 2.5 mm, horizontal orientation. Impingement heights and speeds are given in the figure label.

The standard deviation of the efficiency recorded for horizontal orientation and 25 cm impingement height as a function of temperature is presented in Figure 21.

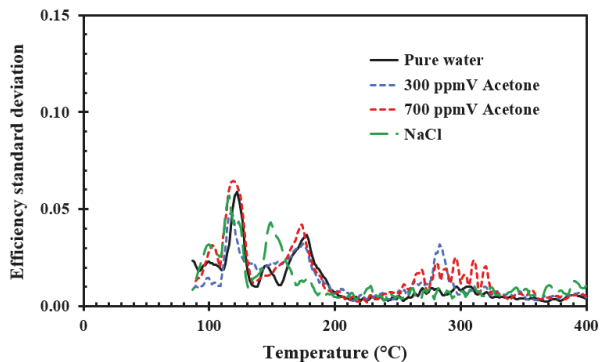


Figure 21. Comparison of cooling efficiency standard deviation for horizontal orientation at 25 cm impingement height and speed 2.2 m/s.

To evaluate whether the efficiency recorded for the aluminum discs with different mixtures of surfactants were significantly different, as well as different compared to pure water, a Student's *t*-test was introduced requiring an $\alpha < 0.05$. The difference in cooling efficiency as presented in Figures 13–20 was, through the complete temperature range, i.e., 85 °C to 400 °C, for all configurations not statistically valid, with only two exceptions. The exceptions were the comparison between 12.5 cm and 50 cm impingement height for the 700 ppm acetone solutions and the conspicuous peak in cooling efficiency for the NaCl solution at 110 °C.

4.3. Error Analysis

Only minor variations in the droplet application rate and droplet diameter were observed. The standard deviation for the water application rate was within 3% and for the droplet diameter, it was within $\pm 1\%$. The 25 cm impingement height was measured to within 1 mm, that is, giving less than 1% error in the calculated droplet speed. Given the rather large standard deviations for the observed water droplet efficiency, the droplet diameter, application rate and droplet speed can be considered sufficiently constant for comparing the results from the different measurement series.

Before each measurement series, the discs were aligned horizontally (0°), 30° and 60° to within 0.5° . Some slight misalignment during the heating and cooling cycles cannot be completely excluded, and this may to some extent influence the results. However, misalignment larger than 1° was not observed after the completion of each measurement series. It is therefore reasonable to believe that differences recorded in the water droplet cooling efficiencies were caused by the parameters altered on purpose.

5. Discussion

When assessing different parameters, such as surface roughness, the expected steam layer thickness is an essential parameter. Using computational methods, Chatzikyriakou et al. [20] showed that the vapor layer exhibits oscillations for sessile water droplets, eventually settling to a thickness in the range of 20–40 μm . This result is also supported by the theoretical value obtained by Wachters et al. [21] for similar droplet conditions (28.9 μm). Some contradictions were presented in [7,22] regarding the surface roughness influence on the heat transfer for the transition boiling and film boiling regime. Whereas some researchers describe increasing surface roughness to increase the heat transfer, others claim the opposite. It is believed that this contradiction can be related to the fact that some heat transfer dependences are valid in certain surface roughness ranges. There are also different ways of producing a given surface roughness; for example, the surface pattern could differ significantly, while still giving the same Ra value. This was the main reason for choosing Ra 0.4 (smooth surface) as a primary surface roughness for the experiments with acetone surfactant additives.

In the present work, there was no flame present during the water droplet cooling of the hot discs. Additionally, when applying water droplets, the discs were always the hottest object, hotter than the generated steam from the evaporating droplets. No condensation would therefore occur on the disc. The presented method could therefore not reveal phenomena such as cRPT [17].

For the horizontally aligned stainless steel discs, the smallest droplets were observed to give a higher cooling efficiency over a wider temperature range. This is probably due to the larger relative contact surface area to the volume of the smaller droplets. The largest droplets demonstrated higher peak efficiency (i.e., higher cooling efficiency at boiling crisis) which was recorded to be in the range of 64–75% for the different configurations. The droplet cooling efficiency increased slightly with increasing impact velocity for 30° and 60° orientation. This is believed to be due to a rise in pressure inside the droplet and slowdown of the steam layer. For horizontal orientation, a higher cooling efficiency over a wider temperature range was observed for the lowest impact velocity. A reason for this could be the two identified boiling regimes/mechanisms of droplet bouncing based on Weber-number (We), as described by Bianco et al. [23]. In the first boiling regime, which represents droplet impingement at high We , drop impact inertia is significantly greater than surface tension. This renders the rebound less elastic. Due to droplet break up, the droplet more easily bounces off the hot metal disc.

For the horizontal configuration, droplet bouncing was more prominent for the largest droplets while the smaller droplets (lower Weber number) tended to attach better to the surface. The droplet cooling efficiency was shown to decrease with increased inclination for the lowest impact velocity (2.2 m/s). For higher droplet velocities, an increase in cooling efficiency for 30° inclination was observed. In line with the results of other researchers [8], a cooling efficiency maximum was observed at 130°C to 210°C . In the film boiling regime, at temperatures above the Leidenfrost temperature (290–300 $^\circ\text{C}$), the cooling efficiency was reduced to about 10%. This result was also in agreement with previous research [8], with the added value in the present study being a concrete value for the cooling efficiency. For industrial fire water applications, a standard water supply rate of $10\text{ L}/\text{min}\cdot\text{m}^2$ gives a cooling capacity of $43\text{ kW}/\text{m}^2$ at 10% cooling efficiency. This cooling heat flux is significantly lower than expected heat fluxes associated with pool and jet fires ($250\text{ kW}/\text{m}^2$ and $350\text{ kW}/\text{m}^2$, respectively) [4].

For the aluminum discs, the water droplet cooling efficiency was not significantly altered by adding acetone surfactant. The Leidenfrost point was only marginally changed for the horizontal orientation and the cooling efficiency increased approximately 2% at higher temperatures. However,

the cooling efficiency at boiling crisis increased by 12% compared to pure water when using 700 ppm acetone and 25 cm impingement height. A similar trend was not observed in the other configurations. The droplet cooling efficiency increased slightly with a decrease in impact velocity. An increase in droplet velocity gave no conclusive indication at temperatures below the Leidenfrost temperature, however a low velocity gave a higher cooling efficiency in the film boiling regime. A reason for this may be as already mentioned and is supported by the study of Biance et al. [23]. The observed Leidenfrost temperature was not significantly altered. Bhatt et al. [16] reported that the droplet speed had to be 13.5–20 m/s for droplets less than 0.45 mm to significantly increase the Leidenfrost temperature when 300 ppm acetone surfactant was added.

A cooling efficiency maximum at 120–140 °C was observed for all aluminum disc tests. This temperature range is significant smaller than observed for the stainless steel tests. This is likely due to an order of magnitude higher thermal conductivity for aluminum versus stainless steel (i.e., 170 W/m·K versus 15 W/m·K). In the film boiling regime, at temperatures above the Leidenfrost temperature (230–240 °C), the cooling efficiency was in the range of 4–10% dependent on the aluminum disc orientation, where increased inclination gave a decrease in cooling efficiency. This is most likely due to impinging droplets more easily bouncing off after their first collision.

In the experiments with emulated seawater (35 g NaCl/kg), two distinct peaks were observed; the first at approximately 110 °C and the second at 130 °C (i.e., the temperature of critical heat flux for the aluminum discs). For the first temperature peak, salt was observed along the edge of the droplet contact area. The salt layer, which started to form on the metal surface, is believed to increase the evaporation rate in the triple-phase (liquid–gas–solid). A similar observation was made by Cui et al. [24].

The nucleate boiling regime was observed to be narrower for the NaCl solution while the transition boiling regime was prolonged and the Leidenfrost temperature was significantly increased (i.e., about 20–30 K) compared to pure water. This is in agreement with the observations of other researchers [25].

In fire water piping, there may be alien objects, like gravel, remains of mussels, etc. Such objects may restrict the flow of the system, in the worst cases render the system inoperable. Fire water systems therefore need to be tested regularly for confirming the system functionality. Using seawater for fire water raises concerns due to corrosion under insulation as well as corrosion attacks on cabling and instrumentation. The limited differences in cooling efficiency between pure water and 35 g/kg NaCl solution observed in the present study therefore do not support that seawater should be the preferred fire water supply.

It should be mentioned that the conspicuous nucleate boiling regime peak in NaCl solution cooling efficiency may be a result of the present study test method. If seawater was applied to the hot surface while the surface temperature was increasing rather than decreasing, the results could be altered in favor of salt water given that more salt may be deposited on the surface, increasing the water droplet surface contact. To test this was not possible with the current setup, and was therefore outside the scope of the present study.

For temperatures above the Leidenfrost temperature, the observed cooling efficiency slightly increased with increasing temperature up to 400 °C. This is most likely caused by the increasing temperature difference between the evaporating levitated droplets and the disc surface. The increase was, however, larger for the aluminum discs than for the stainless steel discs. An interpretation of this finding would require further studies.

During the droplet cooling, temperature gradients will be set up in the disc, especially when using stainless steel as the disc material. However, to analyze this was outside the scope of the present study. For future studies, it would be interesting to do backwards numerical analysis based on the recorded heat loss rates to reveal the magnitude of the internal temperature gradients.

6. Conclusions

The reported low film boiling regime cooling efficiency for pure water, as well as for 35 g/kg NaCl solution, 300 ppm and 700 ppm acetone solutions, demonstrates the importance of activating fire water

deluge or monitors early in case of an industrial fire. Else, it may be very difficult to cool exposed pipes, equipment and structural members. Late activation of fire water will, due to the low cooling efficiency, have limited effect for temperatures at and above the Leidenfrost temperatures. Overall, the additives only marginally improved the water droplet cooling efficiency. It may therefore be concluded that the standard industrial water application rate (i.e., 10 L/min·m²) is insufficient compared to the heat fluxes expected in industrial pool and jet fires.

Author Contributions: T.L. conceived the concept. J.S.B. and M.-M.M. designed the experimental setup. J.S.B. and S.A.B. performed the experiments; J.S.B. analyzed the data; J.S.B., M.-M.M. and T.L. wrote the article; Ø.F. contributed as an advisor throughout.

Funding: J.S.B. was supported by the Norwegian Research Council, Grant No. 257901 and Gassco Inc., Norway, Grant No. PO 4500024195.

Acknowledgments: The authors would like to acknowledge technical support from Gisle Kleppe and Gunnar Thuestad. Support from Gunnar Birkeland, Uni Research Polytec, Terje Øverland and Kjell Erik Kleveland, PDS Protek, in realizing the project is also appreciated. The suggestions from the anonymous reviewers for improving the manuscript are highly appreciated.

Conflicts of Interest: The authors declare no conflict of interest.

References

1. U.S. Chemical Safety and Hazard Investigation Board. Investigation Report Executive Summary. In *Drilling Rig Explosion and Fire at the Macondo Well, Report No. 2010-10-I-OS*; U.S. Chemical Safety and Hazard Investigation Board: Washington, DC, USA, 2010.
2. Kletz, T. What Went Wrong? In *Case Histories of Process Plant Disasters and How They Could Have Been Avoided*, 5th ed.; Institution of Chemical Engineers: London, UK, 2009; ISBN 13:978-1-85617-531-9.
3. Murray, J.A.; Sander, L.C.; Wise, S.A.; Reddy, C.M. *Gulf of Mexico Research Initiative 2014/2015 Hydrocarbon Intercalibration Experiment: Description and Results for SRM 2779, Gulf of Mexico Crude Oil and Candidate SRM 2777 Weathered Gulf of Mexico Crude Oil*; NISTIR 8123; National Institute of Standards and Technology: Gaithersburg, MD, USA, 2016.
4. Norsk Standard. *Technical Safety, NORSOK Standard*, 4th ed.; Standard No. S-001; Norsk Standard: Lysaker, Norway, 2008; 62p.
5. Bjørge, J.S.; Metallinou, M.M.; Log, T.; Frette, Ø. Method for Measuring Cooling Efficiency of Water Droplets Impinging onto Hot Metal Discs. *Appl. Sci.* **2018**, *8*, 953. [[CrossRef](#)]
6. Leidenfrost, J.G. On the Fixation of Water in Diverse Fire. *Int. J. Heat Mass Transf.* **1966**, *9*, 1153–1166. [[CrossRef](#)]
7. Liang, G.; Mudawar, I. Review of drop impact on heated walls. *Int. J. Heat Mass Transf.* **2017**, *106*, 103–126. [[CrossRef](#)]
8. Bernardin, J.D.; Mudawar, I. The Leidenfrost point: Experimental Study and Assessment of Existing Models. *J. Heat Transf.* **1999**, *121*, 894–903. [[CrossRef](#)]
9. Fukuda, S.; Kohno, M.; Tagashira, K.; Ishihara, N.; Hidaka, S.; Takata, Y. Behavior of small droplet impinging on a hot surface. *Heat Transf. Eng.* **2014**, *35*, 204–211. [[CrossRef](#)]
10. Lee, C.H.; Kim, D.Y.; Kim, H.D.; Kim, K.C. Dynamic behavior and micro-explosion characteristics of impinging droplets on a high-temperature surface. *J. Vis.* **2015**, *18*, 59–70. [[CrossRef](#)]
11. Gradeck, M.; Seiler, N.; Ruyer, P.; Maillet, D. Heat Transfer for Leidenfrost drops bouncing onto a hot surface. *Exp. Therm. Fluid Sci.* **2013**, *47*, 14–25. [[CrossRef](#)]
12. Pasandideh-Fard, M.; Aziz, S.D.; Chandra, S.; Mostaghimi, J. Cooling effectiveness of a water droplet impinging on a hot surface. *Int. J. Heat Fluid Flow* **2001**, *22*, 201–210. [[CrossRef](#)]
13. Birdi, K.S.; Vu, D.T.; Winter, A. A study of the evaporation rates of small water drop placed on a solid surface. *J. Phys. Chem.* **1989**, *93*, 3702–3703. [[CrossRef](#)]
14. Misyura, S.Y.; Morozov, V.S. Nonisothermal Evaporation of Layers of Aqueous Salt Solutions. *J. Heat Transf.* **2018**, *141*, 1–9. [[CrossRef](#)]
15. Zhou, X.; Zhou, B.; Jin, X. Study of fire-extinguishing performance of portable water-mist fire extinguisher in historical buildings. *J. Cult. Herit.* **2010**, *11*, 392–397.

16. Bhatt, N.H.; Pati, A.R.; Kumar, A.; Behera, A.; Munshi, B.; Mohapatra, S.S. High mass flux spray cooling with additives of low specific heat and surface tension: A novel process to enhance the heat removal rate. *Appl. Therm. Eng.* **2017**, *120*, 537–548. [[CrossRef](#)]
17. Benedetto, A.D.; Cammarota, F.; Sarli, V.D.; Salzano, E. Effect of Diluents on Rapid Phase Transition of Water Induced by Combustion. *Am. Inst. Chem. Eng.* **2012**, *58*, 2810–2819. [[CrossRef](#)]
18. Log, T. Water Droplets Evaporating on Horizontal Semi-infinite Solids at Room Temperature. *Appl. Therm. Eng.* **2016**, *93*, 214–222. [[CrossRef](#)]
19. Chang, H. The myth of the boiling point. *Sci. Prog.* **2008**, *91*, 219–240. [[CrossRef](#)]
20. Chatzikyriakou, D.; Walker, S.P.; Hewitt, G.F.; Narayanan, C.; Lakehal, D. Comparison of measured and modelled droplet–hot wall interactions. *Appl. Therm. Eng.* **2009**, *29*, 1398–1405. [[CrossRef](#)]
21. Wachters, L.H.J.; Bonne, H.; Van Nouhuis, H.J. The heat transfer from a hot horizontal plate to sessile water drops in the spheroidal state. *Chem. Eng. Sci.* **1966**, *21*, 923–936. [[CrossRef](#)]
22. Misyura, S.Y. The effect of weber number, droplet sizes and wall roughness on crisis of droplet boiling. *Exp. Therm. Fluid Sci.* **2017**, *84*, 190–198. [[CrossRef](#)]
23. Biance, A.L.; Chevy, F.; Clanet, C.; Lagubeau, G.; Quéré, D. On the elasticity of an inertial liquid shock. *J. Fluid Mech.* **2006**, *554*, 47–66. [[CrossRef](#)]
24. Cui, Q.; Chandra, S.; McCahan, S. The effect of dissolving gases or solids in water droplets boiling on a hot surface. *J. Heat Transf.* **2001**, *123*, 719–728. [[CrossRef](#)]
25. Huang, C.K.; Carey, V.P. The effects of dissolved salt on the Leidenfrost transition. *Int. J. Heat Mass Transf.* **2007**, *50*, 269–282. [[CrossRef](#)]



© 2019 by the authors. Licensee MDPI, Basel, Switzerland. This article is an open access article distributed under the terms and conditions of the Creative Commons Attribution (CC BY) license (<http://creativecommons.org/licenses/by/4.0/>).

III



Small Scale Hydrocarbon Fire Test Concept

Joachim Søreng Bjørge ^{1,2,*}, Maria-Monika Metallinou ³, Arjen Kraaijeveld ³ and Torgrim Log ^{3,4}

¹ Q Rådgivning AS/PDS Protek, Øvregata 126, 5527 Haugesund, Norway

² Department of Physics and Technology, University of Bergen, 5020 Bergen, Norway

³ Western Norway University of Applied Sciences, 5528 Haugesund, Norway; monika.metallinou@hvl.no (M.M.M.); Arjen.Kraaijeveld@hvl.no (A.K.)

⁴ Statoil Kårstø, Kårstø, 5562 Tysværåvåg, Norway; tlog@statoil.com

* Correspondence: jsb@q-rad.no; Tel.: +47-9098-1051

Received: 13 October 2017; Accepted: 10 November 2017; Published: 14 November 2017

Abstract: In the oil and gas industry, hydrocarbon process equipment was previously often thermally insulated by applying insulation directly to the metal surface. Fire protective insulation was applied outside the thermal insulation. In some cases, severe corrosion attacks were observed due to ingress of humidity and condensation at cold surfaces. Introducing a 25 mm air gap to prevent wet thermal insulation and metal wall contact is expected to solve the corrosion issues. This improved insulation methodology does, however, require more space that may not be available when refurbishing older process plants. Relocating structural elements would introduce much hot work, which should be minimized in live plants. It is also costly. The aim of the present study is therefore to develop a test concept for testing fire resistance of equipment protected with only air-gap and thermal insulation, i.e., without the fire-protective insulation. The present work demonstrates a conceptual methodology for small scale fire testing of mockups resembling a section of a distillation column. The mockups were exposed to a small-scale propane flame in a test configuration where the flow rate and the flame zone were optimized to give heat flux levels in the range 250–350 kW/m². Results are presented for a mockup resembling a 16 mm thick distillation column steel wall. It is demonstrated that the modern distance insulation in combination with the heat capacity of the column wall indicates 30+ minutes fire resistance. The results show that this methodology has great potentials for low cost fire testing of other configurations, and it may serve as a set-up for product development.

Keywords: small scale fire testing; hydrocarbon fires; low cost

1. Introduction

The hydrocarbon process industry is still important for the modern world economy. It involves physical processes like separation, distillation, cracking, etc., to produce the products that are needed in the market. Equipment, such as distillation columns, usually requires thermal insulation to prevent heat losses or heat gains depending on their temperature span and the ambient conditions. As this is an aging industry, the equipment is gradually upgraded to extend the equipment lifetime.

During the last 3–4 decades, this industry has experienced severe accidents [1,2]. Much effort is therefore put into limiting the fire and explosion risks that are associated with processing the highly combustible hydrocarbon products. However, every year there are still severe fires in the hydrocarbon processing industry [1,3]. Since much of the equipment is working at elevated pressures, a loss of containment in fire-exposed equipment may violently release huge quantities of flammable materials [2,3]. Active and passive fire protection measures are therefore very important to prevent the violent escalation of industrial fires.

Corrosion protection paint was applied to prevent external corrosion of the process equipment. Mineral based thermal insulation (typically 50 mm thickness) was then put in direct contact with this

paint. In order to achieve proper passive fire protection, high temperature resistant mineral based insulation (typically 30–50 mm thickness) was provided outside the thermal insulation. Stainless-steel cladding (typically 0.7 mm thickness) represented the outer surface preventing ingress of rain and snow. The cladding also served as flame deflection in a fire scenario protecting the passive fire protection and the thermal insulation from direct flame exposure. During the 1990's, much research was done to evaluate the fire testing procedures of installed process equipment [4,5]. In general, the selected solutions were demonstrated to give sufficient resistance to hydrocarbon pool fires.

After 20+ years of service, inspection has shown that it is necessary to do maintenance and rehabilitation of process equipment, such as hydrocarbon distillation columns [5]. In some cases, where the units operate below the ambient air dew point, natural convection has supplied humidity to the thermal insulation, finally becoming soaked in water. This ruins the thermal insulation capacity since only 4% moisture by volume can reduce the thermal efficiency by 70% due to the high thermal conductivity of water [1,6]. The aged corrosion protection paint has in several cases not been able to prevent severe corrosion attacks. A complete rehabilitation is therefore often required.

Today, an improved insulation methodology, where an air gap (typically 1" thick) is introduced, prevents the direct contact between the thermal insulation and the steel unit. The thermal insulation is kept at this distance by perforated metal plates (aluminum or stainless steel) that are electrically insulated from the steel wall by non-conducting spacers. The new insulation method adds at least 52 mm to the equipment diameter. In some situations there is, however, not sufficient room available for this added spacing. Relocating structural elements would require much hot work, which should be avoided in live plants, and, shutting down the plant for such work may not be realistic. The possibility to provide room by relocating structural elements is also very costly.

Due to the typical size of such distillation columns, e.g., 4 m diameter and 20–25 m height and the operating pressures, the columns walls are comparatively thick. The walls therefore represent much thermal capacity. It could therefore in principle be a possibility that the complete system, i.e., the wall, air gap, perforated metal plate, thermal insulation, and cladding, would result in sufficiently slow temperature increase in a fire scenario. To demonstrate this by large scale testing is, however, costly. As an alternative, small scale tests may give valuable information. It was therefore decided to look for options for testing the new thermal insulation method in high heat loads.

The present work investigates a concept for the small scale testing of mockups resembling a part of a typical hydrocarbon distillation column, thermally insulated according to the modern requirements. Mockups built according to these requirements were exposed to a small-scale propane flame where the flow rate and flame zone were optimized to limit heat losses and give high heat flux levels, e.g., in the range 250–350 kW/m². The fire dynamics principles of the small-scale testing are outlined, and it is explained how it is possible to achieve heat flux levels that are normally considered only in larger scales. The design of the setup to minimize effects of limited size is discussed. Methods to document the validity of the small-scale testing are provided. Gas temperatures were recorded by mantle thermocouples, as well as a plate thermometer for heat exposure evaluations. Temperatures were also recorded in the mockup cladding, in the thermal insulation and in the steel wall sections. Results are presented for a 16 mm thick wall mockup. The paper describes the theoretical considerations and the physics principles involved. Then, the experiments and the results are presented. Finally, the limitations of the method are discussed regarding the potential exposure to full scale liquid fires at the location of the specific distillation column.

2. Theoretical Considerations

2.1. Fire Dynamics

Fire testing is usually done in standardized furnaces that are fired according to given temperature time curves. Structural building elements are tested in furnaces fired in accordance with the ISO 834 temperature time curve [7]:

$$T = 20 + 345 \cdot \log_{10}(8 \cdot t + 1) \text{ (}^\circ\text{C)} \quad (1)$$

where t (min) is the exposure time. Oil and gas fires are expected to quickly result in very high flame temperatures. The standardized hydrocarbon (HC) test curve developed by the Norwegian Petroleum Directorate is therefore different from the ISO 834 temperature time curve and given by [8]:

$$T = 20 + 1080 \cdot \left(1 - 0.325 \cdot e^{-0.167 \cdot t} - 0.675 \cdot e^{-2.5 \cdot t}\right) \text{ (}^\circ\text{C)} \quad (2)$$

It should be noted that there are also other temperature time curves for less severe fire exposure situations, e.g., façade fire exposure and more severe hydrocarbon fire exposure, such as the French HydroCarbon Modified (HCM) curve. The latter one was developed as a result of several full scale fire tests where temperatures well in excess of 1100 °C were recorded. The HCM curve is given by [9]:

$$T = 20 + 1280 \cdot \left(1 - 0.325 \cdot e^{-0.167 \cdot t} - 0.675 \cdot e^{-2.5 \cdot t}\right) \text{ (}^\circ\text{C)} \quad (3)$$

The three standard temperature time curves are shown in Figure 1.

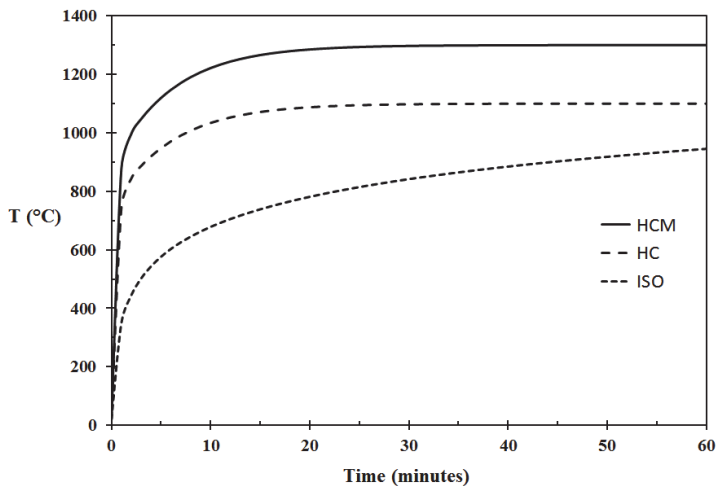


Figure 1. Fire testing temperature time curves.

In industrial fires it is common to distinguish between pool fires resulting from liquid spills and jet fires resulting from the release of pressurized gas. In these two fire regimes, the pool fires are expected to result in heat flux levels of 250 kW/m², while jet fires are expected to result in heat flux levels of 350 kW/m² [10]. The reason for the jet fires giving more severe heat exposure is due to the higher speed of the combustion products giving a higher convective heat transfer coefficient, as well as the increased turbulence level resulting in cleaner burning and higher flame temperatures. The jet fires are also in general more erosive. Standardized testing is usually performed according to the ISO 22899 Jet Fire Test [11]. The 0.3 kg/s propane jet fire, i.e., approximately 14 MW heat release rate, is released

horizontally through a standardized jet nozzle for various time periods exposing e.g., panels, wall and pipe configurations coated with Passive Fire Protection (PFP) materials.

The radiant heat flux that is absorbed by the exposed object is a function of the temperature and emissivity of the receiving surface, as well as the emissivity of the flames. The net heat flux received by an object fully engulfed in flames is given by:

$$\dot{Q}_{net}'' = h(T_f - T_s) + \varepsilon_f \sigma T_f^4 - \varepsilon_s \sigma T_s^4 \quad (\text{W/m}^2) \quad (4)$$

where h (W/m K) is the convective heat transfer coefficient, T_f (K) is the flame temperature, T_s (K) is the temperature of the exposed surface, ε_f is the emissivity of the flames, ε_s is the emissivity of the solid and σ (5.67×10^{-8} W/m² K⁴) is the Stefan-Boltzmann constant. The emissivity of the flames is given by:

$$\varepsilon_f = 1 - \exp(-KL) \quad (5)$$

where K (1/m) is the extinction coefficient and L (m) is the optical flame thickness. Due to the potential size of fires in the oil and gas industry, it is common to assume that the flames are optically thick, i.e., the emissivity is unity.

2.2. The Test Concept

Due to the number of parameters exerting influence on the test severity it is not sufficient to e.g., define 1100 °C recorded by a thermocouple as the target of the flame temperature. Test configuration, heat losses, etc. also needs to be considered. Testing the mockup in a situation that is similar to the real fire is appealing, i.e., where a fire exposes the equipment to be tested. The concept chosen for the present study is shown in Figure 2. It is, however, evident that even though the flames exposing the stainless-steel cladding may be sufficiently hot to comply with e.g., the HC curve, as described in Equation (2), the heat losses from the exposed stainless-steel cladding may reduce the heat exposure substantially. In a small scale, the setup presented in Figure 2 will not work properly due to radiative heat losses.

The convective heat transfer coefficient is dependent on the flame temperature, the hot gas velocity and the turbulence level. It is independent of the flame thickness. However, if the exposed cladding “views” only hot objects, the optical flame thickness becomes much less relevant for heat radiation as long as the exposed surfaces radiate sufficient heat at each other. This may indeed be the case with a fire scenario in a process plant that is dominated by thermally insulated equipment. Reconsidering the set-up to include fire exposed neighbor objects may therefore increase the heat exposure significantly, as shown in Figure 3.

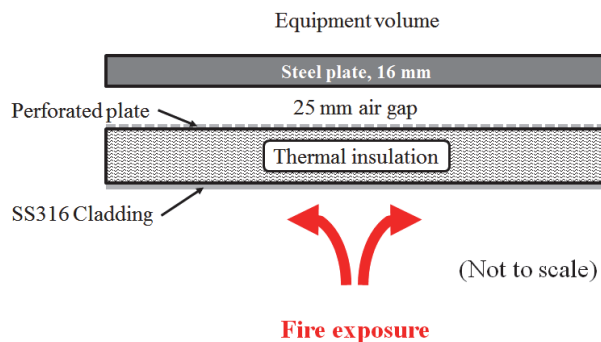


Figure 2. Conceptual sketch 1 of the fire test set-up.

In order for the test set-up shown in Figure 3 to work properly, the fire needs to be sufficiently intense and the dimensions must be large enough to ensure a limited size influence. An axisymmetric set-up, with a central cylindrical fire source would represent a simple test configuration. Since it is easy to get hold of radial propane burners, it was convenient to design the mockup in the cylindrical coordinate system. The steel plate was therefore cut to a disk shape. When compared to a real scale industry fire, the fire insulation in Figure 3, i.e., below the flame volume, represents neighbor equipment radiating at the exposed surface of interest.

In the real setting, there is also a back side of the distillation column to which the heat exposed steel will lose heat by convection and radiation. The test setup was therefore designed, as shown in Figure 4. During preliminary testing it was observed that even the set-up as shown in Figures 3 and 4 was “leaking too much heat” to the surroundings. It was therefore tried to “box” the flame zone somewhat in by light weight heat resistant bricks. The purpose of these was to prevent ingress of ambient air entering into and cooling the lower parts of the flame zone and the lower cladding. The light weight bricks blocked the view from the flame zone to ambient conditions and reradiated heat back to the flame zone as soon as their surfaces got heated. This principle is further explained in Section 4.

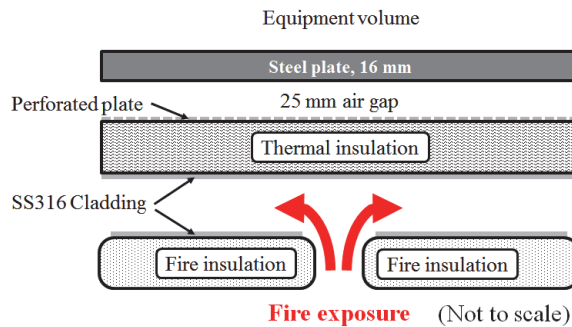


Figure 3. Conceptual sketch 2 of the test set-up where the exposed cladding views heat exposed neighbor objects (fire insulated cladding).

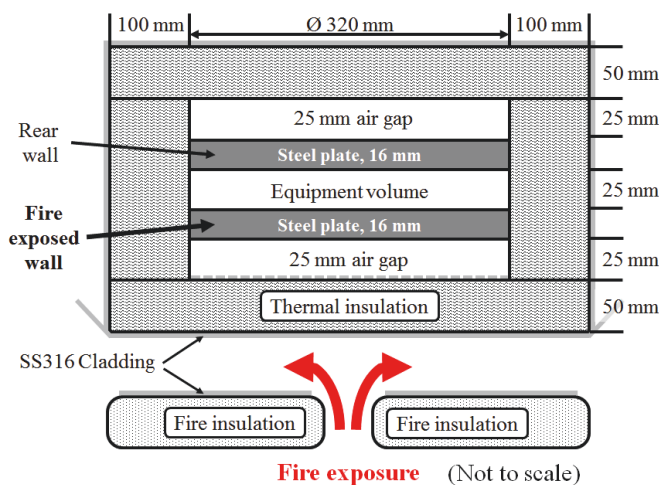


Figure 4. Conceptual sketch of the complete test set-up including mockup.

Distillation columns are often quite large structures, i.e., diameter 4 m and height 20–25 m. When considering a wall thickness only a small fraction of the column diameter, i.e., 16 mm to 4000 mm, the heat flow into the system may be considered one-dimensional. The small scale testing should therefore also be one-dimensional. The radial configuration is very convenient when given a cylindrical burner located at radius zero. Arranging the cylindrical propane fire source vertically, i.e., in positive z-direction, and exposing a horizontal mockup, the heat flow would be one-dimensional through the thermal insulation as long as the size of the mockup is not very large when compared to the deflected flames. The heat exposure should be as independent of radius as possible. Selecting a convenient test specimen diameter is therefore important.

On the other hand, a very low diameter mockup would be more influenced by edge effects due to limited size. It was therefore decided to use steel plate dimension of diameter 20 times the thickness, i.e., diameter 320 mm. This represented a sufficient small scale and a convenient test plate mass (10 kg) for manual handling. Test specimens larger than that would probably result in less uniform heat flow, or required a larger fire source. Limited radial temperature gradients should nevertheless be confirmed by recording temperatures at different locations during fire testing.

2.3. Test Temperatures

The NORSOK S-001 [10] argues that in heat exposure calculations the total heat flux should be set to 250 kW/m² for pool fires and 350 kW/m² for jet fires. The oil and gas companies have therefore recently started specifying 250 kW/m² for pool fires and 350 kW/m² for jet fires, e.g., the Statoil requirements for new installations, TR2237 [12]. For heat transfer calculations, this TR recommends a convective heat transfer coefficient 100 W/m² K, flame emissivity unity and the steel and cladding emissivity 0.85. Flame temperatures of 1050 °C and 1200 °C then corresponds to 250 kW/m² and 350 kW/m² to an object at 20 °C, respectively.

In tests like this, one may introduce cooled total flux meters to record the heat flux levels to the test object. The heat flux meter would, however, in this small-scale setting, not fit in without severely interfering with the heat flux that is received by the test object. Given a combustion chamber propane flame thickness of about 50 mm, the radiation from the exposed solid surfaces quickly dominates the heat flux levels. The best way to ensure proper heat flux levels is then to record the cladding temperatures. This may be done by fixating a thermocouple to the inner cladding surface. Alternatively, introducing a plate thermocouple directly viewing the cladding adds much information about the heat flux levels. A 100 mm by 100 mm by 20 mm thickness type K plate thermometer (100 mm PT, article number 5928050-001, Pentronic AB, Västervik, Sweden), whose function is explained in [13–16], was therefore introduced flush with the fire insulation below the flame zone viewing directly upwards, as shown in Figure 5. It should be noted that this is the opposite of the orientation intended for such plate thermometers. In this orientation, it is mostly exposed to the heat radiation that it can view from the cladding mockup in addition to convective heat that is received from the propane flame. Facing upwards and aligned flush with the fire insulation cladding it had virtually no influence on heat transfer within the flame zone. The surfaces of the PTs are blasted, and heat treated to obtain an emissivity of about 0.9, i.e., about the same value as the suggested by the TR2237 [12]. During the fire, it is believed that all of the surfaces approach at least emissivity 0.9 due to oxidation processes.

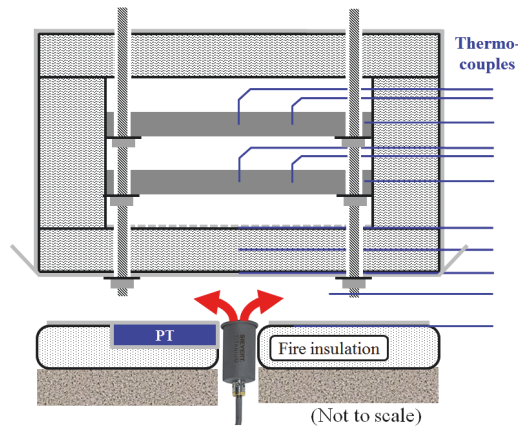


Figure 5. Sketch of mockup including propane gas burner, type K mantle thermocouples, flush mounted plate thermometer (PT), and light weight concrete supporting the fire insulation.

The active part of the plate thermometer, i.e., the stainless-steel plate, had the same thickness as the cladding used in the industry, i.e., 0.7 mm thickness. The flush mounted plate thermometer allowed for a very compact flame volume, exposing the mockup during testing. It should also be noted that the plate thermometer was not designed for the temperatures it was to be exposed to in the present work. It therefore represented an important, but weak, part of the experimental setup which needed to be validated.

To prevent excessive heat exposure to the mockup, the mockup was covered by cladding on the radial surface as well as on the top surface. The direct fire exposed cladding continued 3 cm outside the radius of the mockup and was folded and bent 45° to guide any excess flames away from the mockup, thus reducing the heat stresses and allowing for repeated testing.

3. Materials and Methods

The mockup was arranged with type K thermocouples as indicated in Figure 5. The nearly completed mockup prior to Test 1 is shown in Figure 6. The temperatures were recorded using a datalogger (type 34970A Data Acquisition/Data Logger Switch Unit, Keysight, Santa Rosa, CA, USA (formerly Agilent's Electronic Measurement)).



Figure 6. Mockup nearly ready for fire exposure. (Thermocouples exiting to the right).

A burner (Sievert 346051, Titan 60 mm diameter), which was fed by propane gas, was used as the fire source, see Figure 7. The burner was pre-bent about 30° by the producer and was carefully bent another 60° (bending radius 50 mm) in the present work in order to be arranged horizontally for vertical flames as indicated in Figure 5. It was adjusted to burn with full air access. The gas supply was kept constant during the flame exposure by a flow control unit (Gas control unit, C₃H₈ 225 L/min, build 2612, Brooks Instrument Inc., Hatfield, PA, USA).



Figure 7. Propane burner (Sievert 346051, titanium 60 mm diameter).

The mockup ready for testing is shown in Figure 8a,b for Test 1 and Test 2, respectively. In Test 1, the propane supply was 0.5 g/s. There were no flame containment bricks along the perimeter during this test. In Test 2, the propane supply was 0.75 g/s and light weight bricks (Skamotek 225, Skamol Inc., Nykøping Mors, Denmark) were arranged along the perimeter of the mockup to prevent cold air ingress and limit radiative heat losses from the combustion zone. In addition to contributing in re-radiation, the light weight bricks reduced the view factor of the ambient considerably, as well as ensured gas flow in positive *r*-direction. A photo of the last seconds of Test 2, when some of the light weight bricks were removed for visual inspection, is shown in Figure 9.

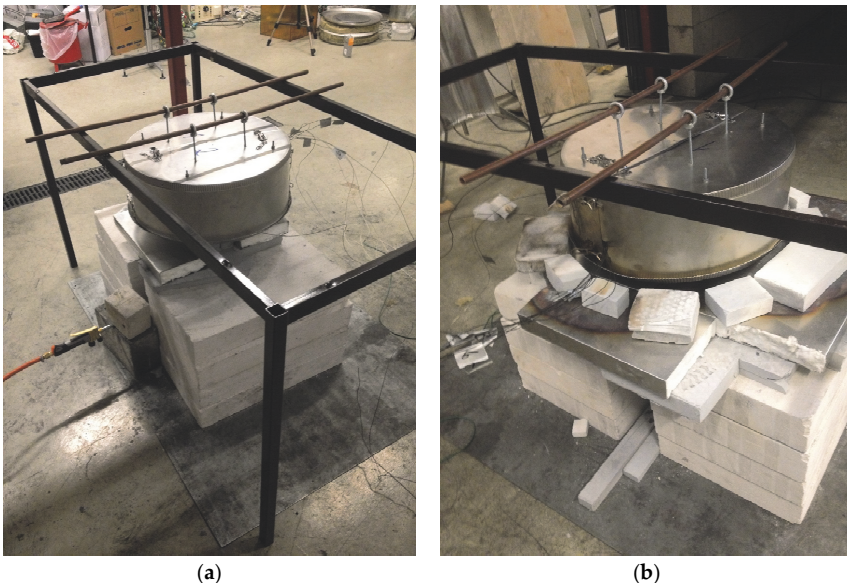


Figure 8. Ready for fire testing; (a) Test 1 and (b) Test 2.



Figure 9. Test 2. (Air flow restrictors removed for visual inspection 30 s before test completion.)

4. Results

The temperatures recorded in Test 1 are shown in Figure 10 (an initial problem with one thermocouple was resolved after about 8 min). The recorded flame temperature was above 1100 °C. The plate thermometer (PT) did, however, record much lower temperatures. The explanation for the discrepancy between the two temperature recordings may be a result of the PT also viewing the ambient temperature outside the flame zone and/or cold air entering the lower part of the flame zone cooling the PT. The PT temperature and the temperature inside the mockup cladding show similar temperatures. The temperature recorded just below the cladding protecting the fire insulation below the flame zone show even lower temperatures. This clearly indicates ambient air ingress cooling the lower parts of the flame zone.

The thermal insulation survived the 30+ min heat exposure, as seen in Figure 11a. The cladding suffered some spalling, but it kept its flame deflection capacity during the fire exposure.

The experience with the open flame zone was a strong motivation for (i) increasing the propane flow, and (ii) introducing flame containing light weight bricks limiting ambient air ingress to the flame zone, and serving as ambient conditions radiation shields and re-radiation units.

The temperatures recorded in Test 2 are shown in Figure 12. It is clearly seen that this test exposed the mockup to a far more severe fire scenario. The temperatures recorded in the flame zone were more than 100 °C higher than in Test 1. For most of the test the flame temperatures, as well as the PT temperatures, were well above 1200 °C.

The thermal insulation was, as shown in Figure 13a,b, severely deteriorated. Traces of glass-like material were observed within the remains of the thermal insulation. Some of the remains showed a powder like structure, which still reduced the heat flow from the flame exposed cladding to the steel plate.

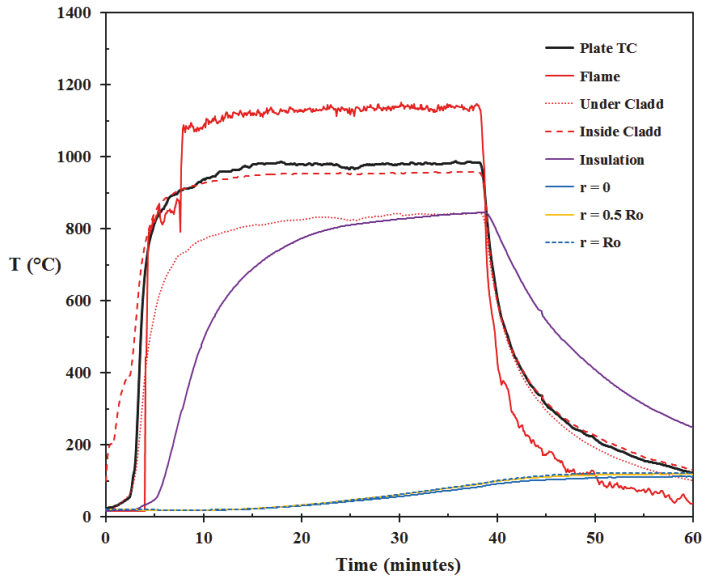


Figure 10. Temperatures recorded in Test 1 (Plate TC is the temperature of the plate thermometer, Flame is the temperature recorded in the flame zone, Under Cladd is the temperature recorded below the lower cladding, Inside Cladd is the temperature recorded inside the upper (exposed) cladding, Insulation is the temperature recorded in the center of the thermal insulation, $r = 0$, $r = 0.5 R_o$ and $r = R_o$ are the temperatures recorded in the exposed 16 mm steel plate at 0 cm, 8 cm and 15.5 cm radius, respectively).

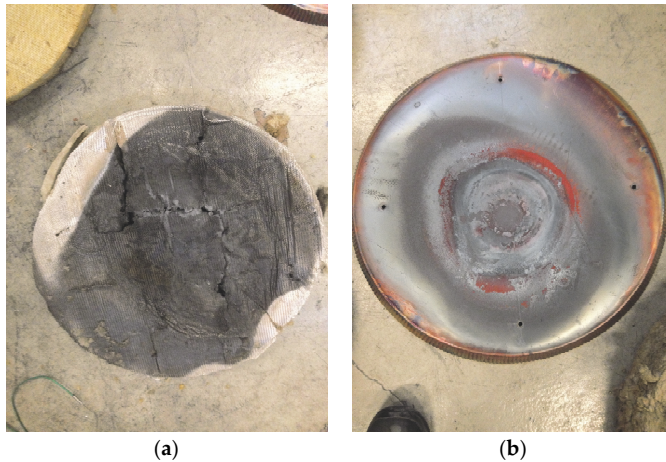


Figure 11. Thermal insulation (a) and cladding (b) after Test 1.

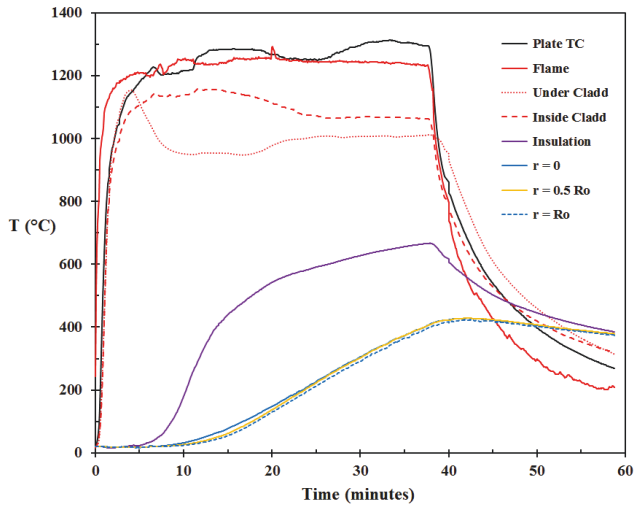


Figure 12. Temperatures recorded in Test 2 (Plate TC is the temperature of the plate thermometer, Flame is the temperature recorded in the flame zone, Under Cladd is the temperature recorded below the lower cladding, Inside Cladd is the temperature recorded inside the upper (exposed) cladding, Insulation is the temperature recorded in the center of the thermal insulation, $r = 0$, $r = 0.5 R_o$ and $r = R_o$ are the temperatures recorded in the exposed 16 mm steel plate at 0 cm, 8 cm and 15.5 cm radius, respectively).

The temperature of the plate thermometer (PT) varied significantly through the test. Spalling, as seen in Figure 14, may influence the temperature to a minor extent. But, as there is only a small heat flow through the thermally insulated PT, there must be other explanations for the varying temperature. Air drafts through the experimental set-up may be a sound explanation.

The temperatures just below the fire insulating cladding during the first 4–5 min closely followed the PT temperatures. This indicates that the ambient air flow keeping the temperature much lower in Test 1 was prevented in Test 2. In Figure 12, it is observed that the temperature below the fire insulation cladding at about 5 min started to decrease. This is probably due to the thermocouple losing contact with the cladding due to buckling. The thermocouple inside the mockup cladding was not fixed and lost contact when the cladding surface buckled. A similar effect was not observed for the plate thermometer, in which, the thermocouple junction is welded to the rear side of the exposed surface. The plate thermometer therefore represented the best source of surface temperature recordings in these tests.



Figure 13. (a) Upper part of exposed thermal insulation after Test 2 and (b) lower part thermal insulation after Test 2.

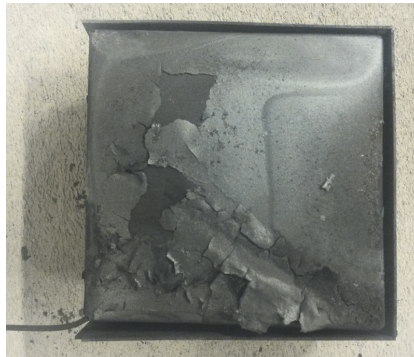


Figure 14. Plate thermometer after Test 2.

The most interesting observation is, however, that the temperatures recorded in the 16 mm thick steel plate for 30+ min stayed below 400 °C. This is a good indication of the total system fire resistance in this particular case where the steel plate represented a significant heat sink. It is also seen that the temperatures at the center of the steel plate, i.e., at $r = 0$, and halfway out to the perimeter, i.e., at $r = 0.5 R_o$, generally do not deviate much. There are, however, some differences between these two temperatures from 10 to 20 min. This may be due to a higher convective heat transfer at the point of propane jet fire impingement, while the gradually increasing radiant heat flux levels average this out. It may, however, also be due to random effects as the thermal insulation starts to disintegrate.

The temperature at the edge of the steel plate, i.e., at $r = R_o$, seems to lag behind about 12–13 °C. This may be explained by an uneven decomposition of the thermal insulation. It should be noted that the center of the PT, i.e., the thermocouple junction, was located at a radius of about 115 mm. It therefore probably did not record the highest temperatures of the system, which was probably within the inner 20–30 mm radius of the exposed cladding. The PT temperatures may therefore be representative for a major part of the tested surface.

Conservatively, the highest temperature of the steel plate, i.e., at $r = 0$, and the temperature of the plate thermometer could be used to describe the survivability of the modern distance insulation in a fire scenario. Based on the current small scale test, this system in the case with 16 mm wall thickness would most likely survive more than 30 min exposure to a hydrocarbon pool fire.

5. Discussion and Conclusions

The scope of the present study was to present a new concept for small scale fire testing of hydrocarbon process equipment. By rethinking fire testing from large flames exposure to heat radiation from thermally insulated stainless-steel surfaces, high temperature thermal exposure could be achieved in a small-scale set-up using a 25 kW test fire. With flame impingement and ambient air flow breakers also working as re-radiation solids, the test setup was capable of producing heat flux levels of 250 kW/m², and probably even approaching 350 kW/m². It was documented that air flow breakers were necessary to make the small-scale testing work as intended.

The target “fire temperature”, given 0.85 in emissivity of the stainless-steel parts, was 1200 °C. The plate thermometer (PT) worked well as an indicator of the fire intensity. Buckling was an issue in the reported tests, both for the mockup cladding and for the fire insulation cladding below the flame zone. The mockup cladding buckled severely, which would also be expected in a real fire. The fire insulation cladding also buckled. It was the first time a PT was tested in an intense fire well above its working temperature by this research group. As mentioned, the plate thermometer did not buckle significantly. It may be that the 100 mm by 100 mm size, as well as the welding, bent edges,

etc. prevented the PT buckling even at temperatures briefly above 1300 °C. Though testing of new equipment was not part of the present study, the authors were quite surprised by the PT performance. It seems promising for future high heat flux level fire testing and research.

It was demonstrated that the thermal insulation was able to keep the temperature of the 16 mm thick steel plate below 400 °C for more than 30 min during exposure to heat flux levels that were well above 250 kW/m². This result may indicate that work and cost may be saved when refurbishing old hydrocarbon processing equipment. It is believed that the 16 mm plate acted as a significant heat sink. Without this heat sink in close proximity to the heat exposed thermal insulation, the insulation may disintegrate faster. The current tests can therefore not be used to evaluate situations where thinner metal walls with less heat capacity are to be protected by thermal insulation.

The concept of small scale testing and using the PT as an indirect non-disturbing heat flux level sensor worked well. Fortunately, the exposed stainless-steel surface of the PT had a thickness that was similar to the cladding used in the industry, i.e., used in the mockup. While a radiometer or total heat flux meter would disturb the experimental setup, the PT, when placed flush with the fire insulation cladding and viewing the exposed mockup surface, resulted in a minimum of flame zone disturbances. In such small scale measurements, the PT is therefore a very interesting device for future studies.

In the present work, only two tests were reported. Preliminary tests not reported did, however, also support the findings of the present study. For larger test programs it would also be necessary to do several repetitions at similar conditions to evaluate the variability in testing. That was outside the present concept study.

A further improvement of the method would be to place more than one plate thermometer in the flame zone. This could give valuable information about any irregularities in heat flux levels, etc. Shielding the equipment better from draft current could give less variation in plate thermometer readings.

A result from fire testing and time to reach e.g., 400 °C is only one of several parameters in risk evaluations regarding fire safety in process plants. Safety for people is the first priority. Time to collapse of pressurized hydrocarbon containing equipment in fires, and potentially a sudden increase in fire severity, must be evaluated against evacuation times. Operation pressure versus design pressure, PSV set-points, i.e., pressure utilization, as well as blow down capacity, also play roles in the final risk evaluation. The fire frequency in the area of interest may also be considered, as well as the problem related to tall and slender structures that represents a threat to neighboring equipment late in a fire scenario. Active fire protection by water cooling may also be considered before a final decision is taken regarding necessary fire resistance of pressurized equipment.

The small scale testing does, however, indicate a potential to reveal important information that may be a part of the complete picture regarding fire risk when modifying existing equipment. When compliance to modern thermal insulation methods would increase the costs and at the same time introduce hot work in a live plant, the presented test methodology may give valuable information in the refurbishment decision processes.

It is recommended to continue the research regarding small scale fire testing of modern thermal insulation methods for thinner, as well as thicker, steel plates. It may also be worthwhile to try to develop small scale fire tests for piping insulation, etc. The small scale method may also have potential as a preliminary test for product development before eventual full scale certified fire testing is undertaken.

Acknowledgments: Statoil Kårstø is acknowledged for funding J.S.B. in this R&D project. The support of Leif Inge Larsen and Ingvald Olai Heska for supplying test materials and producing the mockup is very much appreciated.

Author Contributions: T.L. conceived the project idea and did the first calculations and sketches. A.K. arranged the propane burner and flow control unit and made the basic test rig. J.S.B. mounted the mockup for each test and did preliminary testing as well as Test 1 and Test 2 together with A.K. M.M.M. introduced the plate thermocouples and wrote the paper together with J.S.B. and T.L.

Conflicts of Interest: The funding sponsor encouraged the work and several of the sponsor senior personnel were asked for advice during the progress of the work. T.L. has an advisor position at the funding sponsor. None of the participants in the study have any connections to specific equipment being mentioned in the paper.

References


1. Kletz, T. *What Went Wrong? Case Histories of Process Plant Disasters and How They Could Have Been Avoided*, 5th ed.; Institution of Chemical Engineers: London, UK, 2009; ISBN 13:978-1-85617-531-9.
2. U.S. Chemical Safety and Hazard Investigation Board. *Investigation Report Executive Summary; Drilling Rig Explosion and Fire at the Macondo Well*, Report No. 2010-10-I-OS; U.S. Chemical Safety and Hazard Investigation Board: Washington, DC, USA, 2010.
3. Murray, J.A.; Sander, L.C.; Wise, S.A.; Reddy, C.M. *Gulf of Mexico Research Initiative 2014/2015 Hydrocarbon Intercalibration Experiment: Description and Results for SRM 2779, Gulf of Mexico Crude Oil and Candidate SRM 2777 Weathered Gulf of Mexico Crude Oil*; NISTIR 8123; National Institute of Standards and Technology: Gaithersburg, MD, USA, 2016.
4. Jet Fire Test Working Group. *The Jet-Fire Resistance of Passive Fire Protection Materials*; HSE Report OTI 95 634; Health & Safety Executive—Offshore Technology Report; Jet Fire Test Working Group: Sheffield, UK, 1995; ISBN 0-7176-1166-3.
5. Roberts, T.A.; Shirvill, L.C.; Waterton, K.; Buckland, I. Fire resistance of passive fire protection coatings after long term weathering. *Process Saf. Environ. Prot.* **2010**, *88*, 1–19. [[CrossRef](#)]
6. Collier, K. Insulation. *Chem. Eng. Prog.* **2002**, *98*, 47.
7. International Organization Standardization (ISO). *Fire-Resistance Tests—Elements of Building Construction*; International Organization Standardization: Geneva, Switzerland, 2007.
8. Norsk Standard. *Fire Resistance Tests—Part 1: General Requirements*; NS-EN 1363-1:2012, standard.no; Norsk Standard: Lysaker, Norway, 2012.
9. Taillefer, N.; Carlotti, P.; Larive, C.; Lemerle, C.; Avenel, R.; Pimienta, P. Ten Years of Increased Hydrocarbon Temperature Curves in French Tunnels. *Fire Technol.* **2013**, *49*, 531–549. [[CrossRef](#)]
10. Norsk Standard. *Technical Safety, NORSOK Standard*, 4th ed.; S-001, standard.no; Norsk Standard: Lysaker, Norway, 2008; p. 62.
11. International Organization for Standardization. *Determination of the Resistance to Jet Fires of Passive Fire Protection Materials—Part 1: General Requirements*; International Organization for Standardization: Geneva, Switzerland, 2007; p. 40.
12. Statoil, TR2237. Performance Standards for safety systems and barriers—Onshore. *Statoil Tysværsvåg Norway* **2015**, *3*, 105.
13. Wickström, U. The plate thermometer—A simple instrument for reaching harmonized fire resistance tests. *Fire Technol.* **1994**, *30*, 195–208. [[CrossRef](#)]
14. Ingason, H.; Wickström, U. Measuring incident radiant heat flux using the plate thermometer. *Fire Saf. J.* **2007**, *42*, 161–166. [[CrossRef](#)]
15. Häggkvist, A.; Sjöström, J.; Wickström, U. Using plate thermometer measurements to calculate incident heat radiation. *J. Fire Sci.* **2013**, *31*, 166–177. [[CrossRef](#)]
16. Sjöström, J.; Amon, F.; Appel, G.; Persson, H. Thermal exposure from large scale ethanol fuel pool fires. *Fire Saf. J.* **2015**, *78*, 229–237. [[CrossRef](#)]



© 2017 by the authors. Licensee MDPI, Basel, Switzerland. This article is an open access article distributed under the terms and conditions of the Creative Commons Attribution (CC BY) license (<http://creativecommons.org/licenses/by/4.0/>).

Article

Study of Industrial Grade Thermal Insulation as Passive Fire Protection up to 1200 °C

Joachim Søreng Bjørge^{1,2,*}, Amalie Gunnarshaug^{1,3}, Torgrim Log^{3,4}  and Maria-Monika Metallinou³

¹ Q Rådgivning AS/PDS Protek, Øvregata 126, 5527 Haugesund, Norway; amg@q-rad.no

² Department of Physics and Technology, University of Bergen, 5020 Bergen, Norway

³ Faculty of Engineering and Science, Western Norway University of Applied Sciences, 5528 Haugesund, Norway; torgrim.log@hvl.no (T.L.); monika.metallinou@hvl.no (M.-M.M.)

⁴ Equinor Kårstø, Kårstø, 5562 Tysværåvåg, Norway

* Correspondence: jsb@q-rad.no; Tel.: +47-9098-1051

Received: 17 August 2018; Accepted: 18 September 2018; Published: 19 September 2018



Abstract: It has recently been demonstrated that 50 mm thick industrial grade thermal insulation may serve as passive fire protection of jet fire exposed thick walled steel distillation columns. The present study investigates the performance of thermal insulation in conjunction to 3 mm, 6 mm, 12 mm and 16 mm steel walls, i.e., where the wall represents less heat sink, when exposed to 350 kW/m² heat load. Regardless of the tested steel plate thicknesses, about 10 min passed before a nearly linear steel temperature increase versus time was observed. Thereafter, the thinnest plates systematically showed a faster temperature increase than the thickest plates confirming the wall heat sink effect. To study thermal insulation sintering, 50 mm thermal insulation cubes were heat treated (30 min holding time) at temperatures up to 1100 °C. No clear sign of melting was observed, but sintering resulted in 25% shrinkage at 1100 °C. Thermogravimetric analysis to 1300 °C revealed mass loss peaks due to anti-dusting material at 250 °C and Bakelite binder at 460 °C. No significant mass change occurred above 1000 °C. Differential scanning calorimetry to 1300 °C revealed endothermic processes related to the anti-dusting material and Bakelite mass losses, as well as a conspicuous endothermic peak at 1220 °C. This peak is most likely due to melting. The endothermic processes involved when heating the thermal insulation may to a large part explain the 10 min delay in steel plate temperature increase during fire testing. Overall, the tested thermal insulation performed surprisingly well also for protecting the thin steel plates.

Keywords: passive fire protection; hydrocarbon fires; thermal insulation; thermogravimetric analysis (TGA); differential scanning calorimetry (DSC)

1. Introduction

Petroleum products are an essential source of energy and thereby an important part of the modern world. The hydrocarbon process industry involves complex mechanical interventions with extraction of oil and gas from wells as well as processing to produce the products called for in the market. For many decades, this industry has been, and still is, an essential part of the world economy. In several locations, the oil and gas industry is a mature industry. The lifetime of equipment and process plants must therefore steadily be extended by maintenance, upgrades and modifications. Processes at elevated pressure, combined with highly flammable materials make this an industry with high accident potential. A release of the pressurized and highly flammable material could be disastrous, as evidenced by many major accidents during the last decades [1–3]. Prevention and mitigation of fires and explosions are therefore very important.

If a hydrocarbon leak is ignited, the heat loads to exposed objects may be quite severe, i.e., flame temperatures in the range 1100 °C to 1200 °C and heat loads in the range 250 kW/m² to 350 kW/m² [4]. Heat exposed steel objects lose strength with temperature. Especially at temperatures above 500 °C, the loss of tensile strength is significant [5]. Fire exposed pipes and vessels containing pressurized hydrocarbons may, if weakened by overheating, rupture violently and release the combustible contents giving rise to major escalation of the fire scenario. This may result in a domino effect leading to loss of major parts of offshore platforms and land based production plants. Much effort is therefore put into designing and maintaining protective escalation barriers, e.g., passive fire protection [1,6].

In several hydrocarbon processes, thermal insulation is required to maintain the proper production temperatures. Distillation columns may serve as an example of process equipment where the temperature profiles are carefully designed to obtain good production efficiency and the right quality for the distilled products. Such process units, which may release huge quantities of flammable materials if rupturing in a fire, are normally also protected by mineral based passive fire protection. Previously, the thermal insulation was placed in direct contact with the process equipment metal corrosion protective paint. Externally, the thermal insulation was protected from the natural elements by a 0.7 mm layer of stainless steel cladding. Due to temperature differences in e.g., a distillation column, humid air may be entrained at lower levels. When heated, this humid air travels upwards and is pushed further upwards by new air entrained at lower levels, to locations where the column wall is below its dew point temperature. This results in liquid water draining down through the insulation. Soaked thermal insulation may finally destroy the corrosion protective paint exposing the column steel to liquid water. Severe corrosion may be the consequence of this process and may result in large maintenance costs or, in the worst case, severe hydrocarbons leaks.

To prevent soaked insulation in contact with the column walls, an improved insulation technique introduces a 25 mm air gap between the column walls and the thermal insulation. This has in some cases resulted in too limited available space for adding both 50 mm thick thermal insulation and 50 mm thick passive fire protection as well as the 0.7 mm surface cladding. In a previous study, using small scale testing [7] rather than full scale testing [8], it was demonstrated that 50 mm thermal insulation (ProRox PSM 971, 50 mm, Rockwool), without any passive fire protection (PFP), was sufficient to withstand 30 min jet fire exposure for 16 mm thick steel walls. It was revealed that during the most severe testing, the thermal insulation partly melted. Small scale testing was also performed by Landucci, et al. [9] when investigating composite materials based on basalt fibers as components of the PFP systems.

The present study aims at investigating the passive fire protection performance of the industrial thermal insulation protecting steel walls of 3 mm, 6 mm, 12 mm and 16 mm thickness during 350 kW/m² jet fire exposure. Steel wall temperature versus time was recorded, and it was assumed that the thinner steel walls would obtain higher temperatures early, which could severely influence the thermal insulation degradation processes. In order to study the breakdown of the thermal insulation with temperature, 50 mm cubes of the thermal insulation were heat treated, i.e., 30 min holding time, at varying temperatures up to 1100 °C in a muffle furnace. To further shed light on the thermal insulation behavior at elevated temperatures, thermogravimetric analysis was performed at temperatures up to 1300 °C to reveal mass loss at elevated temperatures. Differential scanning calorimetry to 1300 °C was performed to investigate the high temperature performance of the thermal insulation with respect to identify any potential melting below 1300 °C.

The materials and methods used are explained in Section 2, including some comments on the fire testing criteria. Section 3 presents the results for jet fire testing at 350 kW/m² heat load including the total heat flux to the plates. Shrinking tests at different holding temperatures, and the findings from the thermal gravimetric and differential scanning calorimetric analyses, are also presented in this section. Section 4 presents the discussions and conclusions.

2. Materials and Methods

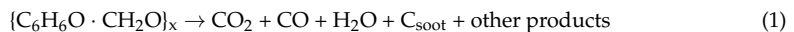
2.1. The Thermal Insulation Studied

The thermal insulation studied was the industrial grade Pipe section mat (PSM) (ProRox PSM 971, thickness 50 mm) delivered by Rockwool Inc. (Copenhagen, Denmark). The technical data for this thermal insulation may be found in Appendix A, Table A1. According to the manufacturer data, the maximum service temperature for this thermal insulation is 700 °C. The thermal conductivity at elevated temperatures is presented in Appendix A, Table A2.

Chemically, the bulk phase of the thermal insulation consists of inorganic oxides. The major components are silica, alumina, magnesia, calcium oxide and iron(III) oxide. Additionally, it also contains minor amounts of sodium oxide, potassium oxide, titanium oxide and phosphorous pentoxide. The detailed chemical composition is given in Appendix A, Table A3.

The thermal insulation is produced by spinning the molten metal oxides at 1500 °C in thin threads, which are subsequently cooled and spun to insulation mats. A Bakelite binder is used to hold the loose spun threads in place during the 10+ year thermal insulation field operation. A mineral based oil is also added in order to act as a dust binder when handling the thermal insulation, e.g., when cutting and fitting the insulation mats for the field application.

During heating, the mineral oil will gradually evaporate/pyrolyze. Bakelite, i.e., polyoxybenzylmethylenglycolanhydride, $(C_6H_6O \cdot CH_2O)_x$, may exhibit complicated degradation processes, which are known to be dependent upon chemicals mixed into the Bakelite [10]. The degradation processes are also dependent on the number of molecular cross links and may be expected to react along several reaction paths. A non-balanced degradation reaction may be represented by:



The degradation temperatures are highly influenced by the number of cross links as well as the other chemicals mixed into the Bakelite [10].

For materials where the thermal conductivity is limited by the pores, it may be shown theoretically [11] that the thermal conductivity will be proportional to the absolute temperature to the third power. The thermal conductivity of the thermal insulation as a function of the absolute temperature to the third power is presented in Figure 1. The linear trend indicates that the thermal conductivity of the thermal insulation is limited by pore radiation, at least until there is a significant thermal degradation of the insulation.

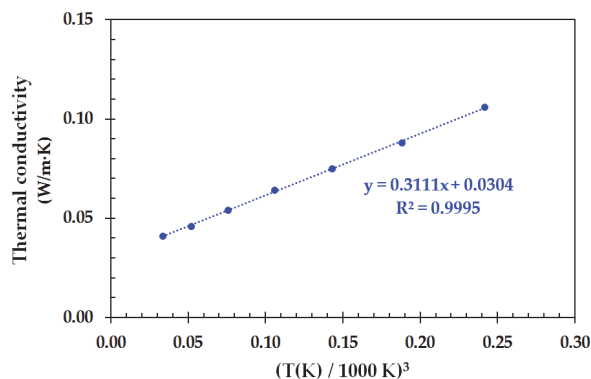


Figure 1. Thermal conductivity of the thermal insulation (ProRox PSM 971, 50 mm) as a function of the absolute temperature to the third power. Data from Appendix A, Table A2.

Sintering is a physical process that may take place in inorganic (ceramic) materials at elevated temperatures. The sintering process is entropy driven [12] and leads to a lower free energy, ΔG . The atoms in the different materials diffuse across the grain boundaries, in this case across the thread boundaries, to form a better mixed material with fewer sharp edges. The atoms diffuse across the boundaries, fusing the threads together such that the materials, at least theoretically, approaches one solid piece.

This atomic diffusion will drive thread surface elimination in different stages, starting from the formation of necks between threads to potential final elimination of the small pores at the end of the sintering process. The linear trend in Figure 1 is a clear indication of the thermal conductivity of the thermal insulation being limited by the pore radiation. Closing the pores by sintering will therefore increase the thermal conductivity of the thermal insulation. This process is indeed applied to create ceramic materials of very high thermal conductivity [13].

For ceramic materials, the sintering process typically starts at a temperature of about 2/3 of the absolute melting temperature [14]. It may therefore be expected that a thermal insulation consisting of porous ceramic materials, such as the thermal insulation studied in the present work, may start to sinter at temperatures several hundred degrees below an associated melting point. Sintering is, however, generally a slow process, which may therefore not make too much problems during a limited time of fire exposure unless the sintering is very fast at the highest temperatures involved in the present testing, i.e., at 1200 °C.

2.2. Fire Test Criterion

An object engulfed in flames receives heat by both convection and radiation. The net heat flux received is given by:

$$\dot{Q}_{net}'' = h(T_f - T_s) + \varepsilon_f \sigma T_f^4 - \varepsilon_s \sigma T_s^4 \quad (\text{W/m}^2) \quad (2)$$

where h (W/m K) is the heat convection coefficient, T_f (K) is the temperature of the flame, T_s (K) is the temperature of the exposed surface, ε_f is the flame emissivity, ε_s is the emissivity of the solid and σ (5.67×10^{-8} W/m² K⁴) is the Stefan-Boltzmann constant. The emissivity of the flame is given by:

$$\varepsilon_f = 1 - \exp(-KL) \quad (3)$$

where L (m) is the optical flame thickness and K (1/m) is the extinction coefficient. Fires in the oil and gas industry may become quite large. Conservatively, it is therefore common to assume that the flames in industrial fires are sufficiently large to be considered optically thick, i.e., $\varepsilon_f = 1$.

Regarding hydrocarbon fires, it is common to principally distinguish the fire to either pool fires caused by liquid spills retained on a surface or jet fires caused by release of ignited pressurized gas. Both these fires are recognized as fuel-controlled fires [4].

For rupture calculations, the actual fire scenarios and heat flux level must be defined. Relevant descriptions for a fire scenario typically include the type of fire, fire duration and size and heat flux levels (both global and peak loads). In heat exposure calculations, the NOR-SOK S-001 and the Scandpower guidelines [4,15] state that the total heat flux for pool fires and jet fires should be set to 250 kW/m² and 350 kW/m², respectively. This is also in accordance with observed heat flux levels obtained from numerous experiments as well as CFD modeling. The oil and gas processing and transport companies have therefore recently specified similar fires loads, e.g., the Equinor requirements for new installations, TR2237 [16]. Given the expected emissivity of a fire exposed object to be about 0.85, flame temperatures of 1050 °C and 1200 °C, respectively corresponds to 250 kW/m² and 350 kW/m² to an object at 20 °C [7].

The ISO 22899 Jet Fire Test [17] is generally used for standardized jet fire testing. This full scale test utilizes a horizontally aligned 0.3 kg/s propane jet, i.e., corresponding to about 14 MW heat release rate, aimed at the object to be tested. In the present small scale test, achieving a fire intensity that brings the 0.7 mm thick cladding, protecting the thermal insulation, up to 1200 °C, was considered

sufficient to claim a 350 kW/m^2 heat load. Plate thermometers were introduced to verify that this was achieved. The fire load criterion for the testing in the present work was therefore defined as a plate thermometer temperature of $1200 \text{ }^\circ\text{C}$ [7].

2.3. The Fire Exposure Test Procedure

The 0.7 mm thick cladding, the 50 mm thick thermal insulation, the required 25 mm air gap and the respective steel plates were aligned horizontally with an axisymmetric vertical propane flame as the fire source. An illustration is given in Figure 2 and the details of the experimental mockup used are presented in [7]. Ten thermocouples (Type K, 1.6 mm diameter, stainless steel mantle, Pentronic AB) were used for temperature recordings during the experiment. These thermocouples are illustrated by the blue lines in Figure 2. Additionally, two 100 mm by 100 mm by 20 mm thick type K plate thermometers (100 mm PT (Plate Thermometer), article number 5928050-001, Pentronic AB, Västervik, Sweden), were used to record an equivalent cladding temperature [7], verifying the test criteria described in Section 2.2. These are illustrated by blue boxes and marked PT in Figure 2. The function of such plate thermometers is explained in depth in [18–21].

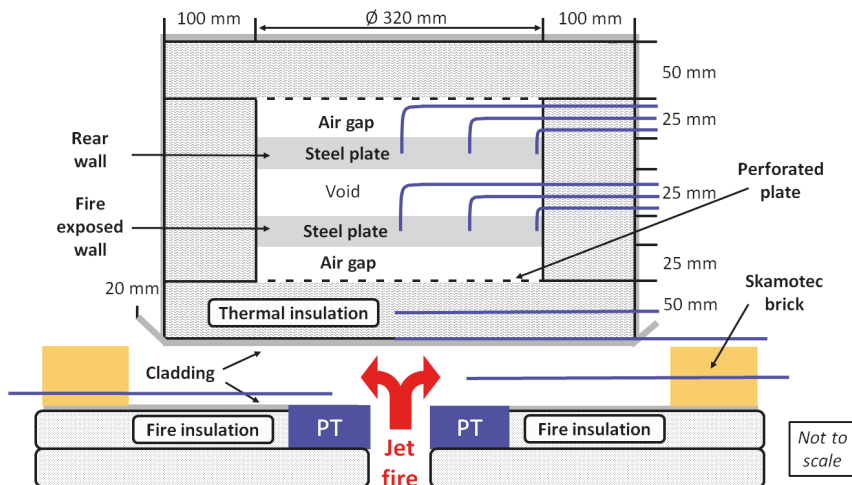


Figure 2. Sketch of mockup including flame zone, type K mantle thermocouples (blue lines), flush mounted plate thermometers (marked PT) and Skamotec bricks.

Aligning the PTs horizontally, facing upwards and flush with the fire insulation representing the lower part of the combustion chamber, they directly viewed the exposed cladding. This orientation gives robust information about the system's heat flux levels. And, aligned flush, the plate thermometers had minimal influence on the flame zone heat transfer. The temperatures of the thermocouples and the plate thermometers were recorded by a data logger (type 34970A Data Acquisition/Data Logger Switch Unit, Keysight, CA, USA).

A 60 mm titan burner (Sievert 346051, Titan, 60 mm diameter) was used as the fire source. The burner was set to burn at full air access, arranged vertically and aligned axisymmetric in the center of the experimental setup. By trial and error, it was found that a 0.6 g/s rate of propane gas was sufficient to reach the required heat load levels. A gas flow control unit (C3H8 225 L/min, build 2612, Brooks Instr. Inc., Hatfield, PA, USA) was used to keep the propane supply constant throughout the test period. The fire tests were generally terminated after 40 min, or earlier if the temperature of the exposed steel plate reached about $600 \text{ }^\circ\text{C}$.

Light weight high temperature concrete bricks (Skamotec 225, Skamol A/S, 100 mm × 100 mm × 50 mm), were placed around the mockup, 1 cm from the exposed cladding edge, to limit air access and prevent heat radiation losses from the flame zone, as indicated in Figure 2. The test mockup during fire exposure is shown in Figure 3.



Figure 3. Fire testing with a propane mass flow rate of 0.6 g/s.

It should be noted that the air access to the flame zone had to be optimized by trial and error. Too restricted air flow along the burner resulted in lower temperatures. This was also the case for excess air entrainment. When finding the optimum, it was quite easy to reproduce fire testing giving 1200 °C plate thermometer temperatures. Fire tests were undertaken for 3 mm, 6 mm, 12 mm and 16 mm steel plate thickness. At least 3 tests were completed for each of the selected steel plate thicknesses.

2.4. Thermal Insulation Heat Treatment Testing

2.4.1. Thermal Insulation Heat Treatment in a Muffle Furnace to 1100 °C

To investigate how the thermal insulation behaved when exposed to elevated temperatures, it was decided to do heat treatment in a muffle furnace. Thermal insulation test specimens (5 cm cubes) were pre-cut 2 days prior to the heat treatment to eliminate any elasticity issues. The heat treatment was done in a muffle furnace (Nabertherm L5/11, Program Controller S17). The furnace had a maximum temperature of 1100 °C, which therefore became the maximum temperature for this heat exposure testing.

One type K thermocouple (1.5 mm diameter) was placed in the center of the test specimen to record the internal test specimen temperature. One similar thermocouple was placed in the upper part of the furnace to record the furnace temperature. The temperature at the furnace display was also recorded.

The heat treatment was done for temperatures in the range 700 °C to 1100 °C, as shown in Table 1. The heating rate was 15 K/min and the holding time at the respective temperatures was 30 min.

Table 1. Holding temperature and number of exposure tests.

| Exposure Temperature (°C) | Number of Tests |
|---------------------------|-----------------|
| 700 | 1 |
| 750 | 1 |
| 800 | 1 |
| 900 | 1 |
| 1000 | 2 |
| 1100 | 2 |

After heat treatment, and cooling to below 300 °C, the height of the tested thermal insulation cubes was recorded at the center of the four vertical sides. The average height was reported for each test specimen.

2.4.2. Thermogravimetric Analysis (TGA) and Differential Scanning Calorimetry (DSC)

Due to the 1100 °C limitation of the available muffle furnace, it was decided to investigate the thermal insulation in more detail and to a temperature of at least 1200 °C. Samples of the thermal insulation were therefore tested in a simultaneous thermogravimetric analysis—differential scanning calorimetry apparatus (NETZSCH STA 449 F1). Test samples (6–8 mg) were taken 10 mm, 25 mm and 40 mm from the thermal insulation surface. The tests were run at a heating rate of 5 K/min, 10 K/min and 20 K/min from room temperature and up to 1300 °C. Tests were conducted in air atmosphere as well as in N₂-atmosphere (to prevent any air oxidation processes).

3. Results

3.1. Results Obtained by Jet Fire Testing

During jet fire testing, the temperatures were recorded at three locations in the exposed steel plate and at three locations in the steel backing plate, i.e., in the steel plate centers ($r = 0$ mm), at half the plate radius ($r = 80$ mm) and close to the full plate radius ($r = 160$ mm). This was done to verify that the system displayed one-dimensional heat flow. A typical temperature recording of a 6 mm thick plate is shown in Figure 4.

In some tests, problems with thermocouple and steel plate mechanical contact appeared, as evidenced in Figure 4 for the thermocouple in the center of the exposed steel plate. This may be due to some tension in the system generated by thermal expansion during the transient heating. In these cases, this temperature recording was not used for further data analysis.

The temperatures versus time recorded for steel plate thickness 3 mm, 6 mm, 12 mm and 16 mm are shown in Figures 5–8, respectively. It should be noted that the temperatures recorded in the flame zone were typically 50–100 °C above the temperature recorded by the plate thermocouples.

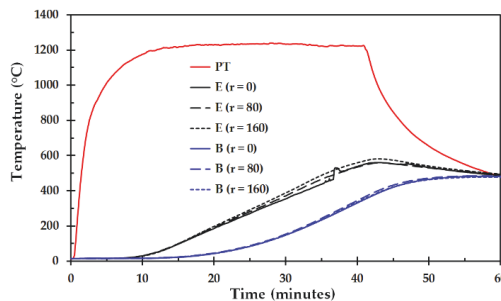


Figure 4. Temperature as a function of time for a representative test (6 mm thick steel plate thickness). Temperatures of the exposed and backing steel plates are marked E and B, respectively. The numbers indicate the radial thermocouple position (in mm). PT represents the plate thermometer.

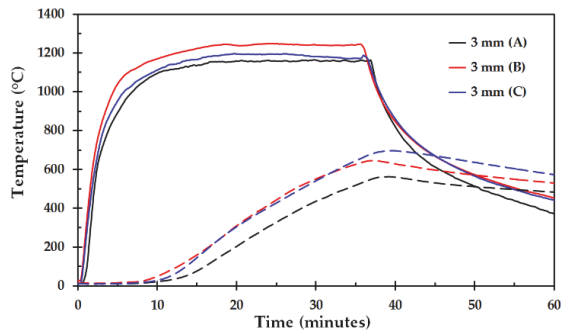


Figure 5. Temperature as a function of time for 3 mm thick steel plate, test A, B and C. Solid lines represent the plate thermometer temperature while the dashed lines represent the temperature of the exposed steel plates.

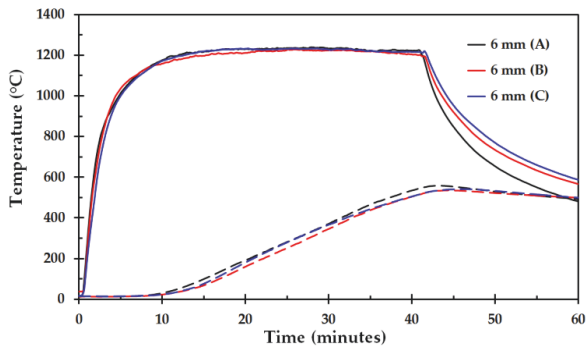


Figure 6. Temperature as a function of time for 6 mm thick steel plate, test A, B and C. Solid lines represent the plate thermometer temperature while the dashed lines represent the temperature of the exposed steel plates.

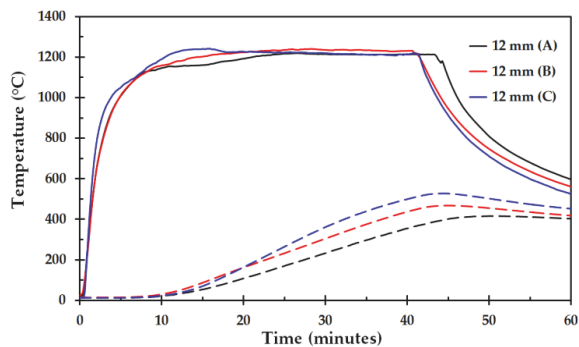


Figure 7. Temperature as a function of time for 12 mm thick steel plate, test A, B and C. Solid lines represent the plate thermometer temperature while the dashed lines represent the temperature of the exposed steel plates.

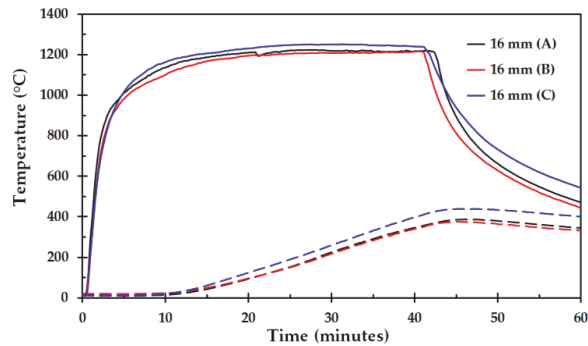


Figure 8. Temperature as a function of time for 16 mm thick steel plate, test A, B and C. Solid lines represent the plate thermometer temperature while the dashed lines represent the temperature of the exposed steel plates.

The average temperatures as a function of time for the different steel plate thicknesses are presented in Figure 9, where each curve represents an average of three separate fire tests. It is clearly seen that the temperature increase is slower for the thicker steel plates as a result of higher steel plate thermal capacity.

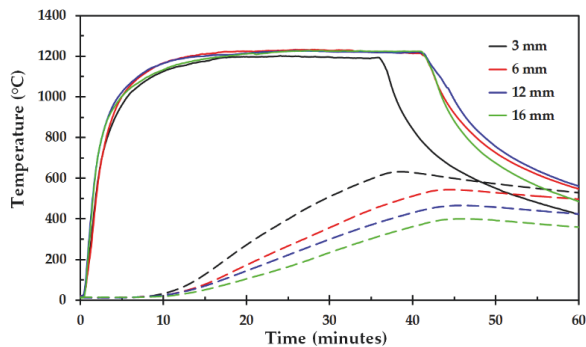


Figure 9. Comparison of 3, 6, 12 and 16 mm steel plate. Every plate thickness represents an average of 3 fire tests.

It is also evident from the Figure 4 through Figure 8 that during the first 10 min very low temperature increase was recorded for any of the steel plate thicknesses. This may partly be explained by the thermal insulation heat capacity, which is about $7 \text{ kJ/m}^2 \text{ K}$. Especially for the thinner steel plates, e.g., the 3 mm plates with a heat capacity $12 \text{ kJ/m}^2 \text{ K}$, the heat capacity of the thermal insulation plays an important part in limiting the temperature increase. The 10 min delay in steel plate temperature increase may, however, also be due to thermal degradation of the components of the thermal insulation. The dust binder will require heat when decomposing. The same holds for the Bakelite. The thermal insulation was also experienced to partly break down during the fire testing. Sintering was always observed, and in some cases, the thermal insulation had partly melted during the fire tests. It is therefore quite likely that endothermic degradation processes initially give some protection of the exposed steel plates, but may finally result in thermal insulation breakdown.

It should be noted that for all the tests, volatiles released from the thermal insulation during the fire testing exited through connections and small openings in the mockup. In some cases these small jets of volatiles ignited and burned when exposed to the ambient air. The fact that the combustion took

place outside the mockup may be taken as a sign of too little oxygen available for combustion within the mockup.

During the fire tests, both the exposed steel plate and the back plate, as presented in Figure 2, may experience a temperature increase during testing. Therefore, the temperatures were recorded for both these steel plates, as shown in Figure 4. Ignoring any heat loss to, or heat gain from, the thermal insulation surrounding the steel plates, the total heat flux to the exposed steel plate may be calculated by:

$$\dot{Q}'' = m_E \cdot C_{E(T)} \cdot \gamma_{E(t)} / A_E + m_B \cdot C_{B(T)} \cdot \gamma_{B(t)} / A_B \quad (4)$$

where m (kg) is the steel plate mass, $C_{(T)}$ (J/kgK) is the specific heat of the steel plate at temperature, T (K), $\gamma_{(t)}$ (K/s) is the temperature versus time slope at time t (s) and A (m²) is the steel plate exposure area. The subscripts E and B represent the exposed and backing steel plates, respectively. The values for the steel plate heat capacity as a function of temperature were taken from [22].

Based on the temperature recordings of the exposed steel plate as well as the back plate, as seen in the sketch of Figure 2, the heat flux as a function of time was calculated by Equation (4). Calculated total heat flux to the steel plates for representative tests are shown in Figure 10. Despite some noise, it is seen that the heat flux development follows the same pattern, at least up to 25 min. The reason for the thinner steel plate to level off may simply be due to the lower temperature difference for this plate as well as a more significant back plate temperature resulting in increased heat loss to the upper insulation. Nevertheless, it is evident that the heat flux to the steel plates are significantly lower than the heat flux of the system, i.e., which was close to 350 kW/m². This indicates that the thermal insulation system, though gradually losing its protective capacity, provides a significant heat protection. It is also evident that the heat protection for the 3 mm steel plate, even after 30 min heat exposure, is comparable to the heat protection of the thicker steel plates. This is important knowledge regarding potential use of the industrial thermal insulation as passive fire protection of thin walled pipes, etc.

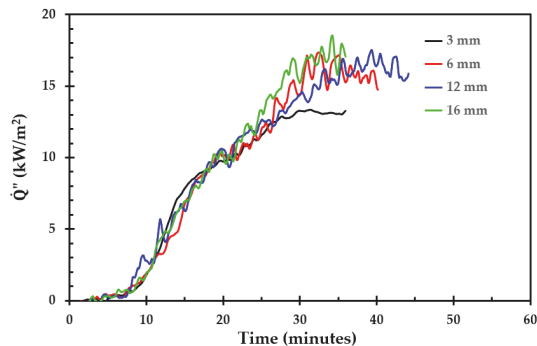


Figure 10. Total heat flux to the steel plates as a function of time. The steel plate thickness is indicated in the figure label.

3.2. Results Obtained by Thermal Insulation Heat Treatment

Due to the thermal degradation of the thermal insulation observed during fire testing, it was decided to do controlled heat treatment tests. This involved heat treatment to 1100 °C in a Muffle furnace, thermogravimetric analysis and differential scanning calorimetry. The results of this testing are presented in the following sub-sections.

3.2.1. Results Obtained by Muffle Furnace Heat Treatment to 1100 °C

The 50 mm cubic test specimens were arranged horizontally according to the heat protection in fires, i.e., the fibers ran horizontally while in the muffle furnace. Testing was done according to Table 1. The temperature development during heating to 1100 °C, 30 min holding time at this temperature, and the subsiding muffle furnace cooling is shown in Figure 11. Two distinct temperature peaks for the thermocouple located within the thermal insulation are observed. The first peak started at about 250 °C and terminated at about 520 °C. The second peak started at about 860 °C and terminated at about 960 °C. The first exothermic process is likely due to dust binder (heavy oil) and Bakelite combustion since the atmosphere in the furnace was ambient air. Due to the thermal insulation porosity, oxygen was available also in the center of the 50 mm thermal insulation cubes. This temperature peak was observed for all the test specimens heated in the muffle furnace.

It may be more challenging to explain the second exothermic reaction. It may be a result of exothermic processes due to oxidation of soot particles from the degradation of the dust binder and/or the Bakelite. Physical (sintering) and/or chemical reactions in the inorganic salts comprising the bulk part of the thermal insulation may also be the source of heat production, e.g., recrystallization, etc. It should be noted that after the heat treatment to 900 °C, 1000 °C and 1100 °C, i.e., at temperatures associated with, or above, the second peak, small soot like particles were observed inside the muffle furnace. Such soot like particles were not observed after the heat treatment to 700 °C, 750 °C or 800 °C. It was, however, outside the scope of the present work to pursue this issue any further.

The height of the originally 50 mm cubic thermal insulation test specimens after 30 min holding time as a function of holding temperature is shown in Figure 12. It appears that there is a change in height between 700 °C and 800 °C, where after there is no major shrinkage until temperatures above 1000 °C. After 30 min at 1100 °C, the shrinkage was still less than 25%. This may indicate that this particular thermal insulation still provides quite significant heat protection up to 1100 °C. Unfortunately, this was the temperature limit of the available muffle furnace, thereby limiting testing at higher temperatures. The two test specimens held 30 min at 1100 °C are shown in Figure 13.

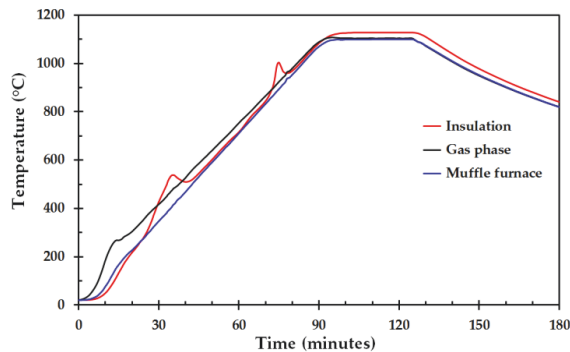


Figure 11. Temperatures recorded in the center of the 50 mm thermal insulation cubes, the gas phase and values displayed at the Muffle furnace (heating rate 15 K/min and 30 min holding time at 1100 °C).

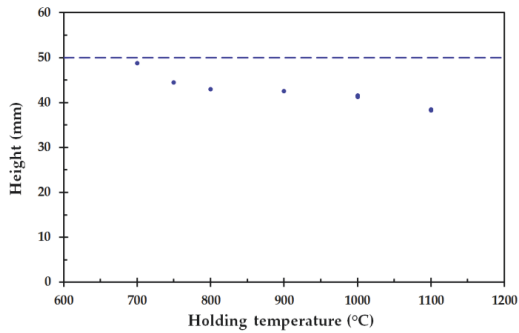


Figure 12. The height of the 50 mm cubic insulation test specimens after 30 min holding time as a function of the holding temperature. The dashed line represents the 50 mm initial height.

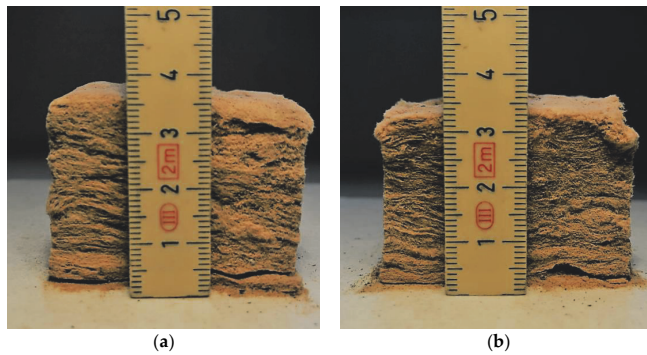


Figure 13. Test specimens (50 mm cubes) after 30 min heat exposure at 1100 °C for (a) test a and (b) test b.

3.2.2. Results Obtained by Thermogravimetric Analysis (TGA) to 1300 °C

Thermogravimetric analysis (TGA) was performed from ambient temperature up to 1300 °C at 5 K/min, 10 K/min and 20 K/min. The TGA results for a sample taken from the middle section of one of the insulation mats used to cut test specimens for fire testing and muffle furnace testing is shown in Figure 14. The results were quite representative for test specimens cut at 10 mm depth and 40 mm depth. The derivative of these curves, i.e., differential thermogravimetric (DTG) analysis, is shown in Figure 15.

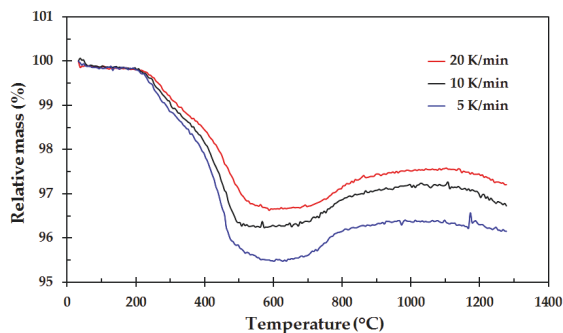


Figure 14. Thermogravimetric analysis of a test specimen from the center of the thermal insulation.

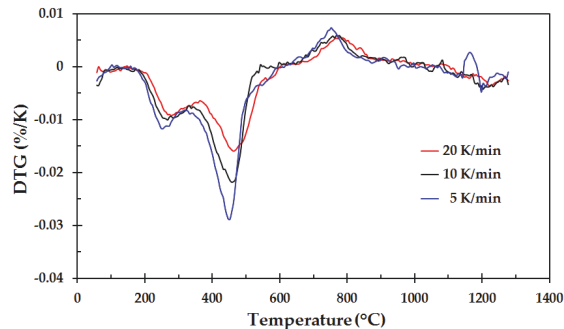


Figure 15. Differential thermogravimetric (DTG) analysis of the results shown in Figure 14.

As seen in Figure 15, the mass loss starts at about 200 °C, with a local minimum in the temperature range 240 °C to 260 °C. This is most likely due to the dust binder mineral oil decomposition/evaporation. The next minimum, with maximum mass loss rates in the range 450 °C to 480 °C, may be a result of Bakelite decomposition. When mixed with other chemicals, the Bakelite may decompose at different temperatures than pure Bakelite, as experienced by Solyman, et al. [10]. The second minimum is therefore most likely due to decomposition of the Bakelite binder, or parts of the Bakelite binder.

From about 700 °C, there seems to be a mass gain, peaking at about 760 °C to 770 °C. The current study has no explanation of this observation. From about 860 °C, there is only some minor mass loss throughout for the remaining heating to 1300 °C.

For some of the tests, the gas emissions were analyzed by fourier transformed infrared spectroscopy (FTIR). The FTIR recordings revealed traces of H₂O, CO₂ and CO during the entire heating period, though the concentration of these gas species were most profound at the start of the heating process and at the end of the heating process. The higher production of these species early in the heating process is probably due to dust binder and Bakelite decomposition. The higher concentration at the end of the heating process may indicate some chemical reactions related to the minerals comprising the thermal insulation fibers, including traces of other minerals than presented in Appendix A, Table A3.

3.2.3. Results Obtained by Differential Scanning Calorimetry to 1300 °C

The differential scanning calorimetry from ambient temperature to 1300 °C was performed simultaneously with the TGA measurements, i.e., for the same samples heated at a rate of 5 K/min, 10 K/min and 20 K/min. The results are shown in Figure 16.

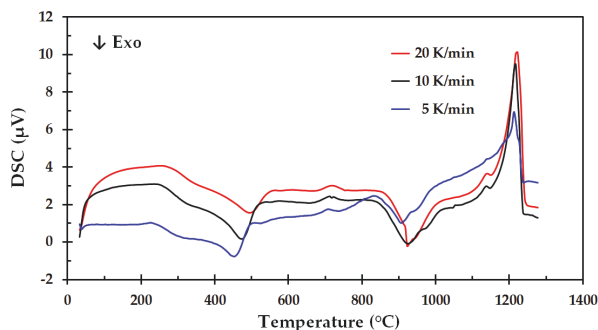


Figure 16. Differential scanning calorimetry (DSC) analysis of the thermal insulation.

At temperatures around 100 °C, there is virtually no heat production or heat consumption by the test run at 5 K/min. Since these tests were conducted in a normal 21% oxygen atmosphere, the heat required for dust binder oil evaporation/pyrolysis may, however, be partly compensated by heat release during oxidation of the released species. Especially for the lower heating rate, i.e., less production of gaseous products, the leakage of oxygen into the covered crucible may allow for relatively more internal combustion than when the pyrolysis rate is higher. The slightly exothermic peaks at 910 °C to 920 °C confirm the findings from the testing in the muffle furnace, i.e., the second temperature peak identified for the 50 mm cube test specimens.

The small endothermic peak at about 710 °C to 720 °C was found on all the DSC tests. This may be due to e.g., crystallization. The exothermic peak at 910 °C to 920 °C may also be a result of crystallization. Simultaneously degradation of the Bakelite and possible Bakelite residues reacting at higher temperatures make the picture quite complicated. In depth treatment of these issues was, however, outside the scope of the present work.

The most conspicuous peaks obtained by the DSC analysis are the highly endothermic physical or chemical reaction peaking at 1212 °C, 1217 °C and 1222 °C, for heating rate 5 K/min, 10 K/min and 20 K/min, respectively. The DSC measurements were too few to consider establishing kinetic parameters for this degradation reaction.

Inspection of the platinum crucibles after TGA/DSC analysis to 1300 °C revealed that the samples had melted completely during the testing. In a multi component inorganic oxide system, as indicated in Appendix A, Table A3, the melting point will not be a defined temperature. It is more likely that there will be gradual melting above the systems eutectic temperature where the composition follows the liquidus lines of the system. It should also be noted that the fast cooling of the spun threads during production of the thermal insulation very likely have resulted in super cooling that did not follow the systems equilibrium phase diagram. It may therefore be quite difficult to interpret the melting process.

The 10 K difference in peak temperature, when increasing the heating rate from 5 K/min to 20 K/min, does, however, indicate that it may be possible to get some information about the kinetics of the observed melting process. An in-depth study of this phenomenon could reveal important information for future modeling of the thermal insulation passive fire protection performance.

3.3. The Thermal Insulation Performance and Break Down

The reason for the delay in temperature increase also for the thinner steel plates may be explained by the characteristics of the thermal insulation including the dust binder and the Bakelite binder. When the exposed thermal insulation surface is heated to e.g., 1000 °C, the exposed part starts to sinter and shrink. This entropy driven process requires some enthalpy, reducing the heat available for further radiation (and conduction) inwards. The heat flux transferred into the thermal insulation is then partly consumed by increasing the temperature of the colder thermal insulation, i.e., the thermal insulation heat capacity needs to be overcome. When the temperature of the next thermal insulation layer starts to increase, heat is also needed to evaporate/pyrolyze the dust binder oil. When the temperature is even higher, heat is needed to decompose/pyrolyze the Bakelite binder. These processes will limit the heat flow to the unexposed parts of the thermal insulation, which early in this process holds a low temperature and displays a very low thermal conductivity. Therefore, there will only be an insignificant heat flow to the metal plates during the first minutes.

As the exposed part of the thermal insulation during fire testing reaches temperatures close to 1200 °C, the degradation (melting) of the thermal insulation requires much heat. However, during this process, the thermal insulation degrades and there will be less thermal insulation thickness to protect the inner parts of the thermal insulation. As the inner parts of the thermal insulation reach higher temperatures, and have lost its dust binder oil and Bakelite binder, it sinters more rapidly as the temperature increases. From about 10 min, this resulted in a nearly linear increase in heat flux to the steel plates, as seen in Figure 10.

The testing confirms that the thermal insulation has a significant effect as passive fire protection. It does, however, also show that the thermal insulation breaks down during this process and becomes less and less protective with time. This is in clear contrast to fire protecting fibers, which typically display 30% to 50% higher thermal conductivity, but retain their protective performance for extended periods even at temperatures above 1200 °C.

3.4. Suggestions for Future Studies

It would be very beneficial if muffle furnace testing of the thermal insulation could be done at holding temperatures at, or even higher than, 1200 °C. This would cover the range of interest for jet fire testing and could give valuable information about break down temperatures and possible break down mechanisms. With more knowledge it may be possible to adjust the thermal insulation mineral composition to gain even better high temperature heat protection.

Differential scanning calorimetry measurements revealing absolute values, e.g., W/g, would be very beneficial for potential future modeling of the fire protection performance of the thermal insulation. When the other information about an oil and gas process area is known, such as fire detection time delays, blowdown times, etc. one may consider whether the thermal insulation could be sufficient for fire protection of the involved pipes and equipment. This could potentially reduce cost when designing new, or refurbishing older, plants and oil platforms.

The fire testing in the present work was done in a way representative for fire exposure. That was worthwhile for demonstrating the performance of the thermal insulation. For future testing, some sort of guarded hot plate setup [23,24], for heat exposure of the thermal insulation, may be considered. At lower temperatures this was done for developing pipeline thermal insulation by Li, et al. [25], who also investigated their new low temperature thermal insulation properties by DSC. A guarded hot plate approach simulating the fire exposure may allow for more controlled heat exposure and more detailed analysis of the thermal insulation behavior during the heat exposure.

Passive fire protection material mats, i.e., quite similar to the thermal insulation, but made of high temperature resistant materials, generally show some higher thermal conductivity than the thermal insulation. They do, however, not break down at 1200 °C. Placing a rather thin layer of fire insulation mat at the fire exposed side of the thermal insulation may therefore be considered. The thickness of this layer could then be designed such that the temperatures of the thermal insulation for a prolonged period could be kept below 1100 °C, ensuring that the thermal insulation would not sinter too severely or break down/melt as fast as in the present study. The system could then potentially protect the steel for a very long period of fire exposure. It would be very interesting to test this concept in a future study.

4. Discussion and Conclusions

The objective of the present study was to investigate the performance of an industrial thermal insulation as passive fire protection of 3 mm, 6 mm, 12 mm and 16 mm steel walls in the configuration currently used in the oil and gas industry for insulating distillation columns. It was also decided to evaluate the mechanisms for thermal insulation degradation during heat treatment at temperatures relevant for 350 kW/m² heat exposure, i.e., up to 1200 °C cladding temperatures.

When doing fire testing, several parameters may vary. An extreme fire would lead to early thermal insulation break down [7] while a too modest fire load would not be valid testing according to the 350 kW/m² test criterion. In the present work, emphasis was put on achieving consistent conditions during fire testing by optimizing the air access into the fire zone versus the propane gas supply. Several tests had to be discarded before this was properly optimized.

Fire testing in the mockup resembling the industrial insulation system and recording the fire exposed wall temperatures showed that the fire protection performance was better for the thicker steel plates. This confirms the importance of the higher thermal capacity of the thicker steel plates. A 10 min delay in temperature increase was, however, revealed for all the plate thicknesses. After this

time delay, the temperature increased systematically faster for the thinner plates due to their lower thermal capacity. The heat flux to the plates as a function of time turned out to be almost similar regardless of the steel plate thickness. This result may be interpreted as better passive fire protection of the thinner steel plates than previously anticipated, and represented a positive surprise in the present study.

Testing 5 cm cubic thermal insulation test specimens showed that there was about 25% thickness shrinkage after holding the thermal insulation 30 min at 1100 °C, thereby indicating that the thermal insulation did not melt at this temperature. Thermogravimetric analysis (TGA) and differential thermogravimetric (DTG) analysis showed mass loss consistent with degradation of the dust binder (oil) and Bakelite binder at temperatures below 700 °C, but indicated no mass loss above 1100 °C. Differential scanning calorimetry (DSC) revealed a major endothermic reaction peaking at just above 1200 °C. It was evident that the sample had melted in the platinum crucible after TGA/DSC to 1300 °C. The endothermic peak at about 1200 °C is therefore most likely due to melting of the mineral based thermal insulation.

The industrial grade thermal insulation studied in the present work may pose some variations in e.g., binder material concentration and bulk phase density. During the fire tests, the thermal insulation did, however, show quite consistent performance. This may be due to the size of the steel plates in the fire tests, i.e., 320 mm diameter. The 10 min delay in temperature increase may therefore be taken as a valid result deserving some explanations. During the fire testing, it was observed that pyrolysis products were released through openings in the mockup. In some tests, these small jets of pyrolysis products burned in contact with the ambient air. This was taken as an indication of ventilation controlled combustion, i.e., there was too little air available in the mockup for any major internal combustion.

The heat requirements for pyrolysing the dust binder oil and the Bakelite, as well as the heat requirements for the melting process at 1200 °C, may to a large extent explain the observed delay in heat flux to the steel plates. But when the thermal insulation gradually increased in temperature, and partly melted, the heat flux to the steel plates increased nearly linearly with time. But still, even when used to protect the thinnest steel plates, i.e., 3 mm thickness, it took more than 20 min to reach a plate temperature of 400 °C.

Due to the many metal oxides comprising the bulk phase of the thermal insulation, the eutectic system may be very hard to analyze. Due to some local variations between batches of the thermal insulation, the eutectic temperature and the melting behavior may also vary.

Realizing that the thermal insulation sintering did not reduce the thermal insulation thickness more than 25% after 30 min at 1100 °C, a design including a thin layer of regular mineral based passive fire protection may be worthwhile a study. If such a layer is added at the exposed side of the thermal insulation, it may help keeping the exposed surface of the thermal insulation at temperatures below 1100 °C for a long time period. This would significantly improve the passive fire protection performance of the combined system.

It is also recommended to do more thermal analysis studies of the thermal insulation to further investigate thermal break down processes. DSC testing at heating rates below 5 K/min and above 20 K/min may possibly allow for revealing information about the kinetics involved in the thermal insulation degradation. Wood pyrolysis may be represented by a set of complex thermal decomposition reactions. Several researchers have, however, concluded that the model should be kept simple unless further research makes it possible to justify added complexity [26–28]. The same approach may be valid also for future research on the degradation of the thermal insulation studied in the present work.

It is also recommended to study heat transfer through the thermal insulation in a setup where other means of heating than a jet fire is considered for more controlled and consistent testing. Such an approach may make it easier to develop a numerical model for utilizing the thermal insulation as passive fire protection, including the thermal insulation breakdown at elevated temperatures. It may also be safer for the experimenters, and require less rigid test safety precautions, since it would not require a propane jet fire exposure.

Author Contributions: T.L. conceived the project idea. J.S.B. and A.G. mounted the mockup for each small scale jet fire test and performed the experiments. A.G. performed the muffle oven experiments, J.S.B, T.L, M.-M.M. and A.G. analyzed the results. J.S.B, M.-M.M. and T.L. wrote the paper.

Funding: J.S.B. was supported by the Norwegian Research Council, Grant No. 257901, Gassco Inc., Norway, Grant No. PO 4500024195 and Equinor, Norway, Grant No. PO 4590081885.

Acknowledgments: The authors would like to acknowledge technical support from G. Kleppe. The support of Leif Inge Larsen and Ingvald Olai Heskja for supplying test materials and producing the mockup is very much appreciated. Equinor Rotvoll performed the TGA and DSC experiments. The data for the thermal insulation supplied by Søren Nyborg Rasmussen, Rockwool, is also much appreciated.

Conflicts of Interest: T.L. has an advisor position at the funding sponsor Equinor. None of the participants in the study have any connections to specific equipment or materials being mentioned in the paper.

Appendix A

The Technical data for the thermal insulation is given in Table A1. The chemical composition of the thermal insulation is given in Table A3.

Table A1. Technical data for the Rockwool Pipe section mat thermal insulation.

| Name | Description | |
|----------------------------------|----------------------------------|------------|
| Material | Stone wool | |
| Operating range | −40 to 700 °C | |
| Name | Performance | Norms |
| Maximum service temperature | 700 °C | EN 14706 |
| Reaction to fire | Euroclass A1 | EN 13501-1 |
| Nominal density | 140 kg/m ³ | EN 1602 |
| Water absorption | ≤1 kg/m ² | EN 1609 |
| | ≤20 kg/m ³ | BP 172 |
| Water vapor diffusion resistance | Sd > 200 m | EN 12086 |
| Air flow resistivity | >60 kPa·s/m ² | |
| Designation code | MW EN 14303-T4-ST(+)-700-WS1-MV2 | EN 14303 |

Table A2. Thermal conductivity of the thermal insulation studied (Rockwool ProRox PSM 971, 50 mm) [29].

| Temperature (°C) | Thermal Conductivity (W/m·K) |
|------------------|------------------------------|
| 50 | 0.041 |
| 100 | 0.046 |
| 150 | 0.054 |
| 200 | 0.064 |
| 250 | 0.075 |
| 300 | 0.088 |
| 350 | 0.106 |

Table A3. Data for the thermal insulation studied (Rockwool ProRox PSM 971, 50 mm) [30].

| Name | Product | Percentage |
|--------------------------|--|--------------|
| Dust binder ¹ | Oil product | <0.5% |
| Binder ¹ | (C ₆ H ₆ O·CH ₂ O) _N | 2.5% (±0.4%) |
| Bulk oxide | SiO ₂ | 40.6–44.6% |
| Bulk oxide | Al ₂ O ₃ | 17.4–20.4% |
| Bulk oxide | MgO + CaO | 23.9–27.9% |
| Bulk oxide | Fe ₂ O ₃ | 5.5–8.5% |
| Bulk oxide | Na ₂ O + K ₂ O | 1.3–4.3% |
| Bulk oxide | TiO ₂ | 0.6–2.6% |
| Bulk oxide | P ₂ O ₅ | Max. 1.2% |

¹ The binder calorific value is 27 MJ/kg according to ISO 1716.

References

- Kletz, T. *What Went Wrong? Case Histories of Process Plant Disasters and How They Could Have Been Avoided*, 5th ed.; Institution of Chemical Engineers: London, UK, 2009; ISBN 13 978-1-85617-531-9.
- U.S. Chemical Safety and Hazard Investigation Board. *Investigation Report Executive Summary*; Drilling Rig Explosion and Fire at the Macondo Well, Report No. 2010-10-I-OS; U.S. Chemical Safety and Hazard Investigation Board: Washington, DC, USA, 2010.
- Murray, J.A.; Sander, L.C.; Wise, S.A.; Reddy, C.M. *Gulf of Mexico Research Initiative 2014/2015 Hydrocarbon Intercalibration Experiment: Description and Results for SRM 2779, Gulf of Mexico Crude Oil and Candidate SRM 2777 Weathered Gulf of Mexico Crude Oil*; NISTIR 8123; National Institute of Standards and Technology: Gaithersburg, MD, USA, 2016. [CrossRef]
- Scandpower. *Guidelines for the Protection of Pressurised Systems Exposed to Fire*; Report No. 27.207.291/R1; Version 2; Scandpower: Kjeller, Norway, 2004.
- Sintef Byggeforsk. *Brannbeskyttelse av Stålkonstruksjoner*; 520.315; Sintef Byggeforsk: Trondheim, Norway, 2004.
- Roberts, T.A.; Shirvill, L.C.; Waterton, K.; Buckland, I. Fire resistance of passive fire protection coatings after long term weathering. *Process Saf. Environ. Prot.* **2010**, *88*, 1–19. [CrossRef]
- Bjørge, J.S.; Metallinou, M.-M.; Kraaijeveld, A.; Log, T. Small Scale Hydrocarbon Fire Test Concept. *Technologies* **2017**, *5*, 72. [CrossRef]
- Jet Fire Test Working Group. *The Jet-Fire Resistance of Passive Fire Protection Materials*; HSE Report OTI 95 634; Health & Safety Executive—Offshore Technology Report: Sheffield, UK, 1995; ISBN 0 7176 1166 3.
- Landucci, G.; Rossi, F.; Nicoletta, C.; Zanelli, S. Designing and testing of innovative materials for passive fire protection. *Fire Saf. J.* **2009**, *44*, 1103–1109. [CrossRef]
- Solyman, W.S.E.; Nagiub, H.M.; Alian, N.A.; Nihal, O.; Shaker, N.O.; Kandil, U.F. Synthesis and characterization of phenol/formaldehyde nanocomposites: Studying the effect of incorporating reactive rubber nanoparticles or Cloisite-30B nanoclay on the mechanical properties, morphology and thermal stability. *J. Radiat. Res. Appl. Sci.* **2017**, *10*, 72–79. [CrossRef]
- Kingery, W.D. Thermal conductivity: XII, Temperature Dependence of Conductivity for Single-Phase Ceramics. *J. Am. Ceram. Soc.* **1955**, *38*, 251–255. [CrossRef]
- Pozzoli, V.A.; Ruiz, M.S.; Kingston, D.; Razzitte, A.C. Entropy Production during the Process of Sintering. *Proc. Mater. Sci.* **2015**, *8*, 1073–1078. [CrossRef]
- Log, T.; Jackson, T.B. Simple and Inexpensive Flash Technique for Determining Thermal Diffusivity of Ceramics. *J. Am. Ceram. Soc.* **1991**, *74*, 941–944. [CrossRef]
- Log, T.; Cutler, R.A.; Jue, J.F.; Virkar, A.V. Polycrystalline t'-ZrO₂(Ln₂O₃) Formed by Displacive Transformations. *J. Am. Ceram. Soc.* **1993**, *28*, 4503–4509. [CrossRef]
- Norwegian Technology Standards Institution. *Norsk Standard, Technical Safety, NORSOK Standard*, 4th ed.; Standard No S-001; Norwegian Technology Standards Institution: Lysaker, Norway, 2008; p. 62.
- Statoil. *Performance Standards for Safety Systems and Barriers—Onshore*; TR2237; Statoil: Tysvær, Norway, 2015; Volume 3, p. 105.

17. International Organization for Standardization. *Determination of the Resistance to Jet Fires of Passive Fire Protection Materials—Part 1: General Requirements*; ISO 22899-1; International Organization for Standardization: Geneva, Switzerland, 2007; 40p.
18. Wickström, U. The plate thermometer—A simple instrument for reaching harmonized fire resistance tests. *Fire Technol.* **1994**, *30*, 195–208. [[CrossRef](#)]
19. Ingason, H.; Wickström, U. Measuring incident radiant heat flux using the plate thermometer. *Fire Saf. J.* **2007**, *42*, 161–166. [[CrossRef](#)]
20. Häggkvist, A.; Sjöström, J.; Wickström, U. Using plate thermometer measurements to calculate incident heat radiation. *J. Fire Sci.* **2013**, *31*, 166–177. [[CrossRef](#)]
21. Sjöström, J.; Amon, F.; Appel, G.; Persson, H. Thermal exposure from large scale ethanol fuel pool fires. *Fire Saf. J.* **2015**, *78*, 229–237. [[CrossRef](#)]
22. Brux, G. *Fire Design of Steel Structures*; Franssen, J.-M., Real, P.V., Eds.; Steel Construction: Berkshire, MA, USA, 2010; Volume 3, pp. 264–264.
23. Jeong, Y.-W.; Koh, T.-H.; Youm, K.-S.; Moon, J. Experimental Evaluation of Thermal Performance and Durability of Thermally-Enhanced Concretes. *Appl. Sci.* **2017**, *7*, 811. [[CrossRef](#)]
24. American Society for Testing and Materials. *ASTM C177: Standard Test Method for Steady-State Heat Flux Measurements and Thermal Transmission Properties by Means of the Guarded-Hot-Plate Apparatus, Annual Book of ASTM Standards*; ASTM International: West Conshohocken, PA, USA, 2004.
25. Li, T.-T.; Zhang, X.; Peng, H.; Jiang, Q.; Dai, W.; Lou, C.-W.; Lin, J.-H. Thermally Bonded PET-Basalt Sandwich Composites for Heat Pipeline Protection: Preparation, Stab Resisting, and Thermal-Insulating Properties. *Appl. Sci.* **2018**, *8*, 510. [[CrossRef](#)]
26. Hostikka, S.; Matala, A. Pyrolysis Model for Predicting the Heat Release Rate of Birch Wood. *Combust. Sci. Technol.* **2017**, *189*, 1373–1393. [[CrossRef](#)]
27. Bal, N.; Rein, G. Relevant model complexity for non-charring polymer pyrolysis. *Fire Saf. J.* **2013**, *61*, 36–44. [[CrossRef](#)]
28. Bal, N.; Rein, G. On the effect of inverse modelling and compensation effects in computational pyrolysis for fire scenarios. *Fire Saf. J.* **2015**, *72*, 68–76. [[CrossRef](#)]
29. Rockwool Inc Homepage. Available online: <https://static.rockwool.com/globalassets/rockwool-uk/downloads/datasheets/hvac/pipe-section-mat-psm.pdf> (accessed on 11 October 2017).
30. Rasmussen, S.N.; ROCKWOOL Inc., Hedehusene, Denmark. Personal communication, 20 February 2018.



© 2018 by the authors. Licensee MDPI, Basel, Switzerland. This article is an open access article distributed under the terms and conditions of the Creative Commons Attribution (CC BY) license (<http://creativecommons.org/licenses/by/4.0/>).

Bibliography

- [1] Wikipedia article. History of the petroleum industry. Last edited April. 2019. Available online: https://en.wikipedia.org/wiki/History_of_the_petroleum_industry (accessed on 10 June 2019).
- [2] Wikipedia article. History of coal mining. Last edited May 2019. Available online: https://en.wikipedia.org/wiki/History_of_coal_mining (accessed on 10 June 2019).
- [3] IEA Statistics OECD/IEA. Fossil fuel energy consumption (% of total), 2014. Available online: <https://data.worldbank.org/indicator/eg.use.comm.fo.zs?end=2015&start=1960&type=shaded&view=chart> (accessed on 10 June 2019).
- [4] BP. *BP Statistical Review of World Energy June 2017*. London: BP Statistical Review of World Energy. Available online: <https://www.bp.com/content/dam/bp/en/corporate/pdf/energy-economics/statistical-review-2017/bp-statistical-review-of-world-energy-2017-full-report.pdf> (accessed on 15 February 2019).
- [5] Norwegian Technology Standards Institution. Norsk Standard, Technical Safety, NORSOK Standard, 4th ed.; Standard No S-001; Norwegian Technology Standards Institution: Lysaker, Norway, **2008**; p. 62.
- [6] Standard Norge. Petroleum and natural gas industries, *Control and Mitigation of Fires and Explosions on Offshore Production Installations*, Requirements and guidelines (ISO 13702); Standard Norge: Oslo, **2015**.
- [7] Lochbaum, D. U.S. Nuclear Plants in the 21st century: The risk of a lifetime. *Union of Concerned Scientists*. **2014**, Available online: https://www.ucsusa.org/sites/default/files/legacy/assets/documents/nuclear_power/nuclear04fnl.pdf (accessed on 26 June 2019).
- [8] U.S. Chemical Safety and Hazard Investigation Board. Investigation Report Executive Summary; Drilling Rig Explosion and Fire at the Macondo Well, Report No. 2010-10-I-OS; U.S. Chemical Safety and Hazard Investigation Board: Washington, D.C., USA, **2010**.
- [9] Kletz, T. *What Went Wrong? Case Histories of Process Plant Disasters and How They Could Have Been Avoided*, 5th ed.; Institution of Chemical Engineers: London, UK, **2009**; ISBN 13:978-1-85617-531-9.

- [10] Murray, J.A.; Sander, L.C.; Wise, S.A.; Reddy, C.M. Gulf of Mexico Research Initiative 2014/2015 Hydrocarbon Intercalibration Experiment: Description and Results for SRM 2779, Gulf of Mexico Crude Oil and Candidate SRM 2777 Weathered Gulf of Mexico Crude Oil; NISTIR 8123; National Institute of Standards and Technology: Gaithersburg, MD, USA, **2016**.
- [11] Skulstad, B.H.P.; Huse, J.R.; Bakken, B.I. *Guidelines for the Protection of Pressurised Systems Exposed to Fire* (27.207.291/R1 – Version 2); Kjeller: Scandpower Risk Management AS, **2004**.
- [12] Jet Fire Test Working Group. *The Jet-Fire Resistance of Passive Fire Protection Materials*; HSE Report OTI 95 634; Health & Safety Executive—Offshore Technology Report; Jet Fire Test Working Group: Sheffield, UK, **1995**; ISBN 0-7176-1166-3.
- [13] Bjørge, J.S.; Metallinou, M.-M.; Kraaijeveld, A.; Log, T. Small scale hydrocarbon fire test concept. *MDPI Technologies*, **2017**, 5(4), 72. DOI: 10.3390/technologies5040072.
- [14] Scandpower. *Guidelines for the Protection of Pressurised Systems Exposed to Fire*; Report No. 27.207.291/R1; Version 2; Scandpower: Kjeller, Norway, **2004**.
- [15] Benarx. Passive fire protection testing and certification. Available online: <http://www.benarx.com/resources/what-fire-protection-do-i-need/> (accessed on 10 June 2019).
- [16] Liang, G.; Mudawar, I. Review of drop impact on heated walls. *Int. J. Heat Mass Transf.* **2017**, 106, 103–126. DOI: 10.1016/j.ijheatmasstransfer.2016.10.031.
- [17] Bjørge, J.S.; Metallinou, M.M.; Log, T.; Frette, Ø. Method for measuring cooling efficiency of water droplets impinging onto hot metal discs. *Applied Sciences*, **2018**, 8(6), 953. DOI: 10.3390/app8060953.
- [18] Bjørge, J.S.; Gunnarshaug, A.; Log, T.; Metallinou, M.M. Study of industrial grade thermal insulation as passive fire protection up to 1200°C. *Safety*, **2018**, 4(3), 41, 1–19. DOI: 10.3390/safety4030041.
- [19] Bjørge, J.B.; Bjørkheim, S.A.; Metallinou, M.M.; Log, T.; Frette, Ø. Influence of acetone and sodium chloride additives on cooling efficiency of water droplets impinging onto hot metal surfaces. *Energies*, **2019**, 12(12), 2358. DOI: 10.3390/en12122358.
- [20] Kazemi, Z. Droplet Impaction on Solid Surfaces Exposed to Impinging Jet Fires. Ph.D. Dissertation, Norwegian University of Science and Technology, Trondheim, Norway, **2006**.
- [21] Drange, L.A. A Study of Selected Problems Related to Accidental Process Fires. Ph.D. Dissertation, University of Bergen, Bergen, Norway, **2011**.
- [22] Opstad, S.A.; Wighus, R. Droplet Sizes from Deluge Nozzles; NBL F09117; SINTEF Report: Trondheim, Norway, **2009**.
- [23] Leidenfrost, J.G. *De Aquae Communes Nonnullis Qualitatibus Tractatus*; Ovenius: Duisburg, Germany, **1756**.

- [24] Leidenfrost, J.G. On the fixation of water in diverse fire. *Int. J. Heat Mass Transf.* **1966**, 9, 1153–1166. DOI: 10.1016/0017-9310(66)90111-6.
- [25] Dahle, I.B.; Dybvig, G.; Ersdal, G.; Bulbrandsen, T.; Hansen, B.A.; Tharaldsen, J.E.; Wiig, A.S. Major accidents and their consequences for risk regulation? In Berenguer, C.; Grall, A.; Guedes Soares, C. *Advances in Safety, Reliability and Risk Management*, CRC Press, **2012**; ISBN 978-0-4-68379-1
- [26] Collier, K. Insulation. *Chem. Eng. Prog.* **2002**, 98, 47.
- [27] International Organization for Standardization. *Determination of the Resistance to Jet Fires of Passive Fire Protection Materials—Part 1: General Requirements*; ISO 22899-1; International Organization for Standardization: Geneva, Switzerland, 2007; 40 p.
- [28] Equinor, TR1660 *Insulation Handbook* v.5, Equinor: Tysvær, Norway.
- [29] Brændeland, G. Risk factors in emergency response. A review of investigations of large incidents in Norway. SINTEF A16037: Trondheim, Norway, **2011**.
- [30] Lauridsen, Ø.; Kristensen, V.; Dørum, K.G.; Hundseid, O.; Etterlid, H.; Hagerup, O.; Tjelta, O.; Førland, I.H.; Zachariassen, S. Hydrocarbon leak on the Ula P facility, 12 September 2012. Investigation report, Petroleumstilsynet: Stavanger, Norway, **2012**.
- [31] Petroleum Safety Authority Norway. The framework regulation. *Regulations relating to health, safety and the environment in the petroleum activities at certain onshore facilities, etc.* Stavanger, Norway, **2018**.
- [32] Petroleum Safety Authority Norway. Technical and operational regulations. *Regulations relating to technical and operational matters at onshore facilities in the petroleum activities, etc.* Stavanger, Norway, **2016**.
- [33] Petroleum Safety Authority Norway. Ord og uttrykk. Available online: <https://www.ptil.no/fagstoff/ord-og-uttrykk/#R> (accessed on 27 June 2019).
- [34] Gassco, Hvitboken Barriere integritet, revision 1, Gassco: Bygnes, Norway.
- [35] Center for Chemical Process Safety. *Guidelines for Engineering Design for Process Safety*. John Wiley & Sons: New York, USA, **2012**
- [36] Rausand, R.; Utne, I.U. Risikoanalyse -teori og metoder; Trondheim, Norway, 2011; ISBN 978-82-519-2446-7.
- [37] Wingerden, K.V. Mitigation of gas explosions using water deluge, *Process Safety Progress*, **2004**, 19 (3), 173–178. <https://doi.org/10.1002/prs.680190309>.
- [38] Health and Safety Executive. Active / passive fire protection. Available online: <http://www.hse.gov.uk/comah/sragtech/techmeasfire.htm> (accessed on 05 July 2019).
- [39] Roberts, T.A.; Shirvill, L.C.; Waterton, K.; Buckland, I. Fire resistance of passive fire protection coatings after long term weathering. *Process Saf. Environ. Prot.* **2010**, 88, 1–19. DOI: 10.1016/j.psep.2009.09.003.

- [40] American Petroleum Institute. *Sizing, Selection, and Installation of Pressure-Relieving Devices, Part I – Sizing and Selection*, 9th ed. (API Std 520). API: Washington, D.C., USA, **2014**.
- [41] American Petroleum Institute. *Pressure-Relieving and Depressuring System*, 6th ed. (API Std 521); API: Washington, D.C., USA, **2014**.
- [42] Wikipedia article. Fire triangle. Last edited May 2019. Available online: https://en.wikipedia.org/wiki/Fire_triangle (accessed on 04 July 2019).
- [43] Bosch, C.J.H.; Weterings, R.A.P.M. *TNO Yellow Book*, Methods for the calculation of physical effects due to releases of hazardous materials. Committee for the Prevention of Disasters: Netherlands, **1996**.
- [44] Eckhoff, R.K. *Explosion Hazards in the Process Industries*, 2nd ed.; Gulf Professional Publishing: Houston, Texas, USA, **2005**; ISBN: 0-9765113-4-7.
- [45] Lawson, J.R. A History of Fire Testing, NIST Technical Note 1628, National Institute of Standards and Technology: Gaithersburg, USA, **2009**.
- [46] International Organization for Standardization (ISO) *Fire-Resistance Tests—Elements of Building Construction*; ISO 834-1:1999; International Organization Standardization: 1214 Vernier, Genève, Switzerland, **2007**.
- [47] Norsk Standard. *Fire Resistance Tests—Part 1: General Requirements*; NS-EN 1363-1:2012, standard.no; Lysaker, Norway, **2012**.
- [48] Taillefer, N.; Carlotti, P.; Larive, C.; Lemerle, C.; Avenel, R.; Pimienta, P. Ten years of increased hydrocarbon temperature curves in French tunnels. *Fire Technol.* **2013**, *49*, 531–549. DOI:10.1007/s10694-012-0259-8.
- [49] Statoil, TR2237. *Performance Standards for Safety Systems and Barriers—Onshore*. Statoil: Tysvær, Norway, **2015**, 3, 105.
- [50] Hurley, M.J.; Gottuk, D.; Hall Jr, J.R.; Harada, K.; Kuligowski, E.; Puchovsky, M.; Torero, J.; Watts Jr, J.M.; Wieczorek, C. *SFPE Handbook of Fire Protection Engineering*, 5th ed.; Springer: London, England, **2016**. DOI 10.1007/978-1-4939-2565-0.
- [51] Drysdale, D. *An Introduction to Fire Dynamics*, 2nd ed.; Wiley: West Sussex, England, reprinted March 2008; ISBN: 0-471-97291-6.
- [52] Wikipedia article. Thermal diffusivity. Last edited February 2019. Available online: https://en.wikipedia.org/wiki/Thermal_diffusivity (accessed on 27 June 2019).
- [53] Chase, M.W. *NIST-JANAF Thermochemical Tables*, 4th ed.; American Institute of Physics: College Park, MA, USA, **1998**. Available online: <https://srdata.nist.gov/jpcrd/jpcrdM9.pdf> (accessed on 5 February 2017).
- [54] Chegini, G.R.; Ghobadian, B. Spray dryer parameters for fruit juice drying, *World J. Agric. Sci.* **2007**, *3*, 230–236.
- [55] Dugas, V.; Broutin, J.; Souteyrand, E. Droplet evaporation study applied to DNA chip manufacturing. *Langmuir* **2005**, *21*, 9130–9136. DOI: 10.1021/la050764y

- [56] Deegan, R.D.; Bakajin, O.; Dupont, T.F.; Huber, G.; Nagel, S.R.; Witten, T.A. Capillary flow as the cause of ring stains from dried liquid drops, *Nature* **1997**, *389*, 827–829. DOI: 10.1038/39827
- [57] Lopes, M.-C.; Bonaccorso, E.; Gambaryan-Roisman, T.; Stephan, P. Influence of the substrate thermal properties on sessile droplet evaporation: Effect of transient heat transport. *Colloids Surfaces A Physicochem. Eng. Asp.* **2013**, *432*, 64–70. DOI: 10.1016/j.colsurfa.2013.04.017
- [58] Log, T. Water droplets evaporating on horizontal semi-infinite solids at room temperature. *Appl. Therm. Eng.* **2016**, *93*, 214–222. DOI: 10.1016/j.applthermaleng.2015.09.108
- [59] Girard, F.; Antoni, M.; Faure, S.; Steinchen, A. Influence of heating temperature and relative humidity in the evaporation of pinned droplets. *Colloids Surfaces A Physicochem. Eng. Asp.* **2008**, *323*, 36–49. DOI: 10.1016/j.colsurfa.2007.12.022
- [60] Misyura, S.Y. The effect of Weber number, droplet sizes and wall roughness on crisis of droplet boiling. *Exp. Therm. Fluid Sci.* **2017**, *84*, 190–198. DOI: 10.1016/j.expthermflusci.2017.02.014
- [61] Nguyen, T.; Nguyen, A.; Hampton, M.; Xu, Z.; Huang, L.; Rudolph, V. Theoretical and experimental analysis of droplet evaporation on solid surfaces. *Chem. Eng. Sci.* **2013**, *69*, 522–529. DOI: 10.1016/j.ces.2011.11.009
- [62] Zhou, X.; Zhou, B.; Jin, X. Study of fire-extinguishing performance of portable water-mist fire extinguisher in historical buildings. *J. Cult. Herit.* **2010**, *11*, 392–397. DOI: 10.1016/j.culher.2010.03.003
- [63] Bhatt, N.H.; Pati, A.R.; Kumar, A.; Behera, A.; Munshi, B.; Mohapatra, S.S. High mass flux spray cooling with additives of low specific heat and surface tension: A novel process to enhance the heat removal rate. *Appl. Therm. Eng.* **2017**, *120*, 537–548. DOI: 10.1016/j.applthermaleng.2017.03.137
- [64] Fukuda, S.; Kohno, M.; Tagashira, K.; Ishihara, N.; Hidaka, S.; Takata, Y. Behavior of small droplet impinging on a hot surface. *Heat Transf. Eng.* **2014**, *35*, 204–211. DOI: 10.1080/01457632.2013.812496
- [65] Lee, C.H.; Kim, D.Y.; Kim, H.D.; Kim, K.C. Dynamic behavior and micro-explosion characteristics of impinging droplets on a high-temperature surface. *J. Vis.* **2015**, *18*, 59–70. DOI: 10.1007/s12650-014-0218-1
- [66] Gradeck, M.; Seiler, N.; Ruyer, P.; Maillet, D. Heat transfer for Leidenfrost drops bouncing onto a hot surface. *Exp. Therm. Fluid Sci.* **2013**, *47*, 14–25. DOI: 10.1016/j.expthermflusci.2012.10.02
- [67] Pasandideh-Fard, M.; Aziz, S.D.; Chandra, S.; Mostaghimi, J. Cooling effectiveness of a water droplet impinging on a hot surface. *Int. J. Heat Fluid Flow* **2001**, *22*, 201–210. DOI: 10.1016/S0142-727X(00)00086-2

- [68] Birdi, K.S.; Vu, D.T.; Winter, A. A study of the evaporation rates of small water drop placed on a solid surface. *J. Phys. Chem.* **1989**, *93*, 3702–3703. DOI: 10.1021/j100346a065.
- [69] Bernardin, J.D.; Mudawar, I. The Leidenfrost point: Experimental study and assessment of existing models. *J. Heat Transf.* **1999**, *121*, 894–903. DOI: 10.1115/1.2826080.
- [70] Sawyer, M.L.; Jeter, M.S.; Abdel-Khalik, S.I. A critical heat flux correlation for droplet impact cooling. *Int. J. Heat Mass Transf.* **1997**, *40*, 2123–2131. DOI: 10.1016/S0017-9310(96)00267-0.
- [71] Chang, H. The myth of the boiling point. *Sci. Prog.* **2008**, *91*, 219–240.
- [72] Majithia, A.K.; Hall, S.; Harper, L., Bowen, P.J. Droplet breakup quantification and processes in constant and pulsed air flows. *Paper id ilass08-4-4*. **2008**.
- [73] Kekesi, T.; Amberg, G.; Wittberg, L.P. Drop deformation and breakup. *Int. J. Multiphase Flow*. **2014**, *66*, 1–10. DOI: 10.1016/j.ijmultiphaseflow.2014.06.006
- [74] International Standard. *Geometrical Product Specifications (GPS)—Surface Texture: Profile Method—Terms, Definitions and Surface Texture Parameters*; ISO 4287; ISO: Geneva, Switzerland, **1997**; 25p.
- [75] Log, T.; Heskestad, G. Temperatures of restricted turbulent fire plumes. *Fire Saf. J.* **1998**, *31*, 101–115. DOI: 10.1016/S0379-7112(97)00068-4.
- [76] Chatzikyriakou, D.; Walker, S.P.; Hewitt, G.F.; Narayanan, C.; Lakehal, D. Comparison of measured and modelled droplet–hot wall interactions, *Appl. Therm. Eng.* **2009**, *29*, 1398–1405. DOI: 10.1016/j.applthermaleng.2008.02.012.
- [77] Wachtters, L.H.J.; Bonne, H.; Van Nouhuis, H.J. The heat transfer from a hot horizontal plate to sessile water drops in the spheroidal state. *Chem. Eng. Sci.* **21**, **1966**, 923–936. DOI: 10.1016/0009-2509(66)85086-8.
- [78] Wickström, U. The plate thermometer—A simple instrument for reaching harmonized fire resistance tests. *Fire Technol.* **1994**, *30*, 195–208, DOI:10.1007/BF01040002.
- [79] Ingason, H.; Wickström, U. Measuring incident radiant heat flux using the plate thermometer. *Fire Saf. J.* **2007**, *42*, 161–166, DOI: 10.1016/j.firesaf.2006.08.008.
- [80] Häggkvist, A.; Sjöström, J.; Wickström, U. Using plate thermometer measurements to calculate incident heat radiation. *J. Fire Sci.* **2013**, *31*, 166–177, DOI: 10.1177/0734904112459264.
- [81] Sjöström, J.; Amon, F.; Appel, G.; Persson, H. Thermal exposure from large scale ethanol fuel pool fires. *Fire Saf. J.* **2015**, *78*, 229–237. DOI: 10.1016/j.firesaf.2015.09.003.
- [82] ahsell. Kraftbrenner Sivert Pro. Available online: <https://www.ahsell.no/33/verktoy/sveis-og-gass/gassbrennerutstyr/388852/> (accessed on 29 June 2019).
- [83] Jeong, Y.-W.; Koh, T.-H.; Youm, K.-S.; Moon, J. Experimental evaluation of thermal performance and durability of thermally-enhanced concretes. *Appl. Sci.* **2017**, *7*, 811.

-
- [84] American Society for Testing and Materials. ASTM C177: Standard Test Method for Steady-State Heat Flux Measurements and Thermal Transmission Properties by Means of the Guarded-Hot-Plate Apparatus, *Annual Book of ASTM Standards*; ASTM International: West Conshohocken, PA, USA, **2004**.
- [85] Li, T.-T.; Zhang, X.; Peng, H.; Jiang, Q.; Dai, W.; Lou, C.-W.; Lin, J.-H. Thermally bonded PET–Basalt sandwich composites for heat pipeline protection: Preparation, stab resisting, and thermal-insulating properties. *Appl. Sci.* **2018**, *8*, 510. DOI: 10.3390/app8040510.



Graphic design: Communication Division, UIB / Print: Skjipes Kommunikasjon AS



uib.no

ISBN: 9788230846513 (print)
9788230863305 (PDF)